Michael D. Machesky

Refining leaf trait methods for paleoclimate reconstruction

submitted in partial fulfillment of the requirements for the degree of

Master of Science in Earth and Environmental Sciences

Department of Earth and Environmental Sciences

The University of Michigan

Accepted by:

Signature	Selena Y Smith (Name)	1 Aug 2023 (Date)
Signature	Nathan D Sheldon (Name)	1 Aug 2023 (Date)
Department Chair Signature	Julia Cole (Name)	20 Aug 2023 (Date)

- [x] Permission granted.
- [ ] Permission granted to copy after: ________________
- [ ] Permission declined.

Author Signature

Earth and Environmental Sciences
UNIVERSITY OF MICHIGAN

Table of Contents

Acknowledgements iii

Abstract iv

Ch. 1 Introduction 1–3

- **1.1 References 3–4**

Ch. 2 Sensitivity of leaf gas-exchange modeled atmospheric CO_2 concentration reconstructions to methods of stomatal measurement 5–24

- **Abstract 5**
- **2.1 Introduction 5–6**
- **2.2 Methods 6–10**
- **2.3 Results 10–13**
- **2.4 Discussion 13–16**
- **2.5 Conclusions 16**
- **2.6 References 17–19**
- **Figures 20–24**

Ch. 3 Insights into climate reconstruction from palm leaf traits 25–57

- **Abstract 25**
- **3.1 Introduction 25–28**
- **3.2 Methods 28–32**
- **3.3 Results 32–34**
- **3.4 Discussion 34–38**
- **3.5 Conclusions 38**
- **3.6 References 39–45**
- **Tables 46–52**
- **Figures 53–57**

Appendix 58–126

Acknowledgements

I would first like to thank my academic advisors Dr. Selena Smith (PEPPR lab) and Dr. Nathan Sheldon (GRiTS lab). The samples for Chapter 3 were acquired with the help of my labmates Jeronimo Morales Toledo in the field and herbarium, and Kelly Martin in the herbarium. My labmates Kelly Martin, Kate Morrison, and Katherine Harpenau also helped with data collection for Chapter 2. Technical assistance was provided by Dr. Michael Hren (University of Connecticut), who ran all of my samples in his isotope ratio mass spectrometer while our machine was out of commission. Undergraduate lab assistant Sarah Lindsey and Earth RISE participant Sofía Martinez-Lozoya aided with data collection for Chapter 3. I would like to thank Lauren VanWagoner for collecting and isotopically analyzing over 100 palm leaf samples as part of her honor's thesis with Selena, that I was able to use here. My labmate Cecilia Howard trained me to use the elemental analyzer and cavity ringdown spectrometer (CRDS), even though I never got a chance to run the CRDS. I would also like to thank Dr. Brad Ruhfel for access to the University of Michigan Herbarium (MICH), Dr. Jordan Teisher for access to the Missouri Botanical Gardens Herbarium (MO), Dr. Ken Cameron for access to the Wisconsin State Herbarium (WIS), Dr. Brett Jestrow for access to the Fairchild Tropical Botanical Garden Herbarium (FTG), and Dr. Matthew Pace for access to the New York Botanical Garden Herbarium (NY). I would also like to thank Stacy Scherman, Brenda Magers, and Troy Crider from the South Carolina Department of Parks, Recreation, and Tourism (permit no. N-7-22), Michael Bradley from the Charleston County Parks and Recreation Commission, Cheri Albin from the Florida Parks Service (permit no. 06162210), Jason Thompson from the Charlotte County Parks and Natural Resources Division, and Keith Duhon from Loyola University New Orleans for allowing me access to collect leaf samples. Finally, I would like to thank all of my friends and family who supported me during my past two years in graduate school. This work was supported by the University of Michigan Department of Earth and Environmental Sciences Scott Turner Award (2021, 2022) and NSF EAR-1949151 to S.Y. Smith.

ABSTRACT

As continued reliance on fossil fuels drives anthropogenic climate change, it is important to understand past changes in climate and how they affected Earth's organisms and ecosystems. Because of their sessile nature and direct interaction with the atmosphere, plants and plant fossils are one of the most important tools for studying climate in a changing world. Quantitative, mechanistic methods have been developed to reconstruct atmospheric CO_2 concentrations (c_a) by modeling leaf-gas exchange using carbon isotope ratios and stomatal traits. Currently, these methods have mostly been used by woody "dicot" plants in mid- to high-latitudes, leaving other plant groups and lower latitudes understudied. In Chapter 1, I introduce the motivation for the study and the questions I set out to answer in the following chapters: (1) how do methods of cuticle preparation affect the results of stomatal analysis? (2) how is climate reflected in palm leaves spatially, temporally, and phylogenetically? In Chapter 2, I investigated how four different methods of preparing leaf cuticles for stomatal analysis (nail polish, dental putty on fresh leaves, putty on dried leaves, and fluorescence on cleared leaves) affect stomatal measurements and resulting c_a calculations. I found that there are significant differences between methods, with fluorescence microscopy on cleared leaves yielding the best results. Thus, I recommend that this method be used when possible, and the use of other methods be calibrated to standardize results. In Chapter 3, I measured several morphological and chemical traits in palm leaves and gathered climate data to test whether palm leaf traits reflected changes in climate spatially, temporally, and phylogenetically. I found that most individual traits are not responding strongly to changes in climate, but there are weak relationships between specific traits and climate in individual species. For *Sabal palmetto*, $\delta^{13}C$ is weakly negatively correlated with c_a, as is stomatal index to both c_a and mean annual precipitation. In *Phoenix dactylifera*, vein length per area is negatively correlated with mean annual temperature, as is C:N to vapor pressure deficit. However, palms did show a low response of intrinsic water use efficiency through time, which may indicate they are either weakly adapting to climate change and may struggle in the near future or that levels of anthropogenic climate change thus far have not been enough to cause them stress. The results suggest given taxa can be used in leaf-gas exchange models to reconstruct c_a, if the carbon assimilation rate and operational stomatal conductance can be better quantified, and corroborate previous research that questions the efficacy of the use of C isotope discrimination (Δ_{leaf}) to reconstruct c_a without the use of stomatal traits.

1. Introduction

As continued reliance on fossil fuels drives global temperature rises, anthropogenic climate change has become the most urgent issue pressing humanity. In order to mitigate its effects on extant organisms and ecosystems, it is important to understand how life on Earth responded to past changes in climate. However, in order to understand organismal responses, we must also have estimates of how exactly Earth's climate changed in the past. These estimates should ideally come from sources independent of one another, and thus the more paleoclimate proxies exist, the better we can assess the ways in which a range of species will respond. Plants interact directly with the atmosphere via their leaves through the processes of photosynthesis and transpiration. Certain traits of plants are sensitive to environmental and climatic factors and will vary between individuals depending on where they grow. Living and fossil leaves are then useful for paleoclimate studies, as they respond to differences in local climatic conditions through both the morphology and chemistry of their leaves (McElwain, 2018).

Plants in the family Arecaceae (palms) are useful for study because of their worldwide low- to mid-latitude distribution across a diverse set of biomes/climate regimes, their commercial importance as a food crop, building material, and as ornamental plants, and their good fossil record extending back to the Late Cretaceous (Dransfield et al., 2008). Fossil palms are already used in paleoclimatology as an indicator of tropical and subtropical conditions, given that their presence in the geologic record necessitates mean cold season temperatures above ~5°C (Greenwood and Wing, 1995; Reichgelt et al., 2018). Presently the majority of paleoclimate reconstruction using plant fossils has been applied at mid and high-latitudes, leaving a gap for such methods to be applied to the tropics and sub-tropics. Palms make a good candidate for low-latitude paleoclimate as today they are mostly restricted to the (sub)-tropical latitudes and have persisted there since their first appearance in the late mid-Cretaceous (Harley, 2006). Furthermore, palms have the potential for a long species duration, as there are a number of genera of palms, including those analyzed in this paper, that have confirmed or suggested fossil counterparts (Dransfield et al., 2008). This makes palms suitable for paleoclimate studies using leaf traits, as they have not changed enough through geologic time to render them inapplicable to present day leaf trait-climate relationships to the past.

A number of plant functional traits have been shown to reflect the environmental and climatic conditions the plant grew in. One example of these traits are stomata – pores most commonly found on the underside of leaves, and which exist on virtually all extant land plants with good potential for preservation in fossils with cuticle preserved (McElwain & Steinthorsdottir, 2017; Clark et al., 2022). The ratio of stomata to total epidermal cells on a leaf, referred to as stomatal index, negatively correlates with atmospheric CO_2 concentrations (pCO_2) in taxon-dependent relationships in both modern and fossil leaves, as plants will increase the number of stomata they have to maximize CO_2 intake in times of low pCO_2 (McElwain & Chaloner, 1995; Royer, 2001; Rundgren & Beerling, 2003). Similarly, stomatal density (the number of stomata on a leaf per unit area), the average length of stomatal pores, and the stable carbon isotope ratio ($\delta^{13}C$) have been combined for use in models to calculate pCO_2 from fossil leaves (Franks et al., 2014; Royer et al. 2018; Konrad et al., 2021; Franks & Beerling, 2009). The density of leaf veins, measured as the ratio of vein length per unit area (VLA), is a functional trait of budding interest to paleoclimatologists. Evolution of high vein densities in angiosperms increased their transpiration capacity and in turn contributed to their global dominance over other plant groups and facilitated the formation of modern rainforest environments (Boyce et al., 2009; Boyce and Lee, 2017). VLA is useful for paleoclimate reconstruction when leaf size is controlled for, as it has been experimentally shown to correlate elevation and has been used to successfully calculate mean annual temperature and pCO_2 (Uhl and Mossbruger, 1999; Blonder and Enquist, 2014). Despite this, VLA remains relatively under-used as a paleoclimatic proxy, and could potentially refine paleoclimatic reconstructions when paired with stomatal or chemical leaf traits.

I aim to combine the use of stomatal index, stomatal density, stomatal pore length, guard cell length, guard cell width, leaf $\delta^{13}C$, and VLA in extant palm leaves to test for relationships with environmental variables, which would allow palm leaf fossils to be used as a quantitative paleoclimate proxy. To do this, I collected leaves from modern and historical specimens of three species of palms with a distribution spanning tropical latitudes across the globe. When beginning to tackle this problem, it became clear that different methods of preparing a leaf cuticle for stomatal analysis may be yielding different results. Thus, I also set out to test whether these different methods affect stomatal density and index measurements, as well as pCO_2 calculations when coupled with $\delta^{13}C$ in the Franks et al. model (2014). For this I applied four different methods of cuticle preparation for stomatal analysis on a set of locally gathered leaves to determine whether results between methods were significantly different. Chapter 2 focuses on the methods comparison of stomatal analysis, while Chapter 3 details the investigation into how climate is reflected in palm leaves on both spatial and temporal scales.

1.1 REFERENCES

Blonder, B., and B. J. Enquist. 2014. Inferring climate from angiosperm leaf venation networks. *The New Phytologist* 204: 116–126.

Boyce, C. K., T. J. Brodribb, T. S. Feild, and M. A. Zwieniecki. 2009. Angiosperm leaf vein evolution was physiologically and environmentally transformative. *Proceedings of the Royal Society B: Biological Sciences* 276: 1771–1776.

Boyce, C. K., and J. Lee. 2017. Plant evolution and climate over geological timescales. *Annual Review of Earth and Planetary Sciences* 45: 61–87.

Clark, J. W., B. J. Harris, A. J. Hetherington, N. Hurtado-Castano, R. A. Brench, S. Casson, T. A. Williams, et al. 2022. The origin and evolution of stomata. *Current biology: CB* 32: R539–R553.

Dransfield, J., N. W. Uhl, C. B. Asmussen, W. J. Baker, M. M. Harley, and C. E. Lewis. Genera Palmarum - The Evolution and Classification of the Palms. Royal Botanical Gardens, Kew, London, UK.

Franks, P. J., and D. J. Beerling. 2009. Maximum leaf conductance driven by CO_2 effects on stomatal size and density over geologic time. *Proceedings of the National Academy of Sciences* 106: 10343–10347.

Franks, P. J., D. L. Royer, D. J. Beerling, P. K. Van de Water, D. J. Cantrill, M. M. Barbour, and J. A. Berry. 2014. New constraints on atmospheric CO_2 concentration for the Phanerozoic. *Geophysical Research Letters* 41: 4685–4694.

Greenwood, D. R., and S. L. Wing. 1995. Eocene continental climates and latitudinal temperature gradients. *Geology* 23: 1044–1048.

Harley, M. M. 2006. A summary of fossil records for Arecaceae. *Botanical Journal of the Linnean Society* 151: 39–67.

Konrad, W., D. L. Royer, P. J. Franks, and A. Roth-Nebelsick. 2021. Quantitative critique of leaf-based paleo-CO2 proxies: Consequences for their reliability and applicability. *Geological Journal* 56: 886–902.

McElwain, J. C. 2018. Paleobotany and Global Change: Important Lessons for Species to Biomes from Vegetation Responses to Past Global Change. *Annual Review of Plant Biology* 69: 761–787.

McElwain, J. C., and W. G. Chaloner. 1995. Stomatal Density and Index of Fossil Plants Track Atmospheric Carbon Dioxide in the Palaeozoic. *Annals of Botany* 76: 389–395.

McElwain, J. C., and M. Steinthorsdottir. 2017. Paleoecology, Ploidy, Paleoatmospheric Composition, and Developmental Biology: A Review of the Multiple Uses of Fossil Stomata. *Plant Physiology* 174: 650–664.

Reichgelt, T., C. K. West, and D. R. Greenwood. 2018. The relation between global palm distribution and climate. *Scientific Reports* 8: 4721.

Royer, D. L. 2001. Stomatal density and stomatal index as indicators of paleoatmospheric CO2 concentration. *Review of Palaeobotany and Palynology* 114: 1–28.

Royer, D. L., K. M. Moynihan, M. L. McKee, L. Londoño, and P. J. Franks. 2018. Sensitivity of a leaf gas-exchange model for estimating paleoatmospheric CO_2 concentration. *Climate of the Past* 15: 795–809.

Rundgren, M., and D. Beerling. 2003. Fossil leaves: Effective bioindicators of ancient CO_2 levels? *Geochemistry, Geophysics, Geosystems* 4.

Uhl, D., and V. Mosbrugger. 1999. Leaf venation density as a climate and environmental proxy: a critical review and new data. *Palaeogeography, Palaeoclimatology, Palaeoecology* 149: 15–26.

2. Sensitivity of leaf gas-exchange modeled atmospheric CO_2 concentration reconstructions to methods of stomatal measurement[1]

ABSTRACT

Mechanistic models using stomatal traits and leaf carbon isotope ratios to reconstruct atmospheric CO_2 concentrations [c_a] are important to understand Phanerozoic paleoclimate. Despite this, methods for preparing leaf cuticles to measure stomatal traits have not been standardized. Three people measured the stomatal density and index, guard cell length, pore length, and guard cell width of leaves from the same *Ginkgo biloba*, *Quercus alba*, and *Zingiber mioga* leaves growing at known CO_2 levels using four different methods of cuticle preparation (fluorescence on cleared leaves, nail polish, dental putty on fresh leaves, and dental putty on dried leaves). There are significant differences between the measurements made using each method, although modeled c_a calculations are less sensitive to method than individual traits, however the choice of C isotopic fractionation by RuBisCo also impacted the accuracy of the results. I suggest using the fluorescence method and directly measure pore length, as it produced the most accurate c_a estimates. Further study should be conducted of the fractionation due to carboxylation of RuBP in individual plant species before use as a paleo-CO_2 barometer.

2.1 INTRODUCTION

Scientists must try to understand the ways in which life responded to global change in the past to understand how life will respond to contemporary climate change. Because plants interact directly with the atmosphere through photosynthesis, living and fossil leaves are useful as recorders of the environmental conditions in which they grew through both morphological and chemical traits (McElwain, 2018). Some of the most well-studied leaf traits for paleoclimate are from stomata: pores on leaf surfaces that regulate gas exchange. Stomata are found on all extant and fossil land plants except for liverworts and are well-preserved across the fossil record, and today are most common on the abaxial surface of leaves (McElwain & Steinthorsdottir, 2017). Especially useful for paleoatmospheric reconstruction is the stomatal index (*SI*) of a plant: the ratio of stomata to the total number of epidermal cells on the bottom of a leaf. Unlike stomatal

[1] Planned submission to Applications in Plant Sciences as **Sensitivity of leaf gas-exchange modeled atmospheric CO_2 concentration reconstructions to methods of stomatal measurement** by Mike D. Machesky, Nathan D. Sheldon, Michael T. Hren, Kelly D. Martin, Kate M. Morrison, Katherine Harpenau, Selena Y. Smith

density (*SD*; the number of stomata per unit area), *SI* is not affected by environmental factors such as temperature, water availability, and irradiance and can therefore be applied to pCO_2 reconstruction independently of other traits (McElwain and Chaloner, 1995; Royer, 2001). Stomatal index has been shown to correlate negatively with pCO_2 in taxon-dependent relationships in both modern and fossil leaves, the number of stomata on plants' leaves are reduced in higher CO_2 conditions to minimize water loss (Royer, 2001; Rundgren & Beerling, 2003). More recently, models were developed to combine the use of the stomatal index, stomatal pore length, and carbon isotope ratio ($\delta^{13}C$) to refine pCO_2 estimates from fossil leaves (Franks et al., 2014; Royer et al. 2018; Konrad et al., 2021; Franks & Beerling, 2009).

Despite the usefulness of stomatal characteristics in paleoclimatic reconstruction, the method for preparing leaf cuticles to measure stomatal size and index has not been standardized. Different methods of leaf cuticle impression could potentially yield results that vary significantly. Specifically, using dried rather than fresh leaves or a fossil may result in smaller stomatal measurements due to sample desiccation and resulting shrinkage. It is important to understand what differences exist between preparation methods for such a widely applied proxy, so that error can be accounted for. I tested whether four methods of leaf cuticle preparation produce comparable stomatal trait data when applied to the same leaves from three different species. I assessed the stomatal density and index, guard cell length, guard cell width, and pore length of each sample using each of the four methods to see whether different methods yielded different results. I also tested whether such differences would be significant enough to alter mechanistic paleoclimate model estimates by comparing pCO_2 values calculated using the Franks et al. (2014) model for each method.

2.2 METHODS

2.2.1 Sample collection

Leaves from *Ginkgo biloba* (n = 16), *Zingiber mioga* (n = 28), and *Quercus alba* (n = 15) were collected from Matthaei Botanical Gardens (n=12, *G. biloba*) and the Arbor Hills neighborhood of Ann Arbor, Michigan in fall 2021 and 2022 (Fig. 2.2). These plants were chosen because of their fossil record, ease of collection access, and the original taxon specific calibrations of *G. biloba* and *Q. robur* from Franks et al. (2014) for use in their model. Additionally, these plants represent a diversity of growth forms and plant groups, as *G. biloba* is a gymnosperm tree, *Q. alba* a dicotyledonous tree, and *Z. mioga* an herbaceous monocot.

2.2.2 Stomatal analysis

Four methods were used to obtain stomatal data. (1) Nail polish. A single, thin layer of clear nail polish was applied to the abaxial surface of each leaf shortly after they were collected. The dried polish was transferred and adhered to a microscope slide using clear packing tape (Hilu and Randall, 1984). (2) Dental putty on fresh leaves (Porter et al., 2019). A cell-level impression of each leaf sample's cuticle was made using AFFINIS light body surface activated silicone-based dental putty (Coltène, Switzerland) on the abaxial surface of each leaf shortly after they were collected. Once dried, a layer of clear nail polish was applied to the putty mold and allowed to dry. The nail polish impression was then transferred and adhered to a microscope slide using clear packing tape. (3) Dental putty on dry leaves. The leaves were dried in a plant press for at least one week. Once fully dried, the process described in method 2 was repeated for each leaf. (4) Fluorescence on cleared leaves. To chemically clear each leaf, ~1 cm^2 portions from the center of leaves were digested using a 5% NaOH solution. Depending on the thickness of the leaf, this took anywhere from two days to two weeks. The leaves were then rinsed in water, bleached, rinsed again, and put through an ethanol dehydration series (50%, 70%, 100%). Samples were stained with 5% safranin-ethanol solution, washed with 70% ethanol and given a final 100% ethanol bath before they were cleared and mounted in cedarwood oil between 0.05" acetate sheets sealed using aluminum tape.

Three different 0.069 mm^2 viewpoints of each sample were imaged using a Nikon Eclipse LV100ND Microscope. Fluorescence was used for the cleared leaves, while each other sample was imaged with transmitted light. Using the cell counter plugin in ImageJ (Schneider et al., 2012), three people independently measured stomatal traits in each image [MM, Kelly D. Martin (all), Kate M. Morrison (*Ginkgo*), Katherine Harpenau (*Quercus, Zingiber*)] after first standardizing methodology by discussion and measuring three images together to ensure the same results. This allowed for the uncertainty associated with human error in cell counting and measurement to be quantified by comparing the differences between each person's measurements. For each image, we counted the number of stomata and epidermal cells to calculate *SI*, and measured the guard cell length, guard cell width, and pore length of three individual stomata using ImageJ (Fig. 1). SI and SD were calculated using the following equations:

$$[1]\ SI = 100 \times \frac{\#Stomata}{(\#Stomata + \#Epidermal\ Cells)}$$

$$[2]\ SD = \frac{\#Stomata}{area\ in\ mm^2}$$

2.2.3 Estimating c_a

Atmospheric pCO_2 (c_a) was calculated for each sample using the Franks et al. (2014) model and updates from Royer et al. (2019). The basis of this model is the relationship between atmospheric CO_2 concentrations and leaf CO_2 assimilation rate (Farquhar and Sharkey, 1982; von Caemmerer, 2000) shown below as equation 3:

$$[3]\ c_a = \frac{A_n}{g_{c(tot)} \cdot (1 - c_i/c_a)}$$

where A_n is the CO_2 assimilation rate by leaves (μmol m^{-2} s^{-1}), $g_{c(tot)}$ is the total operational conductance to CO_2 diffusion from the atmosphere to sites of photosynthesis within the leaf (mol m^{-2} s^{-1}), and c_i/c_a is the ratio of the leaf internal CO_2 concentration (c_i) to that of the atmosphere. For the calculations, A_n values calculated as a function of modeled c_a from Franks et al. (2014) were used. A value of 6.05 μmol m^{-2} s^{-1} calculated for *G. biloba* by Franks et al. (2014) was used for *G. biloba* and a value of 14.9 μmol m^{-2} s^{-1} calculated for *Quercus robur* by Franks et al. (2014) was used for *Q. alba* and *Z. mioga*. *Quercus robur* was the only angiosperm for which an A_n value was calculated by Franks et al., and was therefore assumed to be the closest value for *Q. alba* and *Z. mioga*. $g_{c(tot)}$ is calculated using equation 4:

$$[4]\ g_{c(tot)} = \left(\frac{1}{g_{cb}} + \frac{1}{\zeta g_{c(max)}} + \frac{1}{g_m}\right)^{-1}$$

where g_{cb} is the leaf boundary layer conductance to CO_2 (mol m^{-2} s^{-1}), g_m is the mesophyll conductance to CO_2 (mol m^{-2} s^{-1}), $g_{c(max)}$ is the maximum operational stomatal conductance to CO_2 (mol m^{-2} s^{-1}), and ζ is the fraction of the $g_{c(max)}$ at which the leaf is operating. For each species g_{cb} was assumed to be 2 mol m^{-2} s^{-1}, a value found to be typical of field conditions where with normal photosynthetic gas exchange (Collatz et al., 1991). g_m was assumed to be 0.079 mol m^{-2} s^{-1} for *G. biloba* and 0.194 mol m^{-2} s^{-1} for *Q. alba* and *Z. mioga*, based off of Franks et al.'s (2014) values for *G. biloba* and *Q. robur* respectively which were back calculated from the calculated A_n values using the empirical relationship $g_m = 0.013 \times A_n$ (Epron et al., 1995; Evans and von Caemmerer, 1996). $g_{c(max)}$ was calculated using equation 5, from Franks and Beerling (2009):

$$[5]\ g_{c(max)} = \frac{d}{v} \cdot SD \cdot a_{max} / \left(1 + \frac{\pi}{2}\sqrt{a_{max}/\pi}\right)$$

where d is the diffusivity of CO_2 in air, v is the molar volume of air, and a_{max} is the maximum stomatal aperture, approximated as a fraction β of a circle with diameter equal to stomatal pore length (p), or $a_{max}= \beta(\pi p^2/2)$. Values for d and v were calculated based on equations 6 and 7 (Marrero and Mason, 1972; Royer et al., 2018), with equation 7 based on ideal gas principles:

$$[6]\ d = 1.87 \times 10^{-10} (\frac{T^{2.072}}{P})$$

$$[7]\ v = v_{STP} (\frac{T}{T_{STP}})(\frac{P}{P_{STP}})$$

where T is leaf temperature (K), P is atmospheric pressure (assumed to be 1 atm), T_{STP} is 273.15 K, P_{STP} is 1 atmosphere, and v_{STP} is the molar volume of air at T_{STP} and P_{STP} (0.022414 m^3 mol^{-1}). T used to calculate d and v was assumed to be 292.15 K, based on a mean temperature of 19°C for May through September in Ann Arbor, MI (PRISM, 2022). *SD* was determined using measured values from each leaf sample calculated using equation 2. Two methods were used to determine p, one using direct measurements of pore lengths for each sample and one using the approximate geometric relationship between guard cell length and pore length (p/L) described in Franks et al. (2014) supplementary material. For the latter method, p/L was assumed to be 0.25 for *G. biloba*, 0.3 for *Q. alba*, and 0.6 for *Z. mioga* based on the plant type and stomata size (Franks et al., 2014). The Franks et al. (2014) approximate geometric relationships for β were used for both using the measured and approximated pore length again based on plant type and stomata size. This was 0.6 for *G. biloba*, 1.0 for *Q. alba*, and 0.4 for *Z. mioga*.

The theoretical relationship relating average c_i/c_a to carbon isotope discrimination from the air by a plant (Δ_{leaf}) described in Farquhar et al. (1982) was used to determine c_i/c_a:

$$[8]\ c_i/c_a = [\frac{\Delta_{leaf} - a}{b - a}]$$

where a is the carbon isotope fractionation due to diffusion of CO_2 in air (4.4‰) (Farquhar et al., 1982), b is carbon isotope fractionation due to the carboxylation of ribulose bisphosphate (RuBP) (assumed to be 27–30‰) (Roeske and O'Leary, 1984), and Δ_{leaf} (‰) was determined using the relationship described in Farquhar and Richards (1984):

$$[9]\ \Delta_{leaf} = \frac{\delta^{13}C_{air} - \delta^{13}C_{leaf}}{1 + \delta^{13}C_{leaf}/1000}$$

Each leaf was ground up and a 0.8 mg aliquot was combusted via Elemental Analyzer and analyzed in a MAT 253 Gas Isotope Ratio Mass Spectrometer for its $\delta^{13}C_{leaf}$ values at the Stable

Isotope and Organic Molecular Laboratory at University of Connecticut. These values, and the $\delta^{13}C_{air}$ of -8.6675‰ at the time of collection (Keeling et al., 2001), were used to calculate Δ_{leaf}.

2.3 RESULTS

The size, shape, arrangement, and overall appearance of the stomata and guard cells of each of the three species are each quite distinct (Fig. 2.2). The results of the measurements of *SD*, *SI*, guard cell length, pore length, and guard cell width are displayed in Fig. 2.3. If there were no difference between any two methods, results will theoretically follow a 1:1 line. Points that fall below above the 1:1 line show the method on the y-axis underestimated the value compared to the x-axis, while points above the line overestimated the value.

2.3.1 Fluorescence

Compared to the other methods, fluorescence showed the smallest range in values for guard cell length, pore length, and guard cell width in all species (Fig. 2.3). However, this was not the case for *SD* and *SI*, and in *Z. mioga* fluorescence actually showed the largest range in these measurements. In *G. biloba*, fluorescence showed markedly larger guard cell lengths and guard cell widths than all other methods, with no overlap in their ranges (Fig. 2.3). The guard cell length of fluorescence in *Q. alba* was also larger than the other three methods, although not to such an extreme degree as there was some overlap in their ranges (Fig. 2.3).

2.3.2 Polish

The polish tended to underestimate *SD* compared to fluorescence in *G. biloba*, while it tended to overestimate them in *Q. alba* (Fig. 2.3). Stomatal density measured on polish was not skewed in either direction compared to fluorescence in *Z. mioga* (Fig. 2.3). Stomatal index was mostly overestimated by polish compared to fluorescence in *G. biloba* but was not consistently over or underestimated in *Q. alba* and *Z. mioga* (Fig. 2.3). In both *G. biloba* and *Q. alba*, polish underestimated guard cell length compared to fluorescence, while it was mostly overestimated compared to fluorescence in *Z. mioga* (Fig. 3). Polish tended to overestimate pore length in *Q. alba* and *Z. mioga* compared to fluorescence, while this was not shown in *G. biloba* (Fig. 2.3). Guard cell width was mostly overestimated by polish compared to fluorescence for *Q. alba*, while it was underestimated for *G. biloba* and there was no consistent effect in *Z. mioga* (Fig. 2.3). In *Z. mioga*, polish pore length measurements were larger and showed no overlap with fluorescence (Fig. 2.3). In contrast, guard cell length and guard cell widths in *G. biloba* were smaller and showed no overlap with fluorescence measurements (Fig. 2.3).

2.3.3 Putty on Dried Leaves

Putty on dried leaves tended to underestimate *SD* and overestimate *SI* compared to fluorescence in *G. biloba*, although this was less uniform in *Q. alba* and *Z. mioga* (Fig 2.3). Putty on dried leaves also mostly underestimated guard cell length compared to fluorescence in all three species (Fig. 2.3). Pore length was mostly overestimated by putty on dried leaves compared to fluorescence in *Q. alba* and *Z. mioga*, while no consistent effect was shown in *G. biloba* (Fig. 2.3). Guard cell width was underestimated compared to fluorescence in *G. biloba*, while *Q. alba* and *Z. mioga* showed no consistent effects (Fig. 2.3). There was no overlap between measured ranges of guard cell length and guard cell width in putty on dried leaves and fluorescence for *G. biloba* (Fig. 2.3).

2.3.4 Putty on Fresh Leaves

Putty on fresh leaves underestimated *SI* and overestimated *SD* compared to fluorescence in *G. biloba*, while in *Q. alba* both *SI* and *SD* were underestimated compared to fluorescence (Fig. 2.3). The results for *Z. mioga* showed less significant difference between methods for *SD* and *SI* (Fig. 2.3). Guard cell length, pore length, and guard cell width were all underestimated by putty on fresh leaves compared to fluorescence in *G. biloba* (Fig. 2.3). Guard cell length was underestimated by putty on fresh leaves compared to fluorescence in *Q. alba*, while pore length and guard cell width were overestimated (Fig. 2.3). Pore length and guard cell width from putty on fresh leaves were overestimated in *Z. mioga* compared to fluorescence, while guard cell length did not show a similar effect (Fig. 2.3).

2.3.5 Calculated c_a

In every case, calculating c_a using the measured pore length rather than estimating it as a fraction of guard cell length resulted in the actual c_a of 416.45 ppm falling within the range of calculated values (Fig. 2.4). At the same time, using measured pore length rather than a fraction of guard cell length led to smaller ranges in c_a calculations for *G. biloba* and larger ranges for *Q. alba* and *Z. mioga* (Fig. 2.4). Estimates using guard cell length completely overestimated c_a for *G. biloba* and underestimated c_a for *Q. alba* and *Z. mioga* (Fig. 2.4).

Because the value for *b* used in equation 8 varies between values of 27 and 30‰ (Roeske and O'Leary, 1984), c_a calculations were also made using a *b* value of 30‰. When *b* is assumed to be 30‰, c_a calculations using measured pore length were always lower than the true c_a for each species (Fig. 2.4). Using guard cell length, c_a calculations were consistently higher for *G.*

biloba, except for fluorescence where values were all lower than true c_a (Fig. 2.4). True c_a was within range of *Z. mioga* calculations using guard cell length, however the mean value was always higher than true c_a (Fig. 2.4). Mean estimates for *Q. alba* were all lower than true c_a, and the true c_a was only within the range of estimated values for the two putty methods (Fig. 2.4).

2.3.5.1 Calculations using fraction of Guard Cell Length

Q. alba and *Z. mioga* had the most consistent calculated c_a values across methods, with values never exceeding the true c_a (Fig. 2.4). Estimates from *G. biloba* made using polish, putty on dry leaves, and putty on fresh leaves led to c_a estimates higher than the true value, while the mean fluorescence estimates were higher, but the real c_a was still within the range of values (Fig. 2.4). There was no clear trend in the difference between the c_a calculations for each method in *Q. alba* and *Z. mioga* (Fig. 2.4).

2.3.5.2 Calculations using Measured Pore Length

The true c_a was within the range of calculated c_a values for each species and each method using measured pore length (Fig. 2.4). Fluorescence led to mean c_a values closer to the true value than the other three methods in *G. biloba* and *Z. mioga* (Fig. 2.4). The other three methods produced higher mean c_a estimates for *G. biloba* and lower mean estimates for *Z. mioga* (Fig. 2.4). The mean c_a estimate for *Q. alba* was consistently lower than the true value (Fig. 2.4). For each method, *G. biloba* had the smallest range in estimated c_a values compared to the other species (Fig. 2.4).

2.3.6 Difference between counters

Depending on the measurement being made and the species analyzed, the differences between the values obtained by each of the three counters ranged from very small to significantly different. For each of the three species, mean stomatal density measurements were fairly consistent between counters (Fig. 2.5). Mean stomatal index measurements for *G. biloba* and *Z. mioga* were also fairly consistent between all counters, although for *Q. alba* one counter recorded higher values than the others (Fig. 2.5). Guard cell length is very well constrained between the three counters in *G. biloba*, and less so in *Z. mioga* while still showing a consistency in measurement (Fig. 2.5). However, in *Q. alba*, one counter again shows distinctly different measurements than the other two (Fig. 2.5). Mean pore length in all three species shows some degree of distinction between counters for each species while the data as a whole shows some overlap, although one counter showing more significant differences for *Z. mioga* (Fig. 2.5).

Guard cell width showed the largest differences between counters, with each counter showing almost no overlap from one another for each of the three species (Fig. 2.5).

2.4 DISCUSSION

2.4.1 Difference between methods

Fluorescence is likely the most accurate of the four methods for examining stomatal characteristics because it uses the actual leaf rather than an impression of the cuticle. Applying fluorescent light to cleared leaves allows for cell layers beyond the outermost cuticle to be examined at different magnification. It also allows for greater visibility into the entire structure of stomata beyond this outermost cell layer. In contrast, the other three methods record an impression of only the outermost layer of the leaf cuticle, and in the case of the putty molds an impression of an impression. Smaller guard cell lengths were measured from each method compared to fluorescence in *G. biloba* and *Q. alba*, as were guard cell widths in *G. biloba*. In contrast, pore length measurements were less sensitive to each method in either species. Given that guard cell length and guard cell width are both measurements of the edges of stomata and pore length is not, the impressions are likely not capturing complete stomatal anatomy and are thus more sensitive to methodological differences. *Ginkgo biloba* has sunken stomata and overarching papillae (Grey et al., 2020), which would explain the inability of impressions to represent complete stomata. While *Q. alba* do not have sunken stomata, their stomata are much smaller overall and likely more sensitive to differences in method, explaining the slightly smaller values in guard cell length. This suggests that fluorescence is a more accurate method of examining stomatal traits in these species, as it captures a more complete view of the stomata regardless of stomatal morphology. Scanning electron microscopy (SEM) of leaf cuticles may be able to give further insight into how the three dimensional structure of stomata may affect measurements made using impressions (Matthaeus et al., 2020).

Surprisingly, using dried leaves to measure stomata rather than fresh leaves did not lead to smaller stomatal measurements as was expected due to potential shrinking from desiccation. The only significantly smaller measurements on dried leaves were of guard cell length and guard cell width in *G. biloba* and of pore length in *Q. alba*, however these values were similarly lower for the other impression methods on fresh leaves. This means the stomata are either undergoing similar shrinkage effects from being pressed and dried as they are from being removed from the plant or that this is a result of the impressions themselves. While *Z. mioga* did also appear to show slightly smaller guard cell length in dried leaves but not fresh leaf impressions, pore length and guard cell width were actually larger for all three methods. This again does not support a shrinking of stomata due to desiccation.

2.4.2 Effects on c_a calculations

While individual stomatal measurements could be quite sensitive to differences between the methods, c_a was less sensitive to these differences, especially for measured pore length. Only the fluorescence method for *G. biloba* was able to predict c_a values within range of the true value using guard cell length, while the true c_a was within the predicted range of each method for each species using measure pore length. This shows that using measured pore length, rather than estimating it as a fraction of guard cell length is the best method for calculating c_a. Using measured pore length led to accurate estimations of c_a in all three species, with the smallest range in estimated values for *G. biloba*, one of the plants the Franks et al. model is most commonly applied to. This was to be expected as the model is more accurately calibrated to *G. biloba* than *Q. alba* or *Z. mioga*. The results of the c_a calculations also support fluorescence being the most accurate of the four methods, as it produced mean c_a estimates closest to the true value for *G. biloba* and *Z. mioga*. It may be reasonably assumed that when using any of the other three methods, *G. biloba* would overestimate c_a values while *Q. alba* and *Z. mioga* underestimate them.

The results also show the importance of b in calculation of c_a, as a three per mil difference in this value led to significantly different ranges in calculated c_a values for each method and species. The degree to which carboxylation of RuBP fractionates ^{13}C in each species should be directly measured in extant species or the most closely related extant species for the most accurate results. Furthermore, incorporating other variables such as fractionation due to photorespiration and the CO_2 compensation point in the absence of dark respiration may lead to higher c_a estimates closer to the true value (Royer et al., 2018). Similarly, better refining values for A_n, g_m, β, and T based on these specific taxa may lead to more accurate c_a estimates, and further study of these for each taxa is recommended. The results of both methods reinforce the importance of using as many leaves as possible when estimating c_a using the Franks et al. (2014) model, as leaves growing under the same atmospheric conditions generated ranges sometimes close to 400 ppm using estimated pore length (441–810 for *G. biloba* using putty on dried leaves with b = 27) and in excess of 200 ppm using measured pore length (256–513 ppm for *Q. alba* using fluorescence with b = 27).

Ginkgo is one of the most widely used plants used as a paleo-CO_2 barometer because of the similarity of modern *G. biloba* to the fossil *G. adiantoides* (Tralau, 1968; Royer et al., 2003; Barclay and Wing, 2016). Given that it is so widely used, it is especially important to understand how measurements of *Ginkgo*'s stomata are affected by differences in cuticle preparation method. Of the 16 combinations of cuticle preparation method, means of measuring pore length, and b value, only four yielded accurate c_a calculations. This highlights the need to standardize the results of *Ginkgo* paleo-CO_2 barometry studies using different methods of cuticle preparation. Based on the results of this study, I recommend fluorescence be used and pore length measurements be made directly on the pores rather than as a fraction of guard cell length. Our results also point to a need to measure the actual fractionation of ^{13}C based on the carboxylation of RuBP specific to *Ginkgo*.

2.4.3 Difference between counters

It is evidently very important that those making measurements of stomata are familiar with stomatal morphology and the variation it can have across taxa. Guard cell width measurements from each counter were entirely distinct from each other with no overlap in *G. biloba* or *Z. mioga*. One counter consistently tended to under-measure guard cell width in each of the three species in every method. Similarly, one counter mostly over-measured pore length for each species compared to the others. This stresses the importance of being familiar with stomatal anatomy and using standardized measurement procedures when analyzing stomata, but also suggests that doing replicated counts by different individuals and averaging the results will likely do a better job of capturing variation than relying on a single counter. While I tried to standardize the procedure for cell counting and measurement between each person, people still interpreted the edges of guard cells and which cells to count or not count around the edges of the image differently. These two areas of inconsistency specifically should be addressed clearly when stomatal analysis is done by more than one person to make sure there is less room for personal interpretation.

Zingiber mioga had the most consistency between counters, while *Q. alba* clearly had the least. The consistency of *Z. mioga* measurements is likely due to its larger, non-sunken stomata flanked by pairs of subsidiary cells and hexagonal epidermal cells arranged in a fairly uniform, brick-like manner without subsidiary cells (Fig. 2.2). In contrast, *Q. alba* has much smaller stomata and epidermal cells arranged in a much less uniform manner (Fig. 2.2). Additionally, the leaves of *Q. alba* have denser, reticulate venation making it difficult to avoid leaf veins in images of the cuticle at the level of magnification used. Reexamining *Q. alba* cuticles at a higher magnification may lead to more consistent results across counters.

2.5 CONCLUSIONS

It is important to consider the method of cuticle preparation when reconstructing CO_2 using stomatal parameters, as different methods of cuticle preparation yield significantly different stomatal measurements. While these differences are less pronounced on the actual c_a calculations than on the measurements themselves, it is still important to understand how these calculations may be affected by the method being used. Similarly, it is important to recognize how the effects of each method differ between taxa, as *G. biloba* and *Z. mioga* appeared to be more sensitive to differences between methods than *Q. alba*. When possible, it is recommended that fluorescence be used to make stomatal measurements and that measured pore length be used in all c_a calculations. If any of the other three methods is used, it is important to understand how that affects the c_a estimates of a given species. When pore length cannot be measured and must be estimated using guard cell length, it should be considered how this will affect c_a calculations. Further study into species specific ^{13}C fractionation due to carboxylation of RuBP may also help produce more accurate c_a calculations using stomatal measurements. Additionally, attention should be paid to how measurements are being made when more than one person is involved in making stomatal measurements and procedure should be strictly consistent across any people making measurements.

2.6 REFERENCES

Barclay, R. S., and S. L. Wing. 2016. Improving the *Ginkgo* CO_2 barometer: Implications for the early Cenozoic atmosphere. *Earth and Planetary Science Letters* 439: 158-171.

Collatz, G. J., J. T. Ball, C. Grivet, and J. A. Berry. 1991. Physiological and environmental regulation of stomatal conductance, photosynthesis and transpiration: a model that includes a laminar boundary layer. *Agricultural and Forest Meteorology* 54: 107–136.

Epron, D., D. Godard, G. Cornic, and B. Genty. 1995. Limitation of net CO_2 assimilation rate by internal resistances to CO_2 transfer in the leaves of two tree species (*Fagus sylvatica* L. and *Castanea sativa* Mill.). *Plant, Cell & Environment* 18: 43–51.

Evans, J. R., and S. Von Caemmerer. 1996. Carbon Dioxide Diffusion inside Leaves. *Plant Physiology* 110: 339–346.

Farquhar, G. D., and T. D. Sharkey. 1982. Stomatal Conductance and Photosynthesis. *Annual Review of Plant Physiology* 33: 317–345.

Farquhar, G., and R. Richards. 1984. Isotopic Composition of Plant Carbon Correlates With Water-Use Efficiency of Wheat Genotypes. *Functional Plant Biology* 11: 539.

Franks, P. J., and D. J. Beerling. 2009. Maximum leaf conductance driven by CO2 effects on stomatal size and density over geologic time. *Proceedings of the National Academy of Sciences* 106: 10343–10347.

Franks, P. J., D. L. Royer, D. J. Beerling, P. K. Van de Water, D. J. Cantrill, M. M. Barbour, and J. A. Berry. 2014. New constraints on atmospheric CO2 concentration for the Phanerozoic. *Geophysical Research Letters* 41: 4685–4694.

Gray, A., L. Liu, and M. Facette. 2020. Flanking Support: How Subsidiary Cells Contribute to Stomatal Form and Function. *Frontiers in Plant Science* 11.

Hilu, K. W., and Randall, J. L. 1984. Convenient method for studying grass leaf epidermis. *Taxon* 33: 413–415.

Keeling, C. D., S. C. Piper, R. B. Bacastow, M. Wahlen, T. P. Whorf, M. Heimann, and H. A. Meijer, 2001. Exchanges of atmospheric CO_2 and $^{13}CO_2$ with the terrestrial biosphere and oceans from 1978 to 2000. Global aspects, SIO Reference Series, No. 01-06, Scripps Institute of Oceanography, San Diego, California, USA.

Konrad, W., D. L. Royer, P. J. Franks, and A. Roth-Nebelsick. 2021. Quantitative critique of leaf-based paleo-CO2 proxies: Consequences for their reliability and applicability. *Geological Journal* 56: 886–902.

Marrero, T. R., and E. A. Mason. 2009. Gaseous Diffusion Coefficients. *Journal of Physical and Chemical Reference Data* 1: 3–118.

Matthaeus, W. J., J. Schmidt, J. D. White, and B. Zechmann. 2020. Novel perspectives on stomatal impressions: Rapid and non-invasive surface characterization of plant leaves by scanning electron microscopy. *PLOS ONE* 15: e0238589.

McElwain, J. C. 2018. Paleobotany and Global Change: Important Lessons for Species to Biomes from Vegetation Responses to Past Global Change. *Annual Review of Plant Biology* 69: 761–787.

McElwain, J. C., and W. G. Chaloner. 1995. Stomatal Density and Index of Fossil Plants Track Atmospheric Carbon Dioxide in the Palaeozoic. *Annals of Botany* 76: 389–395.

McElwain, J. C., and M. Steinthorsdottir. 2017. Paleoecology, Ploidy, Paleoatmospheric Composition, and Developmental Biology: A Review of the Multiple Uses of Fossil Stomata. *Plant Physiology* 174: 650–664.

Porter, A. S., C. Evans-FitzGerald, C. Yiotis, I. P. Montañez., and J. C. McElwain. 2019. Testing the accuracy of new paleoatmospheric CO_2 proxies based on plant stable carbon isotopic composition and stomatal traits in a range of simulated paleoatmospheric O_2:CO_2 ratios. *Geochimica et Cosmochimica Acta* 259: 69–90.

PRISM Climate Group, Oregon State University. 2020. PRISM Climate Data. Website https://prism.oregonstate.edu [accessed 2022].

Roeske, C. A., and H. O'Leary. 1984. Carbon isotope effects on the enzyme-catalyzed carboxylation of ribulose bisphosphate. *Biochemistry* 23: 6275–6284.

Royer, D. L. 2001. Stomatal density and stomatal index as indicators of paleoatmospheric CO2 concentration. *Review of Palaeobotany and Palynology* 114: 1–28.

Royer, D. L., L. J. Hickey, and S. L. Wing. 2003. Ecological conservatism in the "living fossil" *Ginkgo*. *Paleobiology* 29: 84-104.

Royer, D. L., K. M. Moynihan, M. L. McKee, L. Londoño, and P. J. Franks. 2018. Sensitivity of a leaf gas-exchange model for estimating paleoatmospheric CO_2 concentration. *Climate of the Past* 15: 795–809.

Rundgren, M., and D. Beerling. 2003. Fossil leaves: Effective bioindicators of ancient CO_2 levels? *Geochemistry, Geophysics, Geosystems* 4.

Schneider, C. A., W. S. Rasband, and K. W. Eliceiri. 2012. NIH Image to ImageJ: 25 years of image analysis. *Nature Methods* 9: 671–675.

Tralau, H. 1968. Evolutionary trends in the genus *Ginkgo*. *Lethaia* 1: 63-101. von Caemmerer, S. 2000. Biochemical Models of Leaf Photosynthesis. Csiro, Collingwood, Australia.

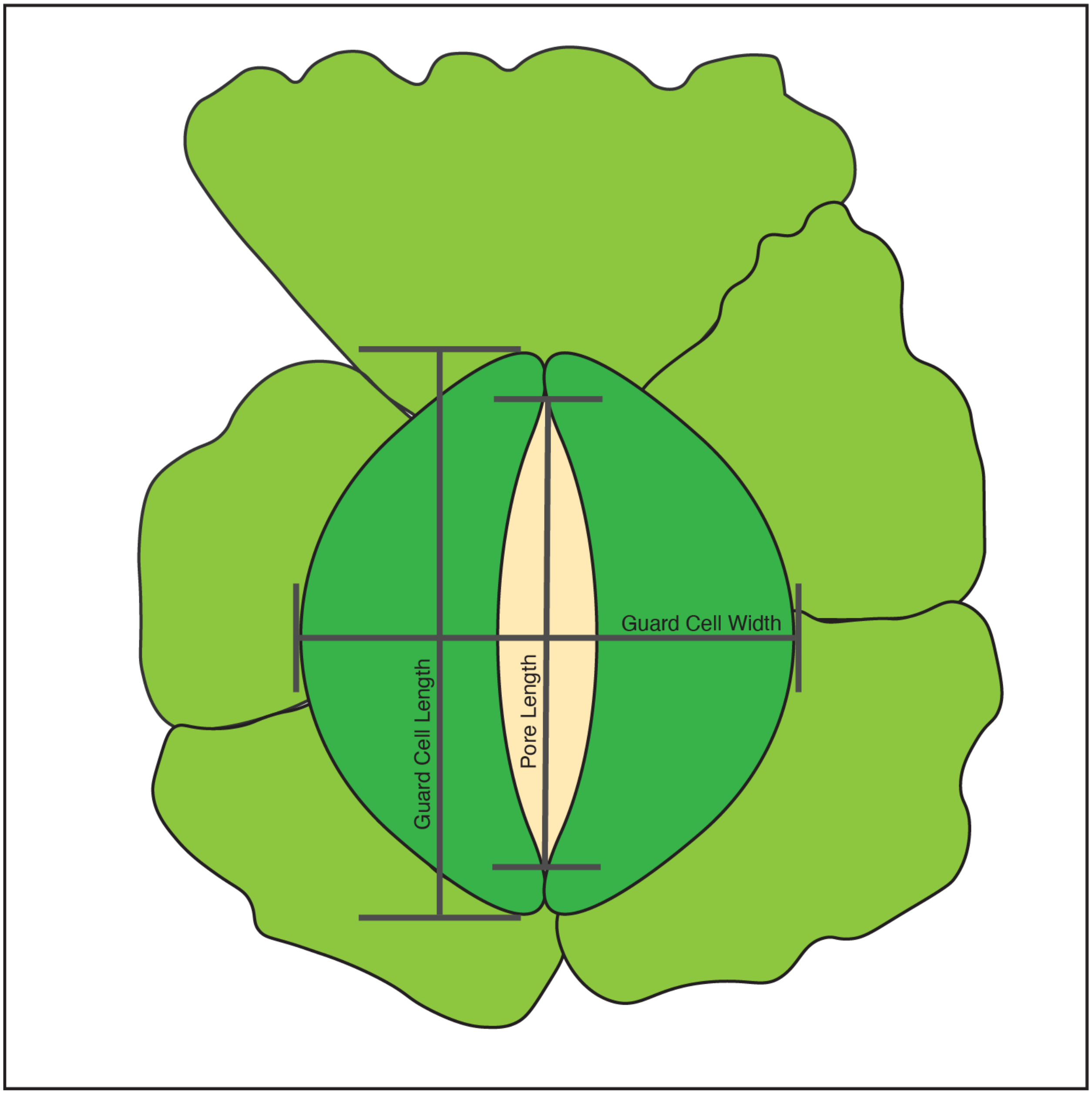

Fig. 2.1: Diagram showing a stoma (beige) and guard cells (darker green) and five subsidiary cells (lighter green) and the three stomatal measurements taken (gray lines).

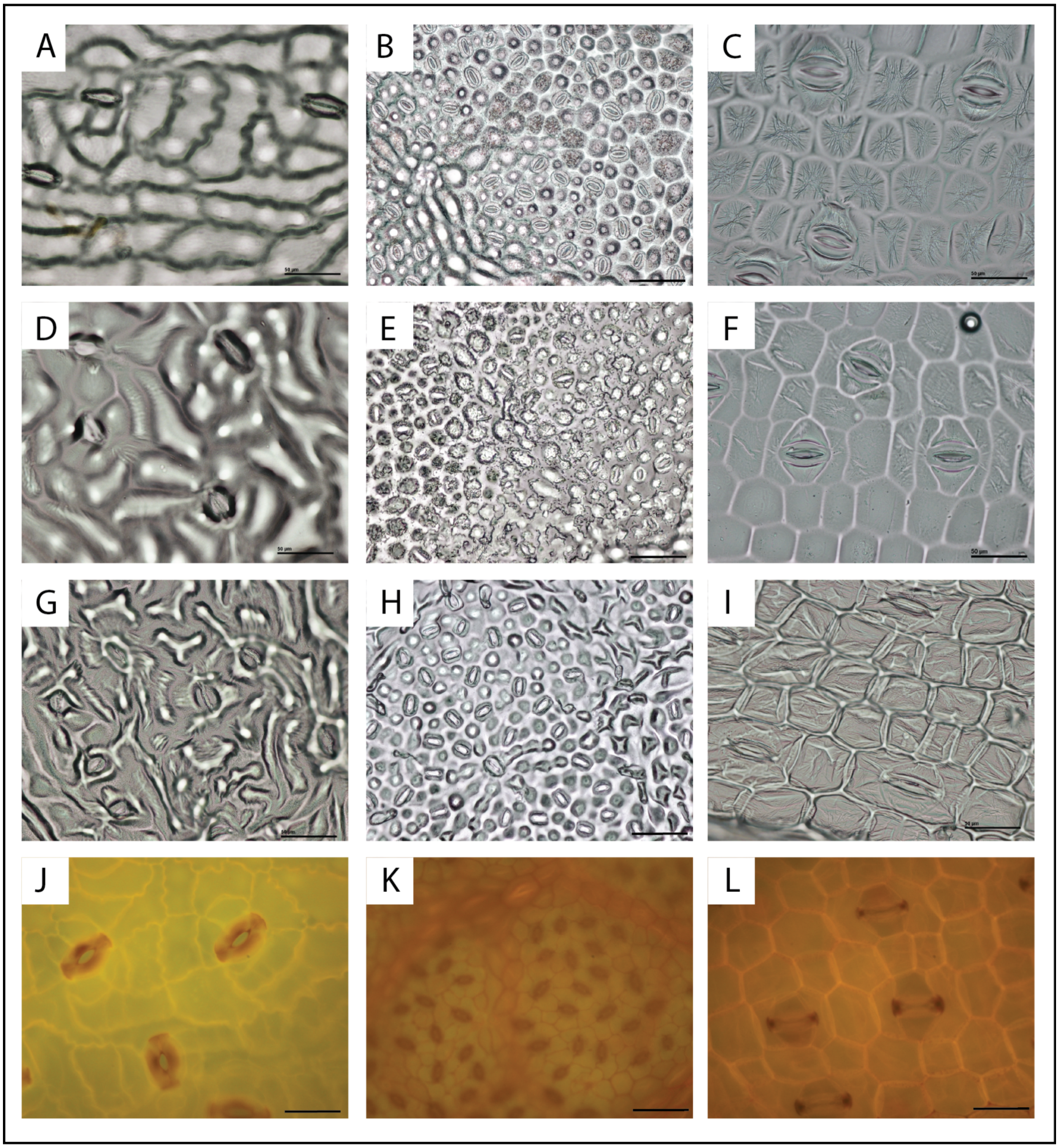

Fig. 2.2: Images of leaf cuticles of each species prepared using each method. A,D, G, J: *Ginkgo biloba;* B, E, H, K: *Quercus alba*; C, F, I, L: *Zingiber mioga.* A–C, Polish. D–F, putty on fresh leaves G–I, putty on dried leaves. J–L, fluorescence on cleared leaves.. Scale bars are 50 µm.

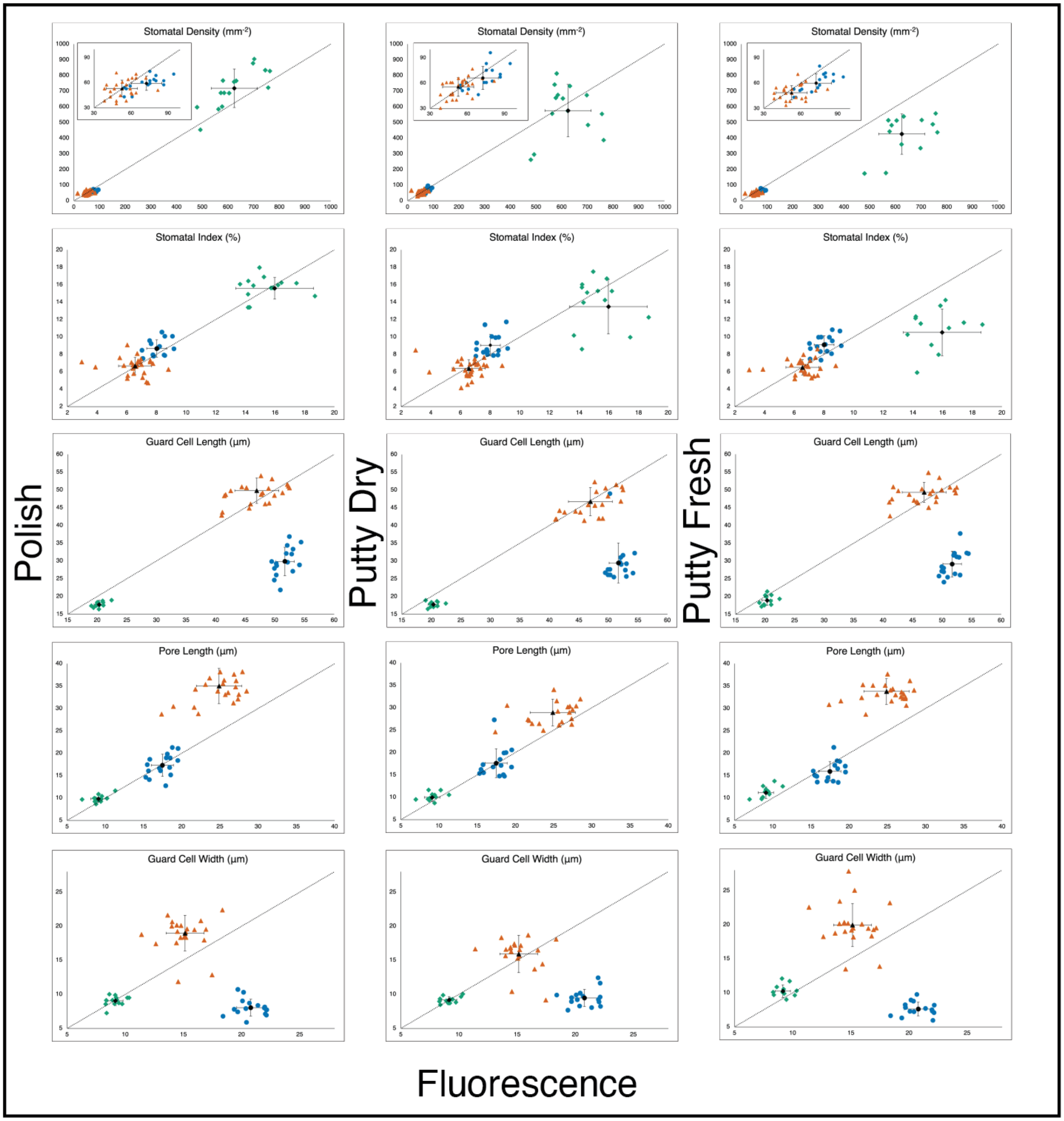

Fig. 2.3: Comparisons of difference between polish, putty on dried leaves, and putty on fresh leaves and fluorescence on stomatal density, stomatal index, guard cell length, pore length, and guard cell width measurements. *G. biloba* represented by blue circles; *Q. alba*, green diamonds; *Z. mioga*, orange triangles. Black symbols represent mean for each species, with error bars showing one standard deviation. Dotted line showing theoretical 1:1 relationship.

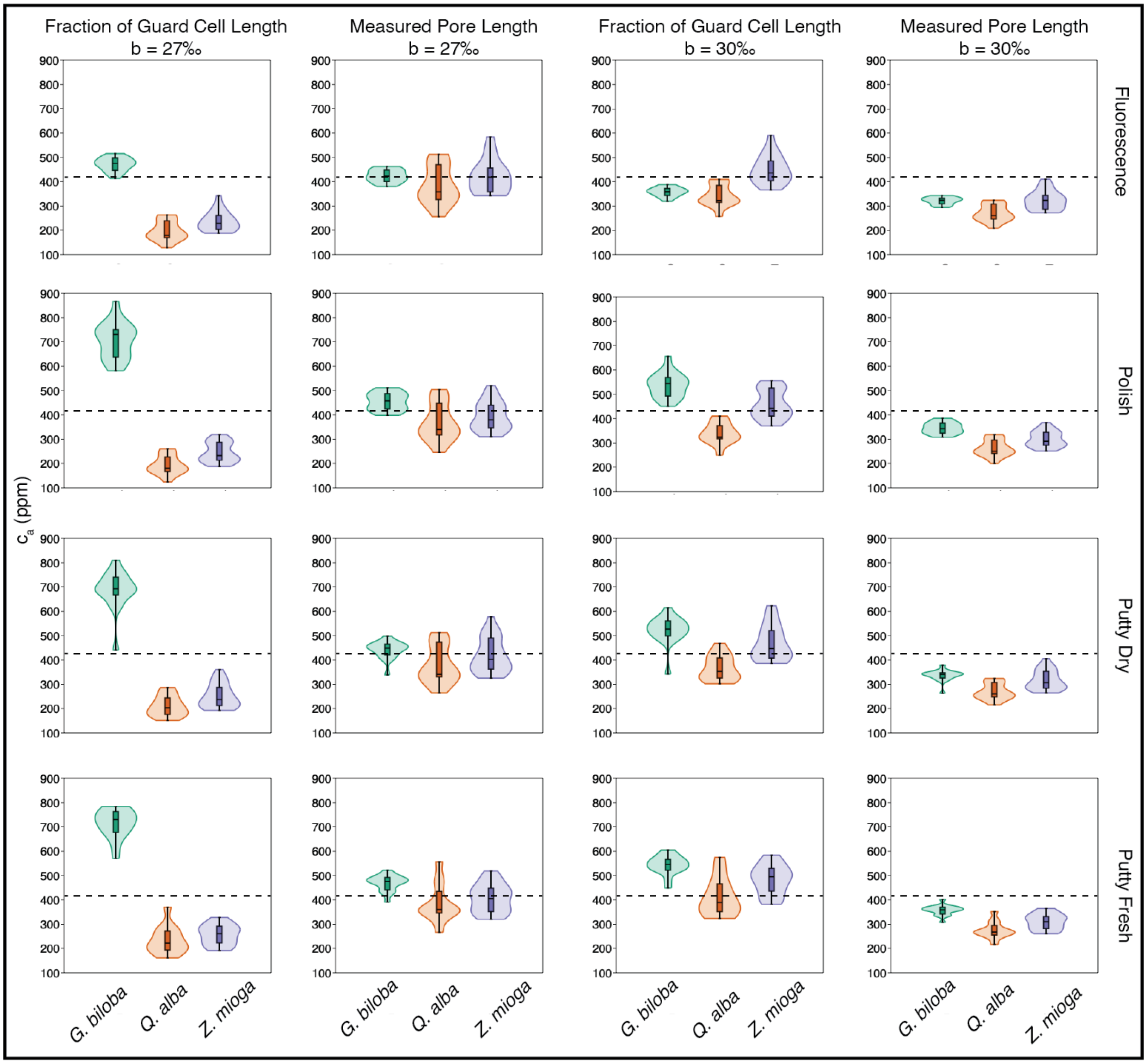

Fig. 2.4: Calculated c_a values for each species using each cuticle preparation method, both measured and estimated pore length, and b values of both 27 and 30‰. Dashed line represents the actual c_a value of 416.45 ppm.

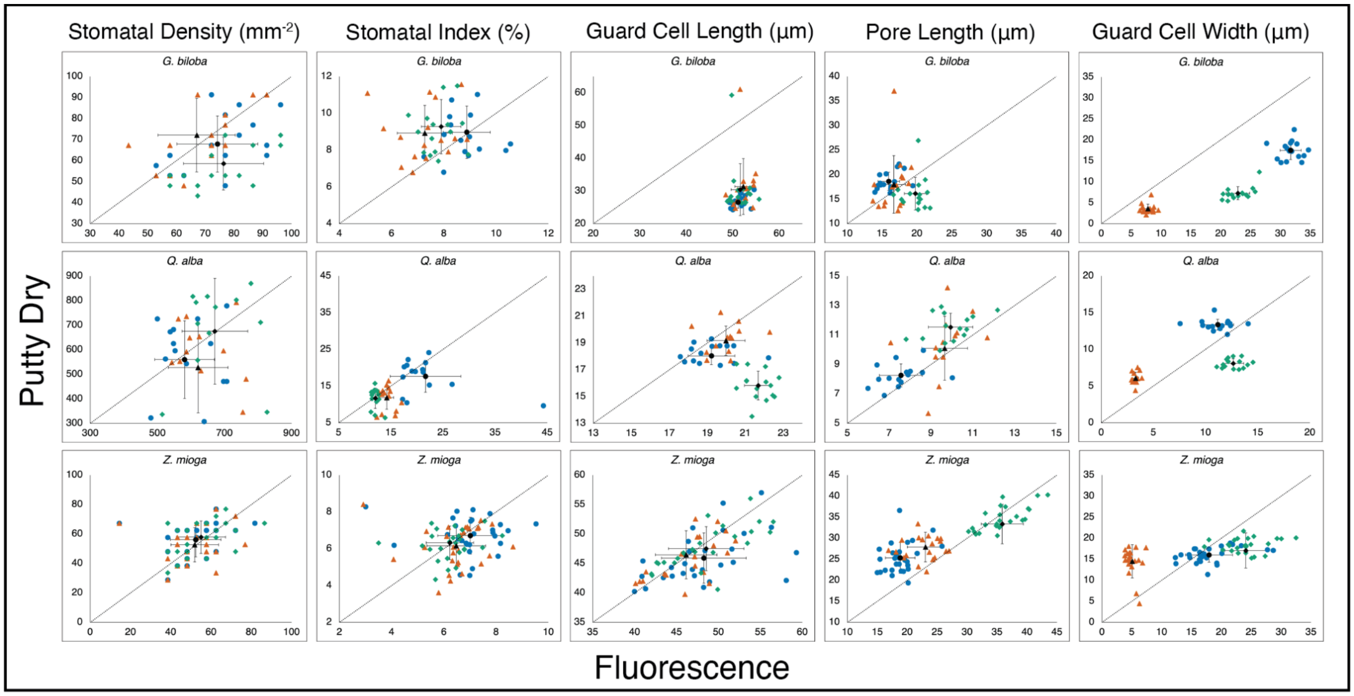

Fig. 2.5: Differences between three counters measured values for stomatal density, stomatal index, guard cell length, pore length, and guard cell width for putty on dried leaves and fluorescence. Counter one's measurements are represented by blue circles; counter two, green diamonds; counter three, orange triangles. Black symbols represent mean for each species, with error bars showing one standard deviation. Dotted line showing theoretical 1:1 relationship.

3. Insights into climate reconstruction from palm leaf traits[2]

ABSTRACT

Plants and plant fossils are important to (paleo)-climatology because they interact directly with the atmosphere through their leaves via the processes of photosynthesis and transpiration. Physiological models have been developed that use measurements of leaf $\delta^{13}C$ and stomatal traits to calculate theoretical leaf-gas exchange as paleo-CO_2 proxies and these are widely used in some plants, like *Ginkgo*, but precise relationships in other groups have not been investigated as thoroughly. Palms (Arecaceae) are of particular interest because of their cosmopolitan low- to mid-latitude distribution, good fossil record, and utility as indicators of (sub)-tropical climatic conditions. I measured a number of morphological and chemical traits and gathered climate data for leaves of *Sabal palmetto*, *Caryota urens*, and *Phoenix dactylifera* as spatial and temporal series and combined them with data for another 98 species of palms to investigate how climate is reflected in palm leaves phylogenetically. The three focal species were tested to see whether palm leaves could accurately reconstruct atmospheric CO_2 concentrations (c_a). I found that with current parameters that while the c_a reconstructions were as precise (± ~25%) as other methods, I was not able to reconstruct c_a accurately using the leaf-gas exchange model on palm leaves. Thus, future work should focus on deriving palm-specific calibrations of non-measured variables to yield more accurate results. I found that palms show a low positive response of intrinsic water use efficiency (iWUE) over the period of Industrialization, which may indicate that they are either weakly adapting to climate change and may struggle in the near future or that levels of anthropogenic climate change thus far have not been enough to cause them stress. Finally, my results also reinforce previous studies that have shown that carbon isotope discrimination does not increase with increasing c_a, and suggests that plant carbon isotopes alone should not be used to reconstruct c_a without including stomatal traits.

3.1 INTRODUCTION

As human activity continues to drive global changes in climate, it is important to understand how Earth's climate changed in the past. Because plants are mostly stationary and interact directly with the atmosphere through photosynthesis and respiration, the fossils they

---

[2] Planned submission to Paleoceanography & Paleoclimatology as **Insights into climate reconstruction from palm leaf traits** by Mike D. Machesky, Nathan D. Sheldon, Lauren van Wagoner, Michael T. Hren, Selena Y. Smith

leave behind can be especially useful for understanding the climatic conditions under which they grew. Physiognomic models such as Climate Leaf Analysis Multivariate Program (CLAMP; Wolfe, 1993; Teodoridis et al., 2011; Yang et al., 2015), Leaf Margin Analysis (LMA; Bailey and Sinnott, 1916; Wolfe, 1979; Wolfe, 1985), and Digital Leaf Physiognomy (DiLP; Peppe et al., 2011) are tools broadly used to reconstruct climate conditions from leaves or leaf fossils. These models rely on certain measurable specific traits in plants that respond to changes in their environment, creating a record of the climate in the morphology of the plant (McElwain, 2018).

However, these models are calibrated for woody "dicot" (non-monocot angiosperm) plants, and they cannot be applied to common fossil taxa including gymnosperms and monocots. This has led to the exploration of relationships between individual plant traits intrinsic to all vascular plants including stomatal characteristics, carbon isotope ratios ($\delta^{13}C_{leaf}$) and discrimination from the atmosphere (Δ_{leaf}), and vein density measured as vein length per area (*VLA*). Stomatal index, the ratio of stomata to total epidermal cells on a leaf, has been shown to correlate negatively with atmospheric CO_2 concentrations (c_a) in taxon-dependent relationships in both modern and fossil leaves, as high stomatal density allows plants to maximize CO_2 intake in times of low atmospheric CO_2 (Royer, 2001; Rundgren & Beerling, 2003). Research has also shown significant non-linear relationships between $\delta^{13}C_{leaf}$ and mean annual precipitation (MAP) in meta-analyses of plants that use the C_3 photosynthetic pathway, whereby dryer conditions contribute to less negative Δ_{leaf} values (Diefendorf et al. 2010; Kohn, 2010), however, that relationship is not present at the species or genus level (Sheldon et al., 2020; Stein et al., 2019, 2021a), suggesting that it instead reflects an ecosystem-integrated relationship (Stein et al., 2021b). VLA has been experimentally shown to correlate with elevation and has been used to calculate mean annual temperature and pCO_2 (Uhl and Mossbruger, 1999; Blonder and Enquist, 2014). Combined study of each of these traits on the same set of leaves has the potential to refine paleoclimate reconstructions using fossil leaves. I set out to test whether combined use of plant traits will accurately reconstruct climatic conditions along both spatial and temporal gradients in palm leaves.

3.1.1 Background

Alternatives to the woody "dicot" based CLAMP, LMA, and DiLP methods include mechanistic models based on the discrimination of carbon isotopes by leaves during photosynthesis as a proxy of water use efficiency, which can be applied to any vascular plant group (Franks et al. 2014; Royer et al. 2018; Konrad et al., 2021; Franks & Beerling, 2009). These models are at their root based on the leaf carbon assimilation model laid out by Farquhar et al. (1980; 1989):

$$[1]\ A_n = g_{c(tot)} \cdot (c_a - c_i)$$

A_n is the leaf CO_2 assimilation rate (µmol $m^{-2}\ s^{-1}$), $g_{c(tot)}$ is the total operational conductance to CO_2 diffusion from the atmosphere to the site of photosynthesis (mol $m^{-2}\ s^{-1}$), and c_a and c_i are the atmospheric CO_2 concentration (ppm) and leaf intercellular CO_2 (ppm) concentration respectively. This equation can then be rearranged to calculate atmospheric CO_2 concentration (equation 2, Fig. 3.1).

$$[2]\ c_a = \frac{A_n}{g_{c(tot)} \cdot (1 - c_i/c_a)}$$

The Franks model is based on this equation, using stomatal size and density to estimate $g_{c(tot)}$, Δ_{leaf} to estimate c_i/c_a, and known c_a dependent assimilation rates of nearest living relative plants to estimate A_n (Franks et al., 2014). Studies of living flora have proven the Franks model effective at estimating atmospheric CO_2 concentrations, but presently it is best practice to use multiple species to constrain for taxon specific variation in estimates (Maxbauer et al., 2014; Londoño et al., 2018; Kowalczyk et al., 2018).

Similarly, *VLA* has also been of interest for applications in paleoclimatic reconstruction. High *VLA* is a trait unique to angiosperms and has been shown to increase a plant's leaf conductance to water vapor, driving both the dominance of angiosperms and the birth of the modern tropical rainforests following the Cretaceous-Paleogene extinction (Boyce et al., 2009; Carvalho et al., 2021). *VLA* is related to hydraulic capacity in leaves (Sack and Frole, 2006; Brodribb et al., 2007; Boyce et al., 2009), and therefore may be useful in refining $g_{c(tot)}$ estimates in the Franks model because leaf mesophyll conductance and hydraulic capacity are linked (Scoffoni et al., 2016).

3.1.2 Why palms?

The majority of paleoclimatic research using plants and plant fossils have focused on dicotyledonous plants and gymnosperms from temperate latitudes, leaving (sub)-tropical and monocotyledonous plants understudied for their potential as proxies. Palms (Arecaceae) are suitable to fill this gap because of their proliferation in tropical and subtropical environments, agricultural importance, and good fossil record dating back to the late Cretaceous (Harley, 2006;

Dransfield et al., 2008). The subfamily Coryphoideae is the best represented group of palms in the fossil record, and the most recognizable fossil leaf morphologies are akin to the modern coryphoid genera *Sabal* and *Phoenix* (Harley, 2006). *Sabal* and *Phoenix* both include species with economic, cultural, and ecological importance that can survive in variable climatic conditions (e.g., *Sabal* can be found in coastal swamps while *Phoenix* are drought tolerant), making them suitable focal groups for this study (Dransfield et al., 2008). The genus *Caryota* was chosen as an outgroup still within Coryphoideae but more distantly related to the other genera (Baker et al., 2009). These three genera are also useful in that they have confirmed or suggested fossil counterparts (Dransfield et al., 2008). Three focal species, *Sabal palmetto*, *Phoenix dactylifera*, and *Caryota urens* (Fig. 3.2) were chosen for their prevalence both in the wild and in herbarium records, their widespread distribution across a variety of low latitude climate regimes, and their confirmed or apparent relationships with fossil taxa (Dransfield et al., 2008).

3.2 METHODS

3.2.1 Sample Collection

3.2.1.1 Spatial data set

Leaf samples were collected from 149 mature *Sabal palmetto* plants across the Atlantic and Gulf coasts of the Southeastern United States in June of 2022. Each plant was photographed and its geographic coordinates were recorded before one ~10 cm leaf segment was clipped from the middle of a healthy, mature frond. The samples were labeled individually and placed in tea bags stored inside a larger plastic bag with silica gel beads (Wilkie et al., 2013). Specimens sampled were at least two meters tall and include both wild and cultivated plants in a variety of natural and urban settings. Upon returning to the lab the samples were stored in an oven at 50°C until dry. Two full voucher specimens were also collected for the University of Michigan Herbarium (MICH).

3.2.1.2 Temporal data set

To expand the geographic area, diversity of climate regimes, and species reflected in the sample set I turned to herbaria. The historic record also allows for inclusion of CO_2 concentration as an environmental variable, as the oldest sample dated back to 1864 and the range tracked Industrialization. Leaf material of *Sabal palmetto* (n = 35), *Phoenix dactylifera* (n = 25), and *Caryota urens* (n = 32) was sampled from voucher specimens at the University of

Michigan Herbarium (MICH), the herbarium at the Missouri Botanical Gardens (MO), the Wisconsin State Herbarium (WIS), the Fairchild Tropical Garden Herbarium (FTG), and the William and Lynda Steere Herbarium of the New York Botanical Gardens (NY) (Fig. 3.3). Approximately one square centimeter of tissue from the center of a leaf frond was collected.

3.2.1.3 Phylogenetic data set

An additional 102 samples from 98 other palms that had been previously analyzed for $\delta^{13}C_{leaf}$ by former student Lauren van Wagoner (undergraduate Honors Thesis, PEPPR lab, University of Michigan) were also sampled from MICH (Fig. 3.2). This sample set represents all five palm subfamilies mostly from the Americas and South and Southeast Asia. Approximately one square centimeter of tissue from the center of a leaf frond was collected.

3.2.2 Stomatal Analysis

A portion of each leaf from samples in the spatial and temporal datasets was reserved to be cleared and assessed for its morphological traits. To clear each leaf chemically, I first digested non-vein tissue using a 5% NaOH solution. Depending on the thickness of the leaf, this took anywhere from two days to two weeks. The leaves were then rinsed in water, bleached, rinsed again, and put through an ethanol dehydration series (50%, 70%, 100%). Samples were stained with 5% safranin-ethanol solution, washed with 70% ethanol and given a final 100% ethanol bath before being cleared and mounted in cedarwood oil between 0.05” acetate sheets sealed using aluminum tape.

Three different 0.069 mm^2 viewpoints (the full image size at 400x magnification) of each sample were imaged using a Nikon Eclipse LV100ND Microscope using fluorescence. For each image, the number of stomata and epidermal cells were counted to calculate *SI*, and measured the pore length of three individual stomata using ImageJ. In images where the pore was not visible, the pore length was estimated as 18 ± 2% of the guard cell length, based on the average fraction of guard cell length to pore length measured in three stomata of 45 samples where pore lengths were visible. *SI* and *SD* were calculated using the following equations:

$$[3]\ SI = 100 \times \frac{\#Stomata}{(\#Stomata + \#Epidermal\ Cells)}$$

$$[4]\ SD = \frac{\#Stomata}{area\ in\ mm^2}$$

3.2.3 Vein Density Analysis

Each cleared leaf was imaged three times using a Nikon SMZ1500 microscope. Three different 5.809 mm^2 (the full image size at 8x magnification) viewpoints of each sample were imaged. Each image was then analyzed in ImageJ (Schneider et al., 2012), using the multipoint line function to trace the lengths of the vein structure, resulting in a 1 pixel wide skeleton of the venation, measuring each segment and noting which are parallel and which are cross veins. I then calculated the total *VLA* as well as the *VLA* of only the parallel veins and only the cross veins.

3.2.4 Geochemical Analyses

A portion of each leaf was reserved for geochemical analysis. Herbarium samples were first washed in Calgon solution using an ultrasonic bath to remove any pesticide or other external residue and subsequently redried in the oven. The leaves were then ground to a powder using a mortar and pestle. Small amounts of liquid nitrogen were applied to aid in the grinding process, as palm leaf tissue is fibrous and breaks down better when brittle. Samples were then loaded into solvent-washed tin capsules, with sample sizes typically between 0.6 and 0.8 µg. I first analyzed each sample for %C and %N using a Costech ECS 4010 elemental analyzer to calculate their C:N; results were calibrated with acetanilide (71.09% C, 10.36% N) and atropine (70.56% C, 4.84% N). Replicate analyses of three samples for each of the three focal species indicate reproducibility of ± 1.34%. Samples were then isotopically analyzed using a MAT 253 Isotope Ratio Mass Spectrometer coupled to a Costech ECS 4010 elemental analyzer. Results were calibrated with IAEA standards (IAEA-CH6: sucrose, $\delta^{13}C = -10.45‰$; IAEA-600: caffeine, $\delta^{13}C = -27.77‰$) and a laboratory internal standard (acetanilide: $\delta^{13}C = -28.17‰$). Reproducibility was better than ± 0.1‰.

3.2.5 Climate data

For samples taken within the continental United States, climate data was gathered from the PRISM Climate Group 800m 1991–2020 30-year normals for monthly precipitation, monthly average temperature, and monthly average VPD to calculate mean annual averages for each variable (PRISM, 2020). Climate data for samples originating outside the continental US was gathered from WorldClim 2.1 (Fick and Hijmans, 2017) at 30s 1970–2000 30-year normals for monthly precipitation, monthly average temperature, and monthly average vapor pressure. I used these data to calculate mean annual averages, and determined VPD using the average temperature for a given month to determine saturation vapor pressure using the National Weather

Service Vapor Pressure Calculator (Brice and Hall, 2023) and subtracting the monthly average vapor pressure. WorldClim values for each variable tended to be slightly smaller for precipitation (σ = 131 mm yr^{-1}), temperature (σ = 1.31 °C), and vapor pressure (σ = 1.08 hPa) compared to PRISM based on regressions of the climate data from either source for 13 sites within the United States, but both data sets are highly correlated (slopes between 0.8 and 0.95, all r > 0.97) and have been previously shown to give compatible results (e.g., Stein et al., 2019).

3.2.6 Estimating c_a

Atmospheric pCO_2 (c_a) was also calculated for each sample using the Franks et al. (2014) model (equation 2) and updates from Royer et al. (2019). For the calculations, A_n values were assumed to be 6.13 µmol m^{-2} s^{-1} based on measurements of *P. dactylifera* made by Al-Khateeb et al. (2020). $g_{c(tot)}$ is calculated using equation 5:

$$[5]\ g_{c(tot)} = \left(\frac{1}{g_{cb}} + \frac{1}{\zeta g_{c(max)}} + \frac{1}{g_m}\right)^{-1}$$

where g_{cb} is the leaf boundary layer conductance to CO_2 (mol m^{-2} s^{-1}), g_m is the mesophyll conductance to CO_2 (mol m^{-2} s^{-1}), $g_{c(max)}$ is the maximum operational stomatal conductance to CO_2 (mol m^{-2} s^{-1}), and ζ is the fraction of the $g_{c(max)}$ at which the leaf is operating. For each species g_{cb} was assumed to be 2 mol m^{-2} s^{-1}, a value found to be typical of field conditions where with normal photosynthetic gas exchange (Collatz et al., 1991). g_m was assumed to be 0.0447 mol m^{-2} s^{-1} based on measurements of *P. dactylifera* made by Al-Khateeb et al. (2020). $g_{c(max)}$ was calculated using equation 6, from Franks and Beerling (2009):

$$[6]\ g_{c(max)} = \frac{d}{v} \cdot SD \cdot a_{max} / \left(1 + \frac{\pi}{2}\sqrt{a_{max}/\pi}\right)$$

where d is the diffusivity of CO_2 in air, v is the molar volume of air, and a_{max} is the maximum stomatal aperture, approximated as a fraction β of a circle with diameter equal to stomatal pore length (p), or $a_{max} = \beta(\pi p^2/2)$. Values for d and v were calculated based on equations 7 and 8 (Marrero and Mason, 1972; Royer et al., 2018), with equation 8 based on ideal gas principles:

$$[7]\ d = 1.87 \times 10^{-10}\left(\frac{T^{2.072}}{P}\right)$$

$$[8]\ v = v_{STP}\left(\frac{T}{T_{STP}}\right)\left(\frac{P}{P_{STP}}\right)$$

where T is leaf temperature (K), P is atmospheric pressure (assumed to be 1 atm), T_{STP} is 273.15 K, P_{STP} is 1 atmosphere, and v_{STP} is the molar volume of air at T_{STP} and P_{STP} (0.022414 m^3 mol^{-1}). T was assumed to be the MAT of the location where the sample was collected. SD was determined using measured values from each leaf sample calculated using equation 4. When possible, p was directly measured using ImageJ. In images where the pore was not visible, p was estimated as 18% of the guard cell length, based on the average fraction of guard cell length to pore length measured in three stomata of 45 samples with visible pores. The Franks et al. (2014) approximate geometric relationships for β were used for both using the measured and approximated pore length again based on plant type and stomata size, in which we assumed β to be 1. The theoretical relationship relating average c_i/c_a to carbon isotope discrimination from the air by a plant (Δ_{leaf}) described in Farquhar et al. (1982) was used to determine c_i/c_a:

$$[9]\ c_i/c_a = [\frac{\Delta_{leaf}-a}{b-a}]$$

where a is the carbon isotope fractionation due to diffusion of CO_2 in air (4.4‰) (Farquhar et al., 1982), b is carbon isotope fractionation due to the carboxylation of ribulose bisphosphate (RuBP) (assumed to be 27–30‰) (Roeske and O'Leary, 1984), and Δ_{leaf} (‰) was determined using the relationship described in Farquhar and Richards (1984):

$$[10]\ \Delta_{leaf} = \frac{\delta^{13}C_{air}-\delta^{13}C_{leaf}}{1+\delta^{13}C_{leaf}/1000}$$

The measured $\delta^{13}C$ of each leaf and $\delta^{13}C_{air}$ for the year each sample was collected (Graven et al., 2017; Keeling et al., 2001) were used to calculate Δ_{leaf}.

3.2.7 Calculating Water-Use Efficiency

The Δ_{leaf} of each sample was also used to calculate its intrinsic water-use efficiency (iWUE), a measure of the amount of carbon assimilated by a plant per unit of water respired. These calculations were made based on the equation derived in Weiwei et al. (2017):

$$[11]\ iWUE = c_a \frac{b-\Delta_{leaf}}{1.6(b-a)}$$

The c_a at the time of collection was used, and again a was assumed to be 4.4‰ and b was assumed to be between 27 and 30‰.

3.3 RESULTS

3.3.1 Chemical Traits

The range in C:N, $\delta^{13}C$, and Δ_{leaf} and mean value for each focal species and for palms as a whole is shown in Table 3.1. *Phoenix dactylifera* had the highest mean C:N as well as the largest range (Table 3.1). The mean C:N and range in values were both similarly lower in *S. palmetto* and *C. urens* (Table 3.1). The mean $\delta^{13}C$ of each species fell within the expected range of C_3 plants of -37 to -20‰, and both *C. urens* and *P. dactylifera* fell entirely within this range (Fig.

3.4). Compared to *S. palmetto* and *C. urens*, *P. dactylifera* showed less negative $\delta^{13}C$ with the smallest range (Fig. 3.4). As a whole palms show a wide range of $\delta^{13}C$ across genera of over 13‰ (Fig. 3.4). The theoretical Δ_{leaf} value of 20‰ was within the range of each of the three focal species, with the mean value for *P. dactylifera* falling close to this expected value (Fig. 3.4). For both *S. palmetto* and *C. urens* the range of Δ_{leaf} values was higher than *P. dactylifera* and they were mostly discriminating against ^{13}C more (Fig. 3.4). Again, palms as a whole showed diverse distributions of Δ_{leaf}, with most showing higher discrimination than theory would suggest and a few genera showing lower (Fig. 3.4).

3.3.2 Morphological Traits

Table 3.2 summarizes the ranges and mean values for *SI*, *SD*, pore length, *VLA*, parallel *VLA*, and cross *VLA* for each of the three focal species as well as all palms included in this study. Compared to *S. palmetto* and *P. dactylifera*, *C. urens* has larger epidermal cells and stomata resulting in smaller *SD* and pore length but also smaller *SI* (Fig. 3.2, Table 3.2). The highest total *VLA* was found in *P. dactylifera*, which also showed the highest parallel *VLA* (Table. 3.2). In contrast, *S. palmetto* showed higher cross *VLA* than either of the other focal species (Table 3.2).

3.3.3 Relationships between Leaf Traits and Climate

The results of ordinary least squares regressions for each measured leaf trait against MAT, MAP, c_a, and VPD for *S. palmetto*, *C.urens*, *P. dactylifera*, and all palms are shown in Tables 3.3 through 3.10. Overall, individual traits did not show many significant relationships with climate variables for any of the three focal species or palms as a whole. There was a weak negative relationship between C:N and c_a in *C. urens* and a moderate positive correlation between C:N and VPD in *P. dactylifera* (Table 3.3). $\delta^{13}C$ had a weak negative correlation with c_a in *S. palmetto* and a weak positive correlation with MAT in *P. dactylifera* (Table 3.4). Δ_{leaf} was weakly negatively correlated with c_a in *P. dactylifera* (Table 3.5). In *S. palmetto*, *SI* was weakly negatively correlated with both MAP and c_a (Table 3.6). *SD* showed only a weak negative correlation with MAT in all palms (Table 3.7). VLA showed a weak positive correlation with c_a in *S. palmetto* and a moderate negative correlation with MAT in *P. dactylifera* (Table 3.8). This moderate negative correlation with MAT also existed in parallel and cross *VLA* for *P. dactylifera*, but parallel and cross *VLA* were not correlated with c_a in *S. palmetto* (Table 3.9, 3.10). Simple multiple regressions similarly showed a lack of significant correlation between multiple climate variables and any single leaf trait.

3.3.4 Water Use Efficiency

Each of the three focal species show weak to moderate correlations between iWUE and time over the period of Industrialization, although the relationship is not significant in *S. palmetto* (Fig. 3.5). These relationships are stronger in each species when carbon fractionation due to carboxylation of RuBP is assumed to be 30‰ rather than 27‰ (Fig. 3.5). iWUE was not correlated with *SI*, *SD*, *VLA*, or pore length in any of the three focal species.

3.3.5 Calculating c_a

The results of c_a calculations using modern *S. palmetto* leaves using assumed *b* values of both 27 and 30‰ are shown in figure 3.6A. The actual c_a value of 415.45 ppm (Keeling et al., 2001) was within the range of calculated c_a for each *b* value, although the bulk of the results were in excess of 500 ppm for each. Using a *b* of 30‰ showed a much smaller range in calculated c_a and a mean value of 616 ppm much closer to the true value than the mean of 946 ppm when b was assumed to be 27‰ (Fig. 3.6A). The results of c_a calculations for historical samples of *S. palmetto*, *C. urens*, and *P. dactylifera* are shown in Fig. 3.6B. All of the calculated values overestimated c_a compared to the actual c_a at the time of collection.

3.4 DISCUSSION

3.4.1 Leaf traits and climate

The three focal species and palms as a whole each showed large ranges in C:N. The large intraspecific ranges of many of the leaf traits is consistent with past study of palm leaf traits (Emilio et al., 2021) and with other groups of more distantly related plants such as gymnosperms (Sheldon et al., 2020). The data show that in *C. urens* there is a weak negative correlation with c_a and a lack of any correlation of C:N to with c_a in the other species. This indicates that with increasing carbon availability in the atmosphere, palms are not increasing their carbon assimilation. *Phoenix dactylifera* displays a moderate positive correlation between C:N and VPD. This may indicate that these palms are increasing their carbon assimilation in response to water stress. The wide range of C:N in palms as a whole and each of the three focal species may be due to differences in soil nutrients, which should be investigated in a future study.

The entire set of palm leaf $\delta^{13}C$ values spanned almost the entire -20 to -37‰ range for C_3 plants (Figure 3.4b; Kohn et al., 2010). Because the family Arecaceae is composed of plants that exhibit a diversity of growth forms, life histories, and climatic tolerances, it is not unreasonable that the range in $\delta^{13}C$ would be large across the family. Similarly, palms as a whole showed a large range in Δ_{leaf} of almost 16‰ (Figure 3.4a). This again likely reflects the great diversity of palms as a family and the many ecological niches they can fill. The decrease in $\delta^{13}C$ in *S. palmetto* through time and with rising c_a shows that they are tracking anthropogenic climate change, as the burning of fossil fuels increases the amount of ^{13}C depleted CO_2 in the atmosphere. However, while $\delta^{13}C$ has decreased in *S. palmetto* with rising c_a through time, they are not showing the expected increase in Δ_{leaf} associated with rising c_a (Ehleringer and Cerling, 1995; Schubert and Jahren, 2012) postulated based upon controlled atmosphere growth experiments, but not observed in previous in naturally grown plants or herbaria records (Stein et al., 2019; Sheldon et al., 2020; Stein et al., 2021a).

The lack of this response may be due to small sample sizes or might indicate that these palms, and palms more generally, are not sensitive to changes in c_a at the scale of anthropogenic climate change. This is not implausible, as the fossil record of Coryphoid palms extends to the Upper Cretaceous and diversifies across the Paleocene and Eocene (Dransfield et al., 2008), meaning palms evolved in a warmer, higher c_a world. This may also be why many palm genera, specifically the oldest lineages, tend to discriminate carbon more than theory would suggest.

It is not surprising that palm $\delta^{13}C$ and Δ_{leaf} were largely not driven by climate. Our results showing a lack of changing $\delta^{13}C$ with MAP, MAT, or VPD or of changing Δ_{leaf} with c_a are in line with previous studies of these relationships in gymnosperms (Sheldon et al., 2020; Stein et al., 2019; Stein et al., 2021a). Similarly, the lack of any significant relationships between Δ_{leaf} and climate do support the findings of Sheldon et al. (2020) that Δ_{leaf} is not correlated with MAT at the species or family level. The lack of response of Δ_{leaf} to c_a is of particular importance for its paleoclimate implications. Studies have shown an increase in Δ_{leaf} in response to increasing c_a in laboratory settings (Schubert and Jahren, 2012; Cui and Schubert, 2016) and have been used to attempt to reconstruct Cenozoic c_a (Cui et al., 2020). However, other research has shown that this relationship does not actually exist outside of the lab (Kohn, 2016; Stein et al., 2019; Sheldon et al., 2020; Stein et al., 2021a; Scher et al., 2022). Our results add to the growing list of studies that disprove the proposed relationship between Δ_{leaf} and c_a, continuing to add serious doubts to the efficacy of studies attempting to reconstruct c_a using carbon isotopes without stomatal traits.

While the other two focal species did not, *S. palmetto* exhibited negative relationships between both *SI* with c_a over time. This is significant because it indicates *S. palmetto* stomata are responding to the increase in c_a over the Industrial era in the way that other plants have shown to (Royer, 2001; Rundgren & Beerling, 2003). Similar to the lack of response in Δ_{leaf}, this may be due to palms not being sensitive to changes in c_a at the scale of anthropogenic climate change. On the other hand, it may simply indicate that at current increases in c_a and global temperatures palms are not stressed and have no need for stomatal anatomy to adapt.

While not showing relationships in all taxa, *VLA* does show a significant positive correlation with c_a in *S. palmetto* and a significant negative correlation with MAT in *P. dactylifera*. While it would make sense that under rising c_a, vein density may increase to accommodate increasing carbon assimilation rates (McElwain et al., 2016), it is puzzling that *VLA* would decrease with increasing temperature in *P. dactylifera* contrary to what past study would suggest (Uhl and Mosbrugger, 1999; Sack and Scoffoni, 2013; Blonder and Enquist, 2014). This could possibly be due to these plants reallocating more water resources into their trunks under higher temperatures, as they show lower net photosynthetic rates at higher temperatures (Arab et al., 2016), but future work on other groups would also be fruitful to determine whether the proposed relationships are specific to the groups of plants in those studies rather than universal.

3.4.2 Water use efficiency

Understanding the intrinsic water use efficiency of plant taxa is important for understanding how well they may adapt to climate change (Battipaglia et al., 2012). Our results show that with rising atmospheric CO_2 concentrations, *C. urens* and *P. dactylifera* are increasing their iWUE in taxon specific relationships. This suggests these plants are adapting to the increase in c_a and may be resilient to future climate change. However, because no significant relationships exist between iWUE and either *VLA*, *SI*, *SD*, or pore length in any of the three focal species, it is unclear what is allowing for this increase in iWUE. One possibility is that changes in leaf size are responsible for this increase in iWUE (Parkhurst and Loucks, 1972), and should be investigated in these palms. On the other hand the trend of increasing iWUE with increasing c_a in *S. palmetto* was statistically insignificant, and this suggests that either these palms are not adapting as well to increasing c_a or that they are not sensitive to c_a increases on this scale. A final possibility is that the lack of response of iWUE over time may be due to insufficient sample size, and that higher resolution sampling may yield different results. Again, the absence of the expected response in *S. palmetto* may be the result of palms having evolved in a world with much higher c_a and global temperatures making them more resilient to stress associated with the current degree of climate change. More alarmingly, this lack of response in iWUE may indicate that palms are not adapting to climate change as well as other plant groups and may at some point hit a physiological threshold where populations begin to struggle. However, there is research suggesting that palms are resilient to drought events with no change to mortality rate or biomass production and increased recruitment rate (Sousa et al., 2020). This is promising and suggests that hopefully anthropogenic climate change will not cause palms to reach a theoretical physiological threshold resulting in population decline, at least in the immediate future.

3.4.3 Calculating c_a

The results of the c_a calculations from both modern and historic samples show that palms have potential as a paleo-CO_2 barometer using the Franks et al. (2014) model, but there is a need for calibrating various model parameters for palms specifically. The overall lower c_a estimates assuming carbon fractionation due to carboxylation of RuBP value of 30‰ compared to 27‰ indicate that the b value for palms is likely closer to 30‰. Reconstructions of c_a using multiple leaves grown under the same c_a were reasonably accurate and precise, with the majority of estimates clustering around the mean of 616 ± 175 ppm with a b of 30‰. This level of precision is suitable for paleoclimatic applications, in particular for periods in the geologic past when CO_2 levels greatly exceeded modern levels (e.g., Paleogene), and is in line with most leading edge paleo-CO_2 proxies where results are accurate to 25–35% of the measure value (Franks et al., 2014; Royer et al., 2019). It is possible that this ~200 ppm offset from the true value could be improved upon and is due to the inaccuracy of the assumed values for non-measured input used in the calculations. The c_a reconstructions from the historical samples typically showed a similar, albeit less consistent, overestimation of c_a. The lack of measurements for factors such as g_{cmax}, A_n, and b in palms means that it is difficult to assume reasonable input values for these variables for different palm species. In the original paper, Franks et al. (2014) included calibrations for multiple woody gymnosperms and a woody dicot, leaving monocots notably absent from the calibrations. If I were to measure these values for each of the three focal species, I may have been able to more accurately reconstruct the c_a in which they grew. It is most important to understand taxon specific A_n, as The results additionally highlight the need for inclusion of as many fossils for analysis as possible when using the Franks et al. model on palm leaves to account for potential variation in model parameters. While the assemblage as a whole was reasonably precise, there were outliers in each case estimating extremely high values compared to the bulk of the samples. Inclusion of multiple leaf fossils for analysis where possible would help ensure c_a estimates using the Franks et al. model on palms are accurate.

3.5 CONCLUSIONS

While many of the studied palm leaf traits were not sensitive to climate, that does not mean there are no lessons to be learned from the results. As one of the older lineages of angiosperms, the lack of relationships between leaf traits and climate may simply be because palms are not sensitive to changes in climate on the scale observable in this study. At the same time, the lack of demonstrated relationship between Δ_{leaf} and c_a add to a growing number of studies suggesting the use of carbon isotopes to reconstruct c_a without stomatal traits are likely inaccurate. While the weak response of iWUE in palms to increasing atmospheric CO_2 may indicate palms are weakly adapting to climate change and may struggle in the future, it may also be because palms are not stressed by current anthropogenic climate change and have not needed to adapt. Further experimental investigation of the response of palm leaf traits to more extreme changes in climate variables may yield different results and are worth undertaking. It is also of note that palms are increasing their iWUE but not their Δ_{leaf} in response to rising c_a, bringing paleoclimate studies which attempt to reconstruct c_a using only Δ_{leaf} into question. Additionally, the results of c_a reconstructions applying the Franks et al. model to palms shows that while current inputs yield reasonably precise but inaccurate results, there is potential for much more accurate results if the model is specifically calibrated to palms species. Leaf gas exchange variables such as assimilation rate and operational stomatal conductance are understudied in non-agriculturally important palm species, and future study investigating these variables could help improve c_a reconstructions from fossil palms.

3.6 REFERENCES

Al-Khateeb, S. A., A. A. Al-Khateeb, M. N. Sattar, A. S. Mohmand, S. A. Al-Khateeb, A. A. Al-Khateeb, M. N. Sattar, and A. S. Mohmand. 2020. Induced in vitro adaptation for salt tolerance in date palm (*Phoenix dactylifera* L.) cultivar Khalas. *Biological Research* 53.

Arab, L., J. Kreuzwieser, J. Kruse, I. Zimmer, P. Ache, S. Alfarraj, K. A. S. Al-Rasheid, et al. 2016. Acclimation to heat and drought—Lessons to learn from the date palm (*Phoenix dactylifera*). *Environmental and Experimental Botany* 125: 20–30.

Bailey, I. W., and E. W. Sinnott. 1916. The Climatic Distribution of Certain Types of Angiosperm Leaves. *American Journal of Botany* 3: 24–39.

Baker, W. J., V. Savolainen, C. B. Asmussen-Lange, M. W. Chase, J. Dransfield, F. Forest, M. M. Harley, et al. 2009. Complete Generic-Level Phylogenetic Analyses of Palms (Arecaceae) with Comparisons of Supertree and Supermatrix Approaches. *Systematic Biology* 58: 240–256.

Battipaglia, G., M. Saurer, P. Cherubini, C. Calfapietra, H. R. McCarthy, R. J. Norby, and M. Francesca Cotrufo. 2013. Elevated CO_2 increases tree-level intrinsic water use efficiency: insights from carbon and oxygen isotope analyses in tree rings across three forest FACE sites. *New Phytologist* 197: 544–554.

Blonder, B., and B. J. Enquist. 2014. Inferring climate from angiosperm leaf venation networks. *The New Phytologist* 204: 116–126.

Boyce, C. K., T. J. Brodribb, T. S. Feild, and M. A. Zwieniecki. 2009. Angiosperm leaf vein evolution was physiologically and environmentally transformative. *Proceedings of the Royal Society B: Biological Sciences* 276: 1771–1776.

Brice, T., and T. Hall. 2023. National Weather Service vapor pressure calculator. Available at website https://www.weather.gov/epz/wxcalc_vaporpressure.

Carvalho, M. R., C. Jaramillo, F. de la Parra, D. Caballero-Rodríguez, F. Herrera, S. Wing, B. L. Turner, et al. 2021. Extinction at the end-Cretaceous and the origin of modern Neotropical rainforests. *Science* 372: 63–68.

Collatz, G. J., J. T. Ball, C. Grivet, and J. A. Berry. 1991. Physiological and environmental regulation of stomatal conductance, photosynthesis and transpiration: a model that includes a laminar boundary layer. *Agricultural and Forest Meteorology* 54: 107–136.

Cui, Y., and B. A. Schubert. 2016. Quantifying uncertainty of past pCO_2 determined from changes in C3 plant carbon isotope fractionation. *Geochimica et Cosmochimica Acta* 172: 127–138.

Cui, Y., B. A. Schubert, and A. H. Jahren. 2020. A 23 m.y. record of low atmospheric CO_2. *Geology* 48: 888–892.

Diefendorf, A. F., K. E. Mueller, Scott. L. Wing, P. L. Koch, and K. H. Freeman. 2010. Global patterns in leaf ^{13}C discrimination and implications for studies of past and future climate. *Proceedings of the National Academy of Sciences* 107: 5738–5743.

Dransfield, J., N. W. Uhl, C. B. Asmussen, W. J. Baker, M. M. Harley, and C. E. Lewis. Genera Palmarum - The Evolution and Classification of the Palms. Royal Botanical Gardens, Kew, London, UK.

Ehleringer, J. R., and T. E. Cerling. 1995. Atmospheric CO_2 and the ratio of intercellular to ambient CO_2 concentrations in plants. *Tree Physiology* 15: 105–111.

Emilio, T., H. Pereira, and F. R. C. Costa. 2021. Intraspecific Variation on Palm Leaf Traits of Co-occurring Species—Does Local Hydrology Play a Role? *Frontiers in Forests and Global Change* 4.

Farquhar, G. D., S. von Caemmerer, and J. A. Berry. 1980. A biochemical model of photosynthetic CO_2 assimilation in leaves of C3 species. *Planta* 149: 78–90.

Farquhar, G. D., K. T. Hubick, A. G. Condon, and R. A. Richards. 1989. Carbon Isotope Fractionation and Plant Water-Use Efficiency. *In* P. W. Rundel, J. R. Ehleringer, and K. A. Nagy [eds.], Stable Isotopes in Ecological Research, Ecological Studies, 21–40. Springer, New York, NY.

Farquhar, G. D., and T. D. Sharkey. 1982. Stomatal Conductance and Photosynthesis. *Annual Review of Plant Physiology* 33: 317–345.

Farquhar, G., and R. Richards. 1984. Isotopic Composition of Plant Carbon Correlates With Water-Use Efficiency of Wheat Genotypes. *Functional Plant Biology* 11: 539.

Fick, S. E., and R. J. Hijmans. 2017. WorldClim 2: new 1-km spatial resolution climate surfaces for global land areas. *International Journal of Climatology* 37: 4302–4315.

Franks, P. J., and D. J. Beerling. 2009. Maximum leaf conductance driven by CO_2 effects on stomatal size and density over geologic time. *Proceedings of the National Academy of Sciences* 106: 10343–10347.

Franks, P. J., D. L. Royer, D. J. Beerling, P. K. Van de Water, D. J. Cantrill, M. M. Barbour, and J. A. Berry. 2014. New constraints on atmospheric CO_2 concentration for the Phanerozoic. *Geophysical Research Letters* 41: 4685–4694.

Graven, H., C. E. Allison, D. M. Etheridge, S. Hammer, R. F. Keeling, I. Levin, H. A. J. Meijer, et al. 2017. Compiled records of carbon isotopes in atmospheric CO_2 for historical simulations in CMIP6. *Geoscientific Model Development* 10: 4405–4417.

Harley, M. M. 2006. A summary of fossil records for Arecaceae. *Botanical Journal of the Linnean Society* 151: 39–67.

Keeling, C. D., S. C. Piper, R. B. Bacastow, M. Wahlen, T. P. Whorf, M. Heimann, and H. A. Meijer, 2001. Exchanges of atmospheric CO_2 and $^{13}CO_2$ with the terrestrial biosphere and oceans from 1978 to 2000. Global aspects, SIO Reference Series, No. 01-06, Scripps Institute of Oceanography, San Diego, California, USA.

Kohn, M. 2016. Carbon Isotope Discrimination in C3 Land Plants is Independent of Natural Variations in pCO_2. *Geochemical Perspectives Letters*.

Kohn, M. J. 2010. Carbon isotope compositions of terrestrial C_3 plants as indicators of (paleo)ecology and (paleo)climate. *Proceedings of the National Academy of Sciences* 107: 19691–19695.

Konrad, W., D. L. Royer, P. J. Franks, and A. Roth-Nebelsick. 2021. Quantitative critique of leaf-based paleo-CO_2 proxies: Consequences for their reliability and applicability. *Geological Journal* 56: 886–902.

Kowalczyk, J. B., D. L. Royer, I. M. Miller, C. W. Anderson, D. J. Beerling, P. J. Franks, M. Grein, et al. 2018. Multiple Proxy Estimates of Atmospheric CO_2 From an Early Paleocene Rainforest. *Paleoceanography and Paleoclimatology* 33: 1427–1438.

Londoño, L., D. L. Royer, C. Jaramillo, J. Escobar, D. A. Foster, A. L. Cárdenas-Rozo, and A. Wood. 2018. Early Miocene CO_2 estimates from a Neotropical fossil leaf assemblage exceed 400 ppm. *American Journal of Botany* 105: 1929–1937.

Marrero, T. R., and E. A. Mason. 2009. Gaseous Diffusion Coefficients. *Journal of Physical and Chemical Reference Data* 1: 3–118.

Maxbauer, D. P., D. L. Royer, and B. A. LePage. 2014. High Arctic forests during the middle Eocene supported by moderate levels of atmospheric CO_2. *Geology* 42: 1027–1030.

McElwain, J. C. 2018. Paleobotany and Global Change: Important Lessons for Species to Biomes from Vegetation Responses to Past Global Change. *Annual Review of Plant Biology* 69: 761–787.

McElwain, J. C., C. Yiotis, and T. Lawson. 2016. Using modern plant trait relationships between observed and theoretical maximum stomatal conductance and vein density to examine patterns of plant macroevolution. *New Phytologist* 209: 94–103.

Parkhurst, D. F., and O. L. Loucks. 1972. Optimal Leaf Size in Relation to Environment. *Journal of Ecology* 60: 505–537.

Peppe, D. J., D. L. Royer, B. Cariglino, S. Y. Oliver, S. Newman, E. Leight, G. Enikolopov, et al. 2011. Sensitivity of leaf size and shape to climate: global patterns and paleoclimatic applications. *New Phytologist* 190: 724–739.

PRISM Climate Group, Oregon State University. 2020. PRISM Climate Data. Website https://prism.oregonstate.edu [accessed 2022].

Roeske, C. A., and M. H. O'Leary. 1984. Carbon isotope effects on enzyme-catalyzed carboxylation of ribulose bisphosphate. *Biochemistry* 23: 6275–6284.

Royer, D. L. 2001. Stomatal density and stomatal index as indicators of paleoatmospheric CO_2 concentration. *Review of Palaeobotany and Palynology* 114: 1–28.

Royer, D. L., K. M. Moynihan, M. L. McKee, L. Londoño, and P. J. Franks. 2018. Sensitivity of a leaf gas-exchange model for estimating paleoatmospheric CO_2 concentration. *Climate of the Past* 15: 795–809.

Rundgren, M., and D. Beerling. 2003. Fossil leaves: Effective bioindicators of ancient CO_2 levels? *Geochemistry, Geophysics, Geosystems* 4.

Sack, L., and C. Scoffoni. 2013. Leaf venation: structure, function, development, evolution, ecology and applications in the past, present and future. *New Phytologist* 198: 983–1000.

Scher, M. A., R. S. Barclay, A. A. Baczynski, B. A. Smith, J. Sappington, L. A. Bennett, S. Chakraborty, et al. 2022. The effect of CO_2 concentration on carbon isotope discrimination during photosynthesis in Ginkgo biloba: implications for reconstructing atmospheric CO_2 levels in the geologic past. *Geochimica et Cosmochimica Acta* 337: 82–94.

Schneider, C. A., W. S. Rasband, and K. W. Eliceiri. 2012. NIH Image to ImageJ: 25 years of image analysis. *Nature Methods* 9: 671–675.

Schubert, B. A., and A. H. Jahren. 2012. The effect of atmospheric CO_2 concentration on carbon isotope fractionation in C_3 land plants. *Geochimica et Cosmochimica Acta* 96: 29–43.

Scoffoni, C., D. S. Chatelet, J. Pasquet-kok, M. Rawls, M. J. Donoghue, E. J. Edwards, and L. Sack. 2016. Hydraulic basis for the evolution of photosynthetic productivity. *Nature Plants* 2: 1–8.

Sheldon, N. D., S. Y. Smith, R. Stein, and M. Ng. 2020. Carbon isotope ecology of gymnosperms and implications for paleoclimatic and paleoecological studies. *Global and Planetary Change* 184: 103060.

Sousa, T. R., J. Schietti, F. Coelho de Souza, A. Esquivel-Muelbert, I. O. Ribeiro, T. Emílio, P. A. C. L. Pequeno, et al. 2020. Palms and trees resist extreme drought in Amazon forests with shallow water tables. *Journal of Ecology* 108: 2070–2082.

Stein, R. A., N. D. Sheldon, and S. Smith. 2019. Rapid response to anthropogenic climate change by *Thuja occidentalis*: implications for past climate reconstructions and future climate predictions. *PeerJ* 7: e7378.

Stein, R. A., N. D. Sheldon, and S. Y. Smith. 2021a. C_3 plant carbon isotope discrimination does not respond to CO_2 concentration on decadal to centennial timescales. *New Phytologist* 229: 2576–2585.

Stein, R. A., N. D. Sheldon, and S. Y. Smith. 2021b. Soil Carbon Isotope Values and Paleoprecipitation Reconstruction. *Paleoceanography and Paleoclimatology* 36: e2020PA004158.

Teodoridis, V., P. Mazouch, R. A. Spicer, and D. Uhl. 2011. Refining CLAMP — Investigations towards improving the Climate Leaf Analysis Multivariate Program. *Palaeogeography, Palaeoclimatology, Palaeoecology* 299: 39–48.

Uhl, D., and V. Mosbrugger. 1999. Leaf venation density as a climate and environmental proxy: a critical review and new data. *Palaeogeography, Palaeoclimatology, Palaeoecology* 149: 15–26.

Weiwei, L. U., Y. U. Xinxiao, J. I. A. Guodong, L. I. Hanzhi, and L. I. U. Ziqiang. 2018. Responses of Intrinsic Water-use Efficiency and Tree Growth to Climate Change in Semi-Arid Areas of North China. *Scientific Reports* 8: 308.

Wilkie, P. 2013. The collection and storage of plant material for DNA extraction: The Teabag Method. *Gardens' Bulletin Singapore* 65.

Wolfe, J. A. 1979. Temperature parameters of humid to mesic forests of eastern Asia and relation to forests of other regions of the Northern Hemisphere and Australia. U.S. Geological Survey Professional Paper 1106. U.S. Geological Survey, Reston, Virginia, USA.

Wolfe, J. A. 1985. Distribution of major vegetational types during the Tertiary. In E. T. Sundquist, and W. S. Broecker [eds.], The carbon cycle and atmospheric CO_2: Natural variations Archean to present, 357–375. American Geophysical Union, Washington, D.C., USA.

Wolfe, J. A. 1993. A method of obtaining climatic parameters from leaf assemblages. U.S. Geological Survey Bulletin 2040. U.S. Geological Survey, Reston, Virginia, USA.

Yang, J., R. A. Spicer, T. E. V. Spicer, N. C. Arens, F. M. B. Jacques, T. Su, E. M. Kennedy, et al. 2015. Leaf form–climate relationships on the global stage: an ensemble of characters. *Global Ecology and Biogeography* 24: 1113–1125.

Table 3.1: Mean and standard deviation values for C:N, $\delta^{13}C$, and Δ_{leaf} for three focal species and palms as a whole. Minimum and maximum values are in parentheses.

Species	C:N	$\delta^{13}C$ (‰)	Δ_{leaf} (‰)
S. palmetto	27.8 ± 6.99 (12.7, 56.6)	-29.81 ± 1.59 (-33.61, -23.94)	21.9 ± 1.51 (17.5, 26.0)
C. urens	29.6 ± 12.9 (11.6, 54.3)	-28.81 ± 1.86 (-32.23, -25.48)	21.8 ± 2.52 (18.0, 25.6)
P. dactylifera	30.2 ± 15.2 (15.6, 68.2)	-26.40 ± 0.941 (-28.20, -25.36)	20.0 ± 1.08 (18.6, 22.0)
All Palms	28.2 ± 8.72 (11.6, 68.2)	-29.32 ± 2.25 (-36.78, -23.10)	22.1 ± 2.31 (16.5, 31.2)

Table 3.2: Mean and standard deviation values for SI, SD, pore length, VLA, parallel VLA, and cross VLA for three focal species and palms as a whole. Minimum and maximum values are in parentheses.

Species	SI (%)	SD (mm^{-2})	Pore Length (μm)	VLA (mm/mm^2)	Parallel VLA (mm/mm^2)	Cross VLA (mm/mm^2)
S. palmetto	11.0 ± 2.66 (6.87–21.5)	637 ± 108 (306–981)	2.76 ± 0.472 (0.582–4.21)	4.753 ± 0.9890 (2.339–6.758)	4.337 ± 1.106 (1.310–6.465)	0.5764 ± 0.3428 (0.1374–1.738)
C. urens	7.71 ± 2.52 (5.04–13.5)	93.1 ± 43.5 (48.1–226)	19.6 ± 7.81 (4.61–34.9)	4.974 ± 1.015 (3.657–8.415)	4.667 ± 1.020 (3.308–8.142)	0.3068 ± 0.08376 (0.1495–0.4894)
P. dactylifera	10.6 ± 4.59 (2.96–16.9)	339 ± 105 (122–497)	3.35 ± 0.358 (2.78–3.82)	6.152 ± 1.571 (4.326–9.662)	5.847 ± 1.522 (4.118–9.311)	0.3049 ± 0.1082 (0.2077–0.5434)
All Palms	10.5 ± 3.00 (2.96–21.5)	534 ± 220 (48.1–981)	4.70 ± 5.95 (0.582–34.9)	4.994 ± 1.354 (2.216–11.31)	4.586 ± 1.353 (1.310–10.08)	0.5536 ± 0.3289 (0.1374–1.738)

Table 3.3: Results of ordinary least squares regressions of C:N against MAT, MAP, c_a, and VPD for *S. palmetto*, *C. urens*, *P. dactylifera*, and all palms. Relationships with a significant R^2 and *p*-value are indicated by *.

Species	Variable	Slope	Intercept	R^2	*p*
Sabal palmetto	MAT	-0.5688	39.651	0.0285	0.025977
Sabal palmetto	MAP	-0.0044	34.08	0.0078	0.2467
Sabal palmetto	c_a	-0.0828	52.459	0.1172	0.86906
Sabal palmetto	VPD	0.013	27.731	0.000006	0.97341
Caryota urens	MAT	-0.9375	50.947	0.0351	0.33014
Caryota urens	MAP	-0.0033	35.076	0.0431	0.27972

Caryota urens	c_a	-0.1894	96.622	0.1843*	0.022621*
Caryota urens	VPD	1.3876	20.236	0.0318	0.35455
Phoenix dactylifera	MAT	1.6114	-8.7511	0.0516	0.41575
Phoenix dactylifera	MAP	-0.0079	39.027	0.0944	0.26527
Phoenix dactylifera	c_a	0.4314	-103.05	0.261	0.051635
Phoenix dactylifera	VPD	2.3411	9.3502	0.413*	0.0097676*
All Palms	MAT	-0.2573	33.702	0.0049	0.30128
All Palms	MAP	-0.0038	33.698	0.0263	0.0165
All Palms	c_a	-0.0806	55.083	0.0526	0.05811
All Palms	VPD	0.9557	20.776	0.0386	0.0035788

Table 3.4: Results of ordinary least squares regressions of $\delta^{13}C$ against MAT, MAP, c_a, and VPD for *S. palmetto*, *C. urens*, *P. dactylifera*, and all palms. Relationships with a significant R^2 and *p*-value are indicated by *.

Species	Variable	Slope	Intercept	R^2	p
Sabal palmetto	MAT	0.0743	-31.35	0.0088	0.22502
Sabal palmetto	MAP	-0.0011	-28.173	0.009	0.22108
Sabal palmetto	c_a	-0.027	-18.59	0.2215*	0.031198*
Sabal palmetto	VPD	-0.1485	-28.65	0.0161	0.1001
Caryota urens	MAT	-0.2009	-24.223	0.0798	0.14589
Caryota urens	MAP	-0.000004	-28.804	-0.000004	0.99254
Caryota urens	c_a	-0.0014	-28.325	0.0005	0.91156
Caryota urens	VPD	-0.0248	-28.646	0.0005	0.91107
Phoenix dactylifera	MAT	0.2367	-32.083	0.3208*	0.0348*
Phoenix dactylifera	MAP	0.0004	-26.819	0.0657	0.37626
Phoenix dactylifera	c_a	0.0121	-30.092	0.0402	0.49172
Phoenix dactylifera	VPD	-0.1112	-25.493	0.0594	0.40066

All Palms	MAT	-0.0696	-27.373	0.0058	0.064492
All Palms	MAP	-0.0005	-27.837	0.0395	0.11128
All Palms	c_a	-0.002	-28.406	0.0001	0.29147
All Palms	VPD	0.2287	-30.318	0.0563	0.53239

Table 3.5: Results of ordinary least squares regressions of Δ_{leaf} against MAT, MAP, c_a, and VPD for *S. palmetto*, *C. urens*, *P. dactylifera*, and all palms. Relationships with a significant R^2 and *p*-value are indicated by *.

Species	Variable	Slope	Intercept	R^2	*p*
Sabal palmetto	MAT	-0.0334	22.625	0.002	0.56624
Sabal palmetto	MAP	0.0006	21.093	0.0026	0.50885
Sabal palmetto	c_a	0.0118	16.812	0.0463	0.34676
Sabal palmetto	VPD	0.195	20.407	0.0309	0.02235
Caryota urens	MAT	0.2433	16.225	0.1086	0.093281
Caryota urens	MAP	-0.0001	22.034	0.0037	0.76293
Caryota urens	c_a	-0.012	26.009	0.0322	0.37044
Caryota urens	VPD	0.0792	21.258	0.0046	0.73703
Phoenix dactylifera	MAT	-0.2489	25.98	0.2681	0.057867
Phoenix dactylifera	MAP	-0.0003	20.349	0.0335	0.53096
Phoenix dactylifera	c_a	-0.0318	29.711	0.2104	0.09909
Phoenix dactylifera	VPD	0.0801	19.352	0.0233	0.60268
All Palms	MAT	0.0977	20.459	0.0094	0.064134
All Palms	MAP	0.0007	21.235	0.0555	0.0000031235
All Palms	c_a	-0.0165	27.959	0.0068	0.28037
All Palms	VPD	-0.2631	24.272	0.0618	0.0018821

Table 3.6: Results of ordinary least squares regressions of SI against MAT, MAP, c_a, and VPD for *S. palmetto*, *C. urens*, *P. dactylifera*, and all palms. Relationships with a significant R^2 and *p*-value are indicated by *.

Species	Variable	Slope	Intercept	R^2	*p*

Sabal palmetto	MAT	-0.0857	12.791	0.0054	0.43851
Sabal palmetto	MAP	-0.0067	20.501	0.1505*	0.0000243*
Sabal palmetto	c_a	-0.0398	26.397	0.1512*	0.044055*
Sabal palmetto	VPD	0.1662	9.6799	0.0107	0.27455
Caryota urens	MAT	0.1577	3.9697	0.0298	0.5224
Caryota urens	MAP	0.0003	7.2881	0.0052	0.79127
Caryota urens	c_a	0.0006	7.4438	0.00004	0.98447
Caryota urens	VPD	0.3225	5.4843	0.0621	0.35217
Phoenix dactylifera	MAT	0.4552	-0.3773	0.0251	0.70768
Phoenix dactylifera	MAP	0.00001	10.548	0.000001	0.99774
Phoenix dactylifera	c_a	-0.0209	17.214	0.0113	0.82075
Phoenix dactylifera	VPD	0.321	6.891	0.1216	0.39727
All Palms	MAT	-0.2004	14.788	0.0287	0.042226
All Palms	MAP	-0.0014	12.477	0.0338	0.027406
All Palms	c_a	-0.0253	19.092	0.0371	0.15906
All Palms	VPD	0.2989	8.1072	0.0516	0.0061724

Table 3.7: Results of ordinary least squares regressions of SD against MAT, MAP, c_a, and VPD for *S. palmetto*, *C. urens*, *P. dactylifera*, and all palms. Relationships with a significant R^2 and *p*-value are indicated by *.

Species	Variable	Slope	Intercept	R^2	*p*
Sabal palmetto	MAT	-0.2762	642.34	0.00003	0.94735
Sabal palmetto	MAP	0.0259	599.99	0.0015	0.65159
Sabal palmetto	c_a	0.1867	540.8	0.0017	0.81346
Sabal palmetto	VPD	-2.8795	659.41	0.0018	0.62254
Caryota urens	MAT	6.5973	-62.834	0.143	0.090935
Caryota urens	MAP	-0.0084	107.59	0.0162	0.58203
Caryota urens	c_a	-0.3698	220.37	0.0587	0.28336
Caryota urens	VPD	9.4127	29.535	0.1654	0.067308

Phoenix dactylifera	MAT	17.771	-85.39	0.1157	0.21476
Phoenix dactylifera	MAP	0.0732	268.61	0.1901	0.1042
Phoenix dactylifera	c_a	-1.1398	696.44	0.0523	0.4318
Phoenix dactylifera	VPD	-3.9078	374.9	0.0256	0.56878
All Palms	MAT	-33.194	1249.3	0.1405*	0.000000185*
All Palms	MAP	-0.0609	620.61	0.012	0.14077
All Palms	c_a	0.1147	337.01	0.0002	0.89847
All Palms	VPD	13.489	428.53	0.017	0.079169

Table 3.8: Results of ordinary least squares regressions of VLA against MAT, MAP, c_a, and VPD for *S. palmetto*, *C. urens*, *P. dactylifera*, and all palms. Relationships with a significant R^2 and *p*-value are indicated by *.

Species	Variable	Slope	Intercept	R^2	p
Sabal palmetto	MAT	0.0591	3.5224	0.0171	0.098122
Sabal palmetto	MAP	-0.0005	5.4535	0.0051	0.3671
Sabal palmetto	c_a	0.0153	-0.439	0.1944*	0.0083436*
Sabal palmetto	VPD	0.0322	4.4994	0.002	0.56945
Caryota urens	MAT	0.0671	3.4443	0.0307	0.46014
Caryota urens	MAP	0.0004	4.2935	0.0818	0.22148
Caryota urens	c_a	0.0067	2.5974	0.0388	0.46997
Caryota urens	VPD	-0.1597	6.0055	0.069	0.26332
Phoenix dactylifera	MAT	-0.4658	17.369	0.5494*	0.035357*
Phoenix dactylifera	MAP	-0.0007	6.8582	0.0685	0.53135
Phoenix dactylifera	c_a	0.0305	-3.1402	0.1155	0.41019
Phoenix dactylifera	VPD	0.5447	2.185	0.2048	0.26024
All Palms	MAT	0.0845	3.1591	0.03	0.0014751
All Palms	MAP	-0.0001	5.2184	0.0051	0.38814

All Palms	c_a	0.0028	4.3601	0.0027	0.77618
All Palms	VPD	-0.0041	5.031	0.00003	0.83409

Table 3.9: Results of ordinary least squares regressions of parallel VLA against MAT, MAP, c_a, and VPD for *S. palmetto*, *C. urens*, *P. dactylifera*, and all palms. Relationships with a significant R^2 and *p*-value are indicated by *.

Species	Variable	Slope	Intercept	R^2	*p*
Sabal palmetto	MAT	0.0992	2.2714	0.0386	0.012549
Sabal palmetto	MAP	-0.0009	5.6026	0.0134	0.14424
Sabal palmetto	c_a	0.0039	3.7281	0.0311	0.31593
Sabal palmetto	VPD	0.1053	3.5089	0.0174	0.095399
Caryota urens	MAT	0.0622	3.2499	0.0261	0.4965
Caryota urens	MAP	0.0004	3.9895	0.0803	0.22591
Caryota urens	c_a	0.0073	2.0734	0.0447	0.43364
Caryota urens	VPD	-0.1617	5.7121	0.07	0.25954
Phoenix dactylifera	MAT	-0.432	16.251	0.5036*	0.048636*
Phoenix dactylifera	MAP	-0.0006	6.4599	0.0549	0.57643
Phoenix dactylifera	c_a	0.0328	-4.1504	0.1424	0.35668
Phoenix dactylifera	VPD	0.54	1.19138	0.2145	0.24777
All Palms	MAT	0.1145	2.1061	0.0547	0.00032752
All Palms	MAP	-0.0002	4.8992	0.01	0.1293
All Palms	c_a	0.0006	4.9336	0.0002	0.89378
All Palms	VPD	0.0346	4.3425	0.0023	0.46622

Table 3.10: Results of ordinary least squares regressions of cross VLA against MAT, MAP, c_a, and VPD for *S. palmetto*, *C. urens*, *P. dactylifera*, and all palms. Relationships with a significant R^2 and *p*-value are indicated by *.

Species	Variable	Slope	Intercept	R^2	*p*
Sabal palmetto	MAT	0.0046	0.4817	0.0008	0.71443
Sabal palmetto	MAP	0.0004	0.0269	0.0262	0.040133

Sabal palmetto	c_a	-0.0005	0.6437	0.007	0.63353
Sabal palmetto	VPD	-0.013	0.6786	0.0028	0.50859
Caryota urens	MAT	0.0049	0.1944	0.0243	0.51165
Caryota urens	MAP	0.000002	0.2041	0.0002	0.95428
Caryota urens	c_a	-0.0006	0.5241	0.0489	0.3676
Caryota urens	VPD	0.0021	0.2934	0.0017	0.86325
Phoenix dactylifera	MAT	-0.0338	1.118	0.609*	0.022307*
Phoenix dactylifera	MAP	0.00009	0.3983	0.2529	0.20397
Phoenix dactylifera	c_a	-0.0023	1.0102	0.1403	0.36058
Phoenix dactylifera	VPD	0.0046	0.2712	0.0031	0.89566
All Palms	MAT	-0.0068	0.7012	0.0033	0.3855
All Palms	MAP	0.00004	0.488	0.0074	0.19188
All Palms	c_a	-0.0015	0.9922	0.0306	0.075926
All Palms	VPD	-0.0031	0.5754	0.0003	0.79204

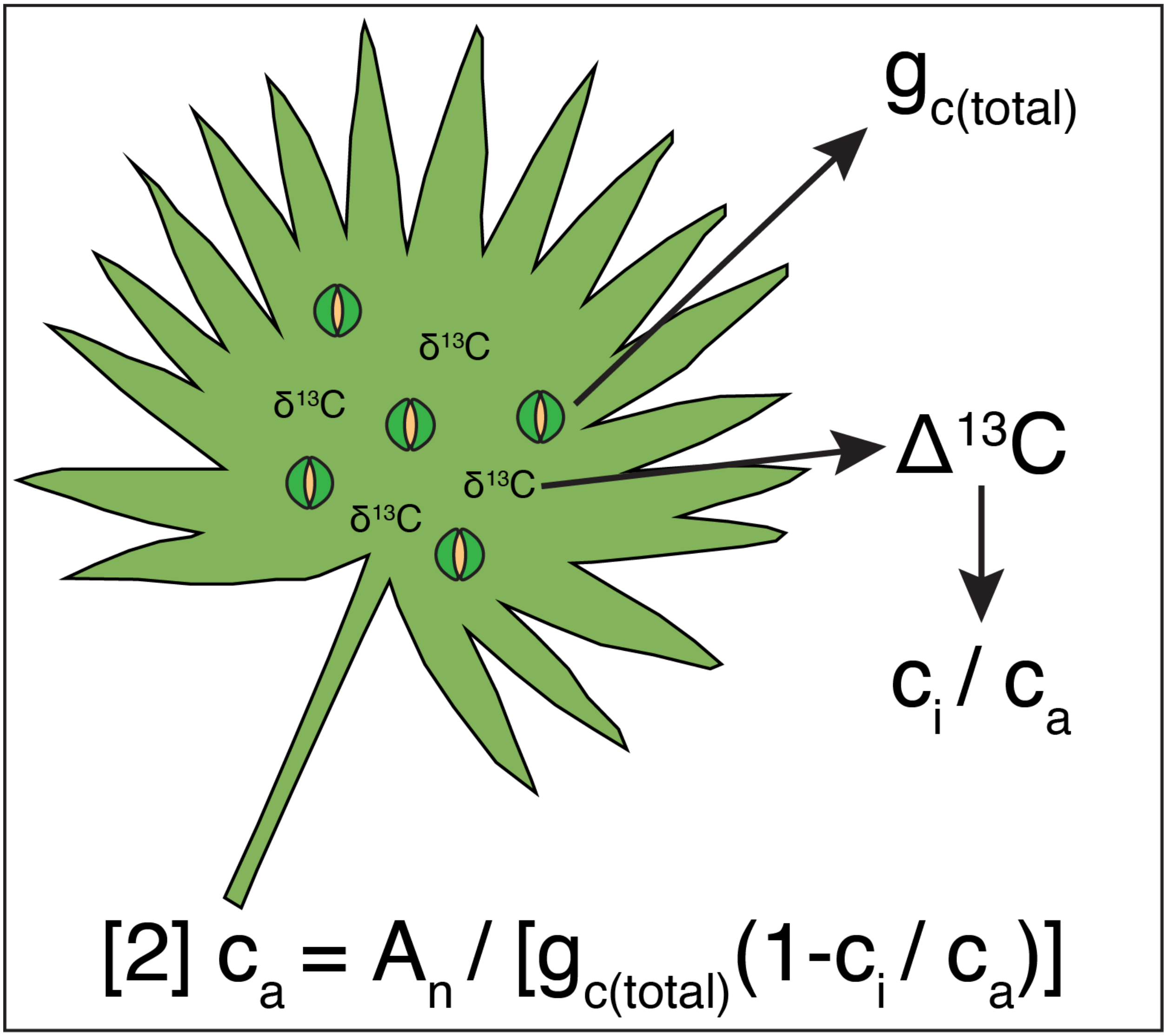

Fig. 3.1: Diagram of the Franks et al. model using CO_2 assimilation rate (A_n), total stomatal conductance ($g_{c(total)}$), and difference between atmospheric CO_2 concentration (c_a) and leaf internal CO_2 concentration (c_i) to reconstruct c_a.

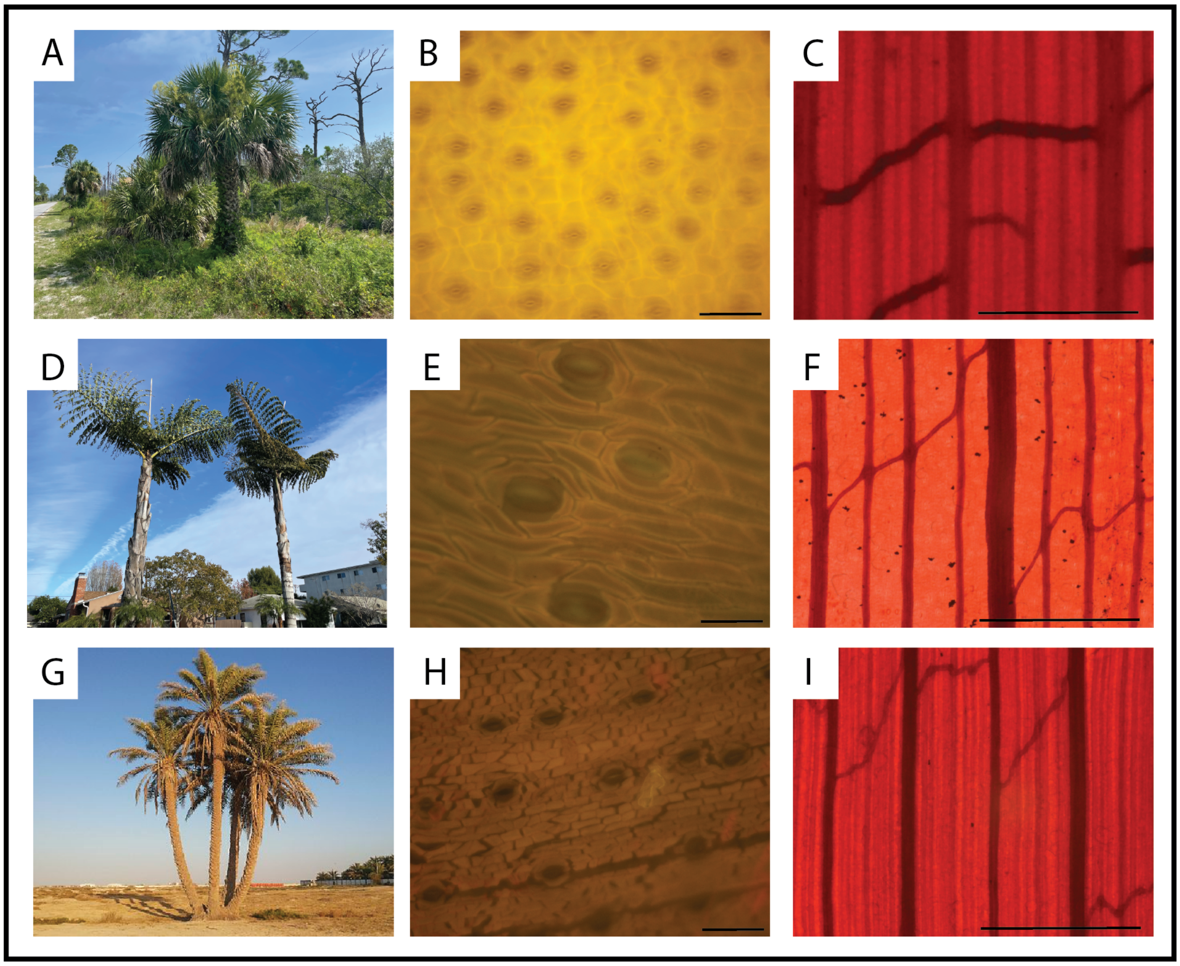

Fig. 3.2: Growth form, cuticle, and venation of *S. palmetto* (A, B, C), *C. urens* (D, E, F), and *P. dactylifera* (G, H, I). Scale bars are 50 µm. Image G credit: Ahmed1251985 (https://commons.wikimedia.org/wiki/File:4_date_palms_1.jpg#file)

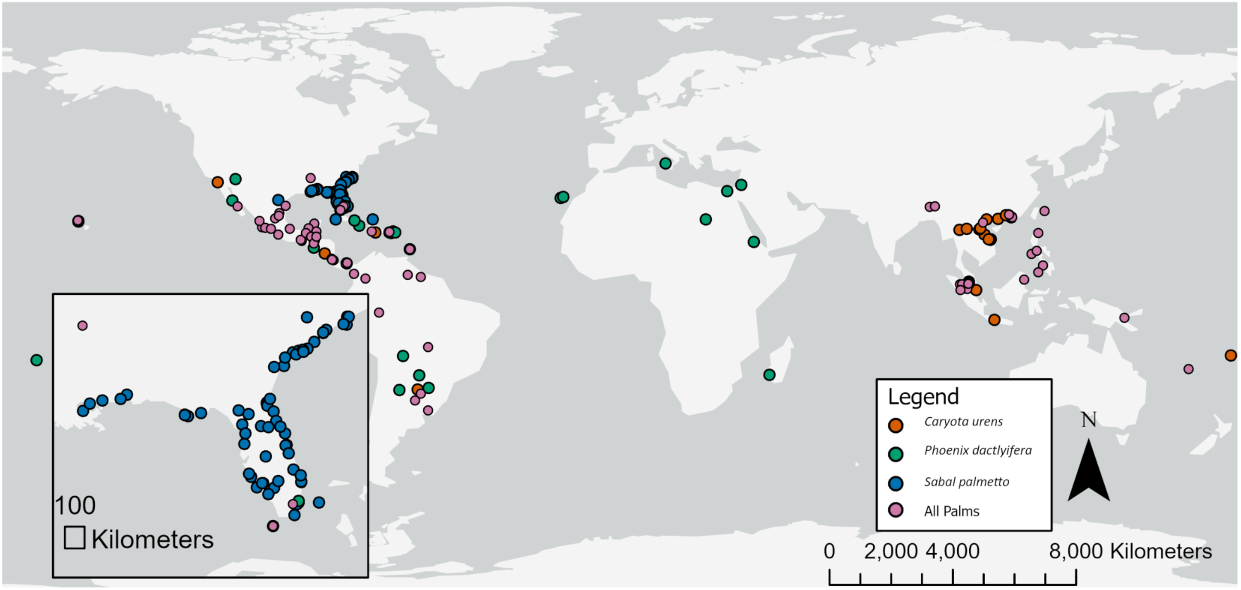

Fig. 3.3: Collection sites for each leaf sample.

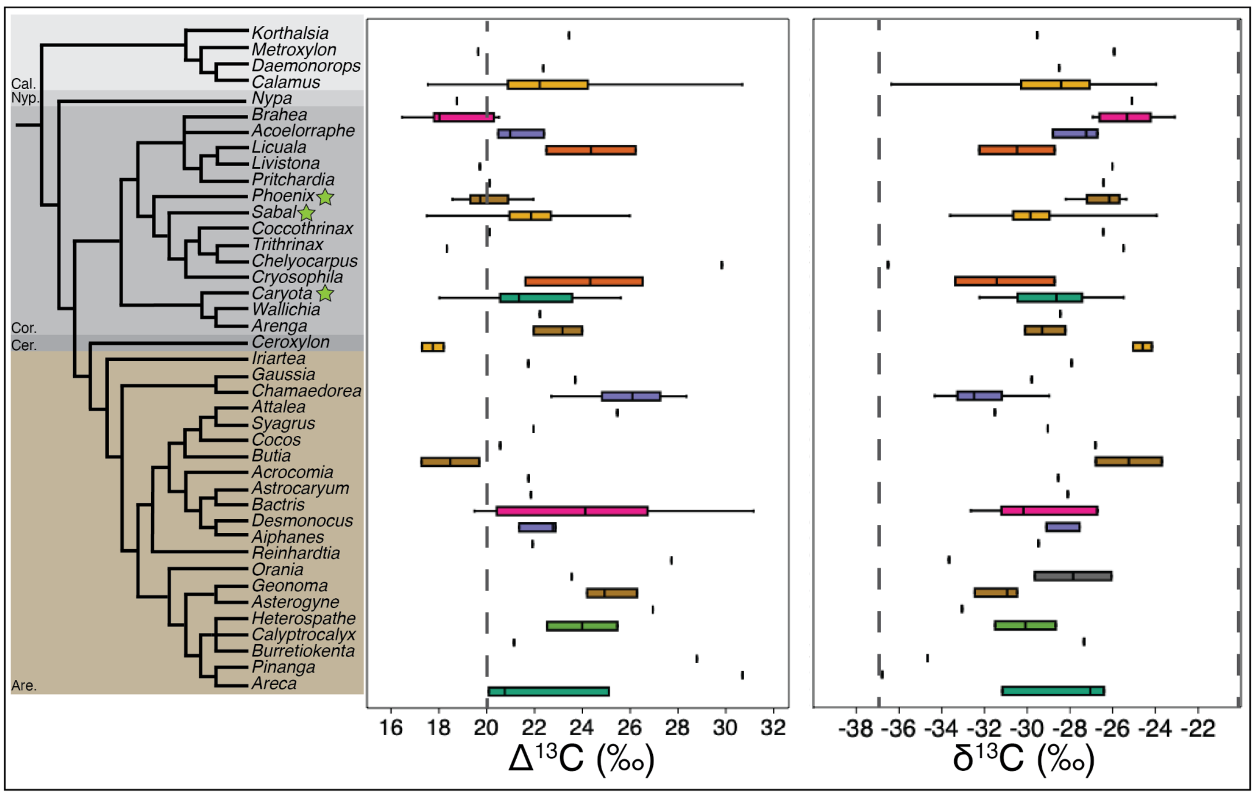

Fig. 3.4: $\Delta^{13}C$ and $\delta^{13}C$ distribution of each palm genus, focal genera are indicated by star. Dashed gray line on $\Delta^{13}C$ shows the theoretical value of 20‰. Dashed gray lines on $\delta^{13}C$ show the typical range of C_3 plants between -20 and -37‰ (Kohn et al., 2010). Phylogenetic relationships based on Baker et al. (2009). Subfamilies of Arecaceae were abbreviated as follows: Cal. = Calamoideae, Nyp. = Nypoideae, Cor. = Coryphoideae, Cer. = Ceroxyloideae, Are. = Arecoideae.

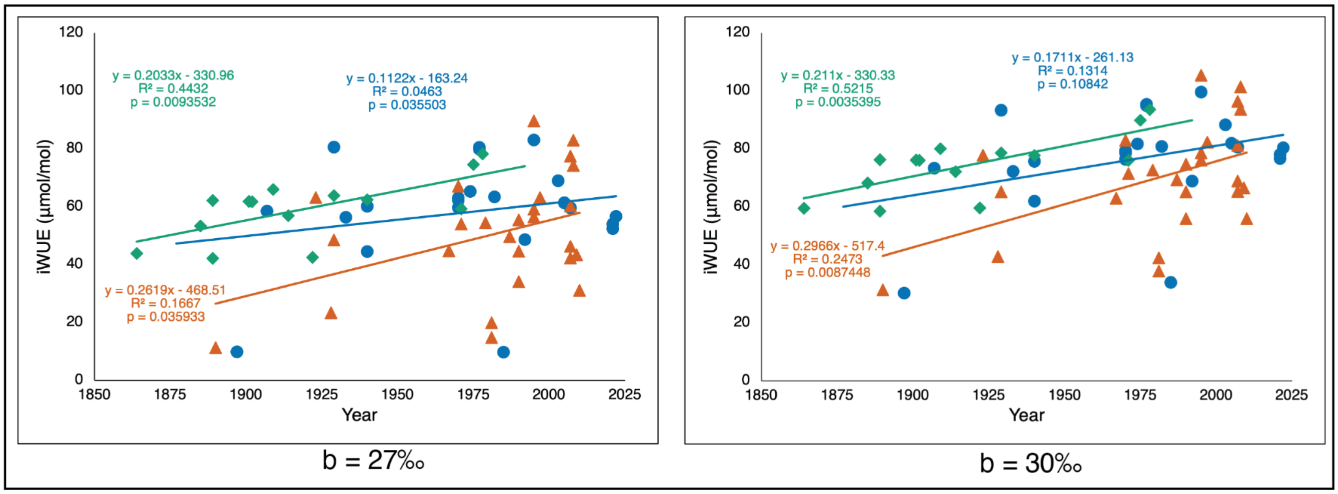

Fig. 3.5: Intrinsic water use efficiency over time for *S. palmetto* (blue circles), *C. urens* (orange triangles), and *P. dactylifera* (green diamonds) with assumed carbon fractionation due to carboxylation of RuBP of both 27 and 30‰.

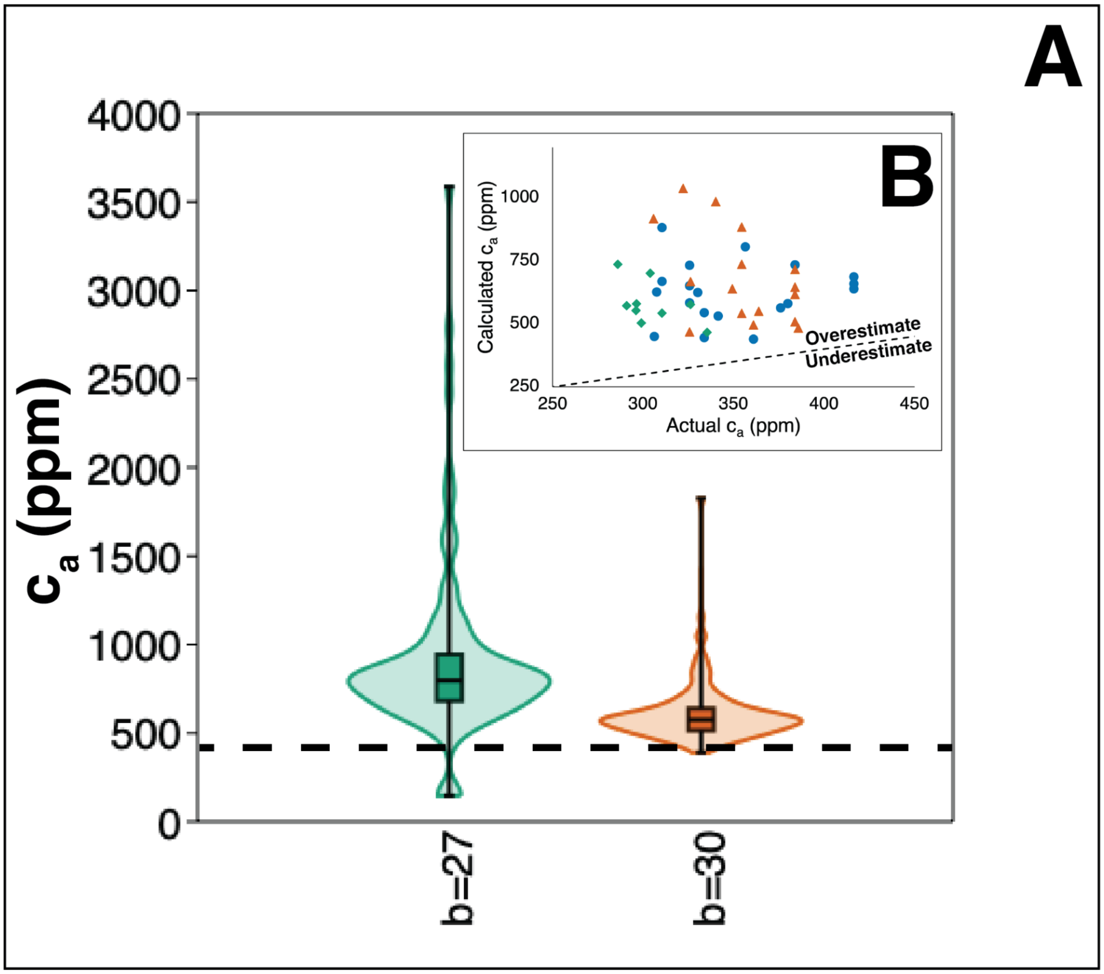

Fig. 3.6: A. Results of c_a calculations from modern *S. palmetto* assuming carbon fraction due to carboxylation of RuBP of both 27 and 30‰. Dashed line shows true c_a value of 416.45 ppm (Keeling et al., 2001). B. Results of c_a calculations from historical samples of *S. palmetto* (blue circles), *C. urens* (orange triangles), and *P. dactylifera* (green diamonds) compared to c_a at the time of collection. Dashed line represents a 1:1 relationship where samples above the line overestimate c_a and samples below the line underestimate c_a.

APPENDIX

CHAPTER 2 SUPPLEMENTAL MATERIAL

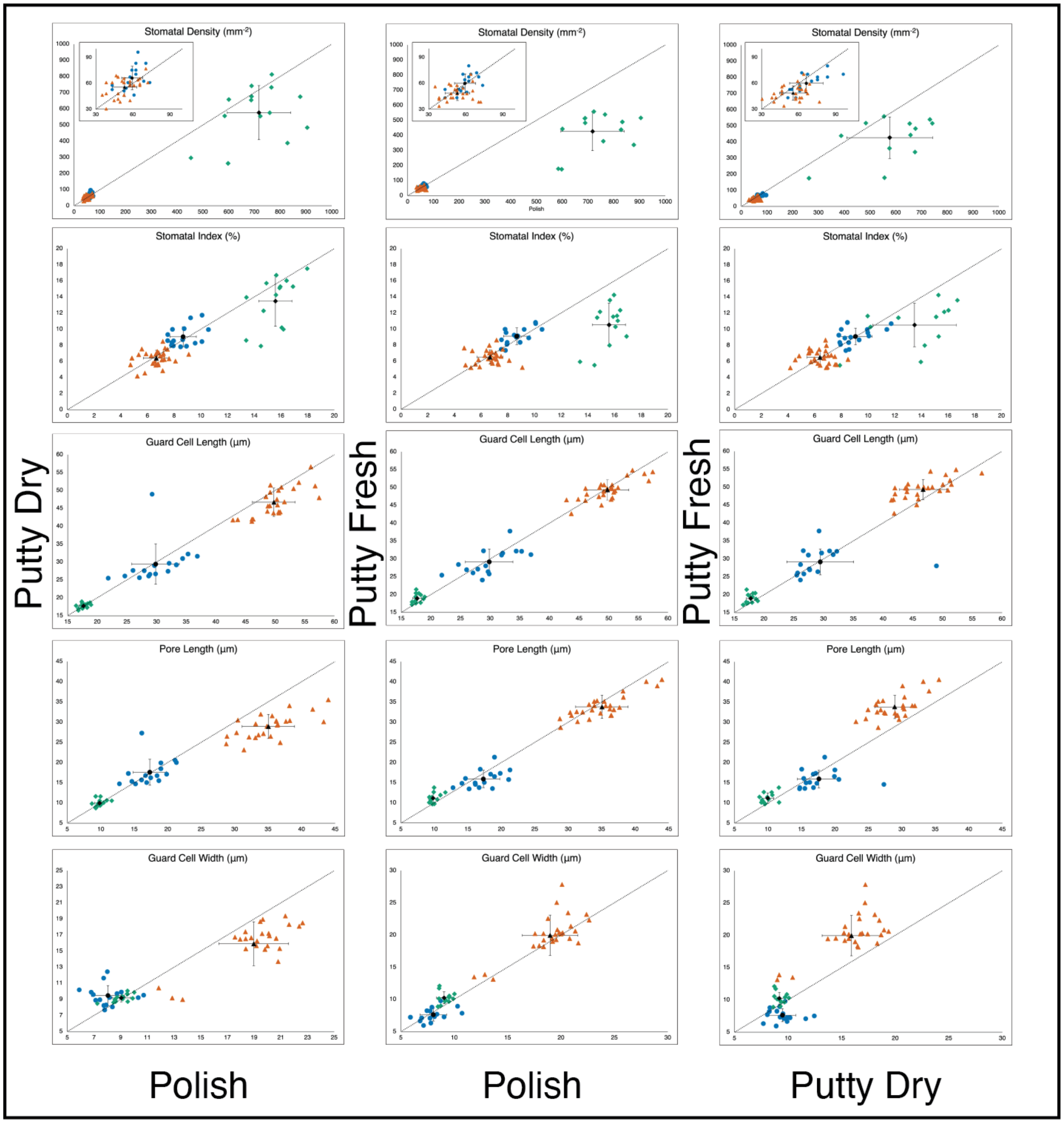

Supplemental Fig. 2.1: Comparisons of difference between polish, putty on dried leaves, and putty on fresh leaves and fluorescence on stomatal density, stomatal index, guard cell length, pore length, and guard cell width measurements. *G. biloba* represented by blue circles; *Q. alba*, green diamonds; *Z. mioga*, orange triangles. Black symbols represent mean for each species, with error bars showing one standard deviation. Dotted line showing theoretical 1:1 relationship.

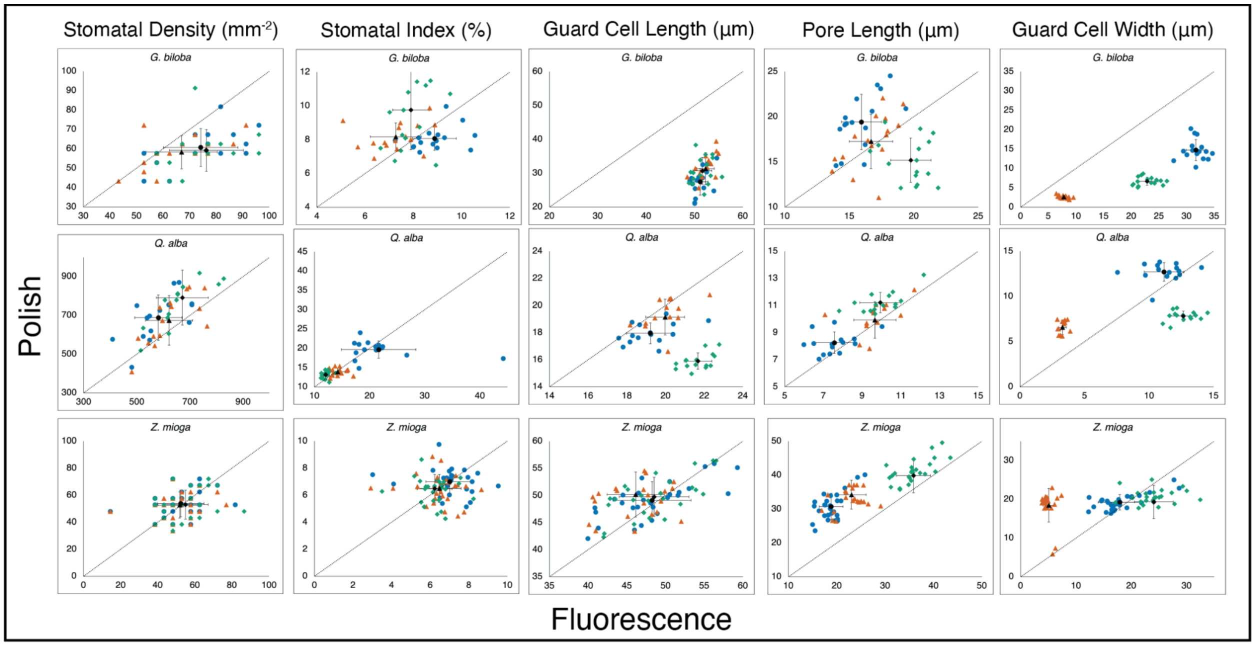

Supplemental Fig. 2.2: Differences between three counters measured values for stomatal density, stomatal index, guard cell length, pore length, and guard cell width for nail polish and fluorescence. Counter one's measurements are represented by blue circles; counter two, green diamonds; counter three, orange triangles. Black symbols represent mean for each species, with error bars showing one standard deviation. Dotted line showing theoretical 1:1 relationship.

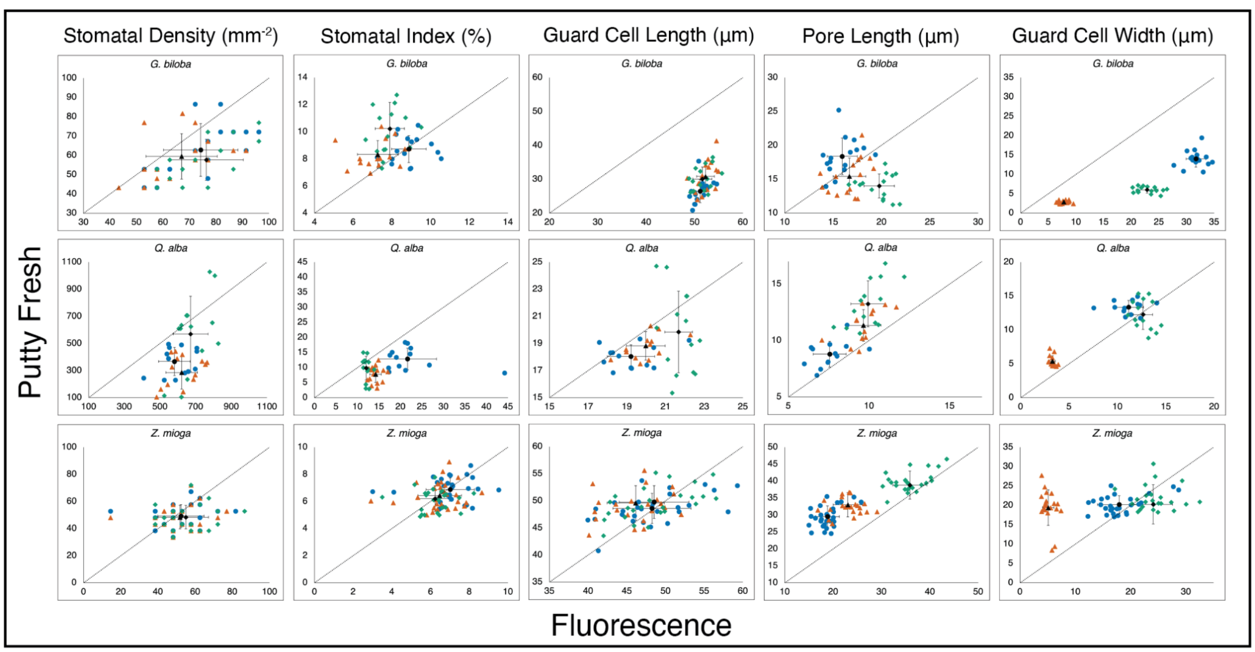

Supplemental Fig. 2.3: Differences between three counters measured values for stomatal density, stomatal index, guard cell length, pore length, and guard cell width for putty on fresh leaves and fluorescence. Counter one's measurements are represented by blue circles; counter two, green diamonds; counter three, orange triangles. Black symbols represent mean for each species, with error bars showing one standard deviation. Dotted line showing theoretical 1:1 relationship.

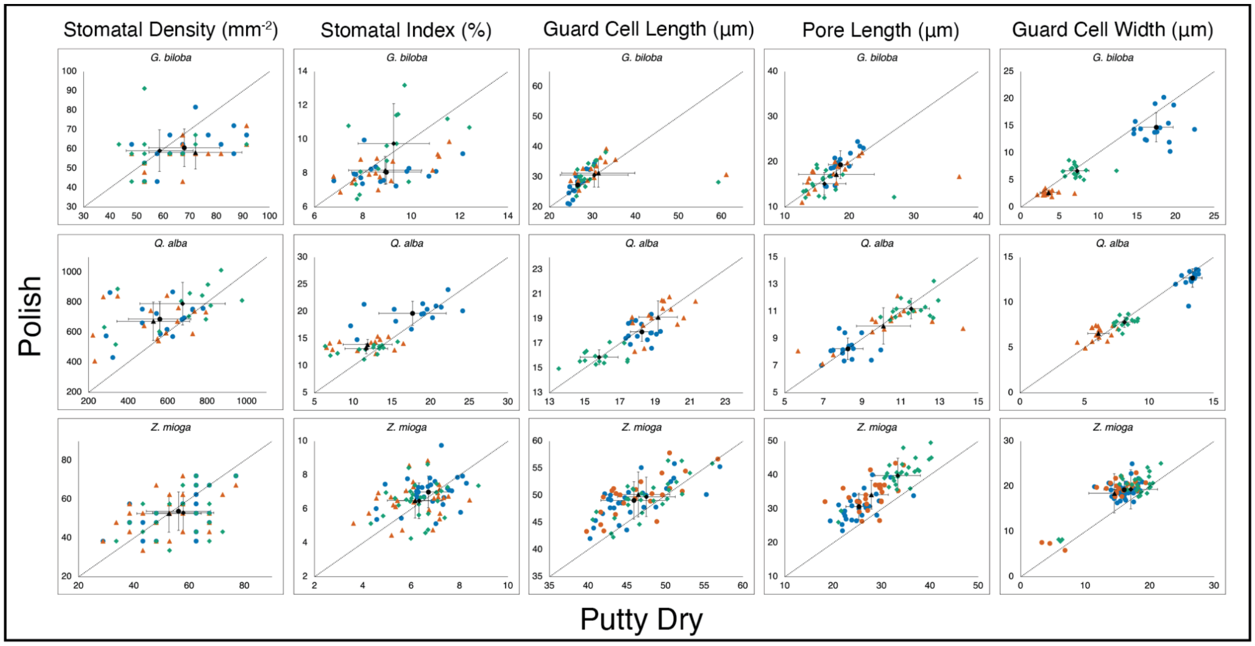

Supplemental Fig. 2.4: Differences between three counters measured values for stomatal density, stomatal index, guard cell length, pore length, and guard cell width for polish and putty on dried leaves. Counter one's measurements are represented by blue circles; counter two, green diamonds; counter three, orange triangles. Black symbols represent mean for each species, with error bars showing one standard deviation. Dotted line showing theoretical 1:1 relationship.

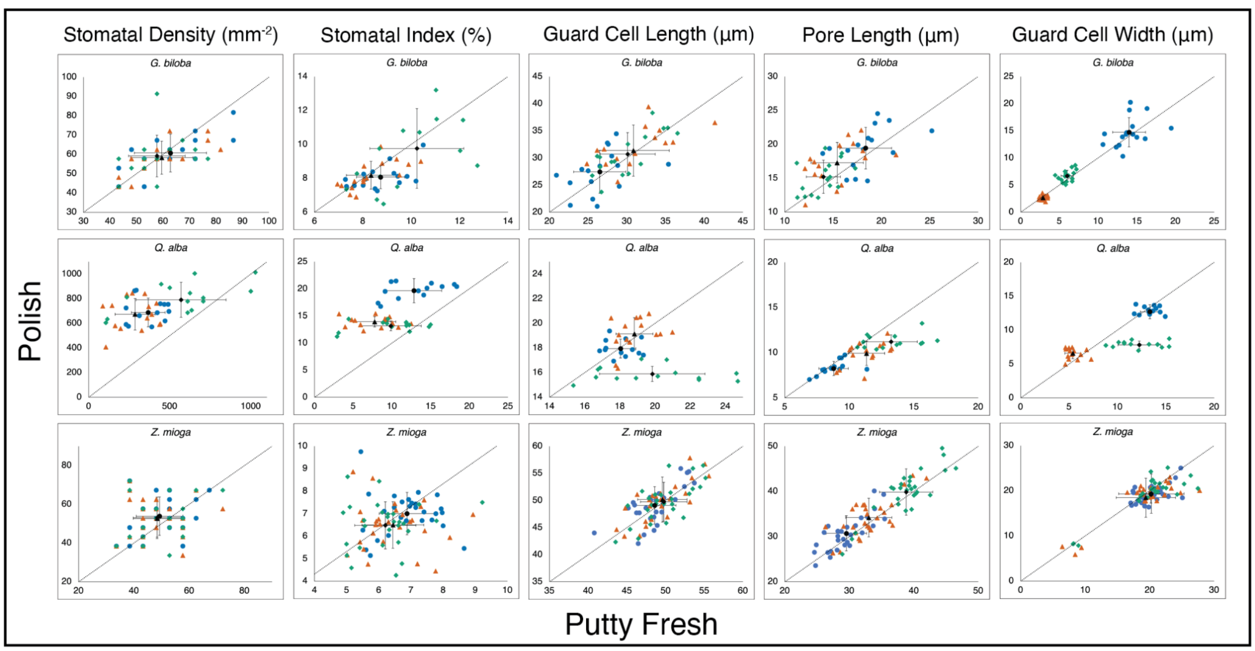

Supplemental Fig. 2.5: Differences between three counters measured values for stomatal density, stomatal index, guard cell length, pore length, and guard cell width for polish and putty on fresh leaves. Counter one's measurements are represented by blue circles; counter two, green diamonds; counter three, orange triangles. Black symbols represent mean for each species, with error bars showing one standard deviation. Dotted line showing theoretical 1:1 relationship.

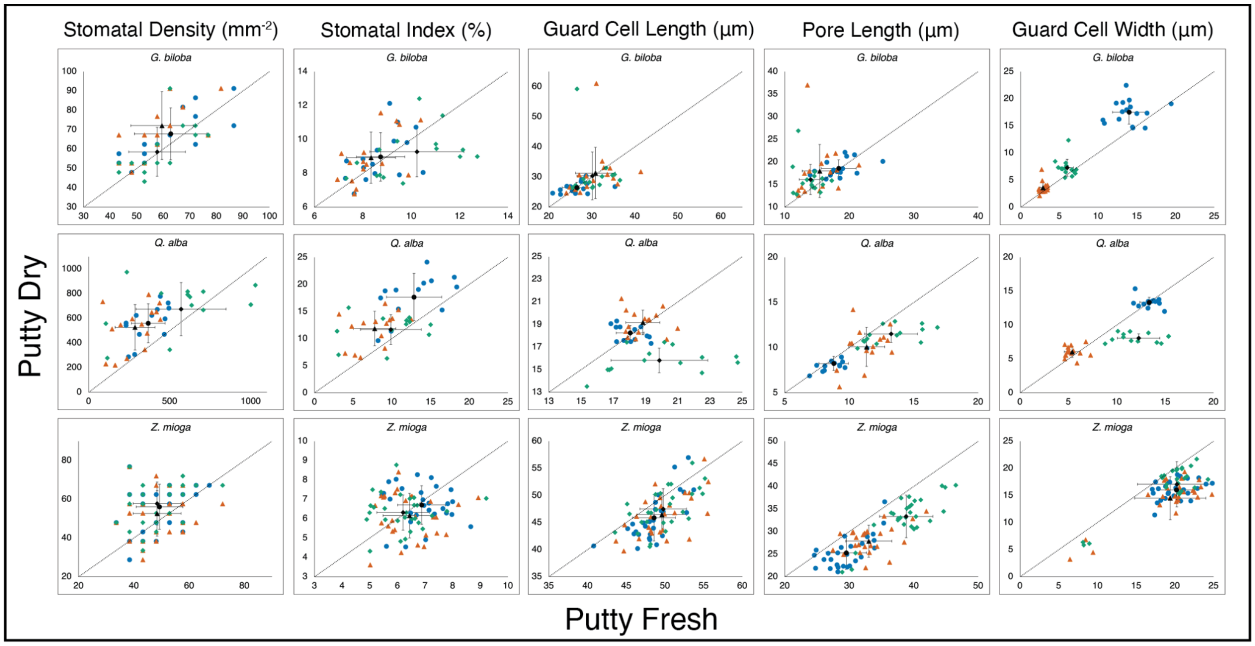

Supplemental Fig. 2.6: Differences between three counters measured values for stomatal density, stomatal index, guard cell length, pore length, and guard cell width for putty on dried leaves and putty on fresh leaves. Counter one's measurements are represented by blue circles; counter two, green diamonds; counter three, orange triangles. Black symbols represent mean for each species, with error bars showing one standard deviation. Dotted line showing theoretical 1:1 relationship.

CHAPTER 3 SUPPLEMENTAL MATERIAL

Supplemental Table 3.1: Collection information for each palm sample.

Sample name	Species	Herbarium /Field Sample	Location	Latitude	Longitude	Year	Collector
SP001	*Sabal palmetto*	Herb.	Jacksonville, FL	30.332201	-81.655649	1893	A.H. Curtiss
SP002	*Sabal palmetto*	Herb.	Cocoa, FL	28.383977	-80.741227	1938	A.S. Rhoads
SP003	*Sabal palmetto*	Herb.	Ocala National Forest, FL	29.24667	-81.91167	2007	A. Townesmith and K.M. Meyer
SP004	*Sabal palmetto*	Herb.	Francis Marion National Forest, SC	33.09806	-79.46917	1998	J. Stone and S. Bodine
SP005	*Sabal palmetto*	Herb.	Bear Island, SC	32.613036	-80.443761	1991	S.R. Hill
SP006	*Sabal palmetto*	Herb.	Big Pine Key, FL	24.669851	-81.353962	1940	E.P. Killip
SP007	*Sabal palmetto*	Herb.	Wadmalaw Island, SC	32.681835	-80.176346	1981	R.W. Read
SP008	*Sabal palmetto*	Herb.	Folly Beach, SC	32.655173	-79.940375	1970	S.W. Leonard
SP009	*Sabal palmetto*	Herb.	Tybee Island, GA	32.000201	-80.845692	1907	W. Trelease
SP010	*Sabal palmetto*	Herb.	Jacksonville, FL	30.332201	-81.655649	1877	A.H. Curtiss
SP011	*Sabal palmetto*	Herb.	Laredo, TX	27.503564	-99.507559	1901	Nichols
SP012	*Sabal palmetto*	Herb.	Lemon Island, SC	32.377384	-80.817894	1974	D.E. Boufford
SP013	*Sabal palmetto*	Herb.	Smith's Island, NC	33.88405	-77.980241	1897	N/A
SP014	*Sabal palmetto*	Herb.	Collier County, FL	26.41667	-81.3	1992	J.S. Miller, M. Merello, and J.K. Myers

Sample name	Species	Herbarium /Field Sample	Location	Latitude	Longitude	Year	Collector
SP015	*Sabal palmetto*	Herb.	Nueva Gerona, Cuba	21.878847	-82.810193	1904	A.H. Curtiss
SP016	*Sabal palmetto*	Herb.	Eldora, Florida	28.912868	-80.812806	1985	W.J. Hahn
SP017	*Sabal palmetto*	Herb.	Sanibel Island, Florida	26.443506	-82.111435	1970	L.J. Musselman
SP018	*Sabal palmetto*	Herb.	Aripeka, Florida	28.432361	-82.664412	1929	H. O'Neill
SP019	*Sabal palmetto*	Herb.	Brickell Hammock, Florida	25.76007	-80.195876	1933	H. O'Neill
SP020	*Sabal palmetto*	Herb.	Edisto Beach State Park, South Carolina	32.512601	-80.30028	1977	B. Hansen and J. Hansen
SP021	*Sabal palmetto*	Herb.	Smith's Island, NC	33.88405	-77.980241	1897	N/A
SP022	*Sabal palmetto*	Herb.	Folly Beach, SC	32.655173	-79.940375	1970	S.W. Leonard
SP023	*Sabal palmetto*	Herb.	Polk County, Florida	27.862579	-81.690618	1940	P.S.
SP024	*Sabal palmetto*	Herb.	Levy County, Florida	29.324802	-82.766995	1970	M. Nee, R. Peet, T. Cochrane, and R. Read
SP025	*Sabal palmetto*	Field	Florence, SC	34.2257	-79.79608	2022	M. Machesky and J. Morales Toledo
SP026	*Sabal palmetto*	Field	Florence, SC	34.2257	-79.79608	2022	M. Machesky and J. Morales Toledo
SP027	*Sabal palmetto*	Field	Florence, SC	34.2257	-79.79608	2022	M. Machesky and J. Morales Toledo
SP028	*Sabal palmetto*	Field	Wilmington, NC	34.2372877	-77.9486687	2022	M. Machesky and J. Morales Toledo

Sample name	Species	Herbarium /Field Sample	Location	Latitude	Longitude	Year	Collector
SP029	*Sabal palmetto*	Field	Wilmington, NC	34.2446	-77.88113	2022	M. Machesky and J. Morales Toledo
SP030	*Sabal palmetto*	Field	Oak Island, NC	33.91108	-78.11705	2022	M. Machesky and J. Morales Toledo
SP031	*Sabal palmetto*	Field	Oak Island, NC	33.91108	-78.11705	2022	M. Machesky and J. Morales Toledo
SP032	*Sabal palmetto*	Field	Oak Island, NC	33.91108	-78.11705	2022	M. Machesky and J. Morales Toledo
SP033	*Sabal palmetto*	Field	Oak Island, NC	33.91108	-78.11705	2022	M. Machesky and J. Morales Toledo
SP034	*Sabal palmetto*	Field	Myrtle Beach, SC	33.64899	-78.92892	2022	M. Machesky and J. Morales Toledo
SP035	*Sabal palmetto*	Field	Myrtle Beach, SC	33.64899	-78.92892	2022	M. Machesky and J. Morales Toledo
SP036	*Sabal palmetto*	Field	Myrtle Beach, SC	33.64899	-78.92892	2022	M. Machesky and J. Morales Toledo
SP037	*Sabal palmetto*	Field	Myrtle Beach, SC	33.64899	-78.92892	2022	M. Machesky and J. Morales Toledo
SP038	*Sabal palmetto*	Field	Myrtle Beach, SC	33.64989	-78.92892	2022	M. Machesky and J. Morales Toledo
SP039	*Sabal palmetto*	Field	Myrtle Beach, SC	33.651	-78.92892	2022	M. Machesky and J. Morales Toledo
SP040	*Sabal palmetto*	Field	Myrtle Beach, SC	33.65306	-78.92892	2022	M. Machesky and J. Morales Toledo
SP041	*Sabal palmetto*	Field	Myrtle Beach, SC	33.65306	-78.925456	2022	M. Machesky and J. Morales Toledo
SP042	*Sabal palmetto*	Field	Myrtle Beach, SC	33.65306	-78.92504	2022	M. Machesky and J. Morales Toledo
SP043	*Sabal palmetto*	Field	Murrells Inlet, SC	33.50139	-79.06791	2022	M. Machesky and J. Morales Toledo
SP044	*Sabal palmetto*	Field	Murrells Inlet, SC	33.50136	-79.06747	2022	M. Machesky and J. Morales Toledo

Sample name	Species	Herbarium /Field Sample	Location	Latitude	Longitude	Year	Collector
SP045	*Sabal palmetto*	Field	Murrells Inlet, SC	33.50176	-79.06713	2022	M. Machesky and J. Morales Toledo
SP046	*Sabal palmetto*	Field	Murrells Inlet, SC	33.50243	-79.06732	2022	M. Machesky and J. Morales Toledo
SP047	*Sabal palmetto*	Field	Murrells Inlet, SC	33.50293	-79.06626	2022	M. Machesky and J. Morales Toledo
SP048	*Sabal palmetto*	Field	Murrells Inlet, SC	33.50333	-79.06675	2022	M. Machesky and J. Morales Toledo
SP049	*Sabal palmetto*	Field	Murrells Inlet, SC	33.50396	-79.06622	2022	M. Machesky and J. Morales Toledo
SP050	*Sabal palmetto*	Field	Murrells Inlet, SC	33.51654	-79.05064	2022	M. Machesky and J. Morales Toledo
SP051	*Sabal palmetto*	Field	Isle of Palms, SC	32.78596	-79.78546	2022	M. Machesky and J. Morales Toledo
SP052	*Sabal palmetto*	Field	Isle of Palms, SC	32.78611	-79.78546	2022	M. Machesky and J. Morales Toledo
SP053	*Sabal palmetto*	Field	Isle of Palms, SC	32.78623	-79.78597	2022	M. Machesky and J. Morales Toledo
SP054	*Sabal palmetto*	Field	Isle of Palms, SC	32.7868	-79.78609	2022	M. Machesky and J. Morales Toledo
SP055	*Sabal palmetto*	Field	Isle of Palms, SC	32.78739	-79.7861	2022	M. Machesky and J. Morales Toledo
SP056	*Sabal palmetto*	Field	Isle of Palms, SC	32.78798	-79.78664	2022	M. Machesky and J. Morales Toledo
SP057	*Sabal palmetto*	Field	Isle of Palms, SC	32.78761	-79.78703	2022	M. Machesky and J. Morales Toledo
SP058	*Sabal palmetto*	Field	Isle of Palms, SC	32.78737	-79.78657	2022	M. Machesky and J. Morales Toledo
SP059	*Sabal palmetto*	Field	Charleston, SC	32.73345	-79.99225	2022	M. Machesky and J. Morales Toledo
SP060	*Sabal palmetto*	Field	Charleston, SC	32.73299	-79.99239	2022	M. Machesky and J. Morales Toledo

Sample name	Species	Herbarium /Field Sample	Location	Latitude	Longitude	Year	Collector
SP061	*Sabal palmetto*	Field	Charleston, SC	32.73269	-79.99298	2022	M. Machesky and J. Morales Toledo
SP062	*Sabal palmetto*	Field	Charleston, SC	32.73349	-79.99359	2022	M. Machesky and J. Morales Toledo
SP063	*Sabal palmetto*	Field	Charleston, SC	32.73392	-79.99433	2022	M. Machesky and J. Morales Toledo
SP064	*Sabal palmetto*	Field	Charleston, SC	32.7351	-79.99067	2022	M. Machesky and J. Morales Toledo
SP065	*Sabal palmetto*	Field	Charleston, SC	32.73653	-79.99185	2022	M. Machesky and J. Morales Toledo
SP066	*Sabal palmetto*	Field	Charleston, SC	32.73392	-79.99054	2022	M. Machesky and J. Morales Toledo
SP067	*Sabal palmetto*	Field	Charleston, SC	32.73273	-79.98964	2022	M. Machesky and J. Morales Toledo
SP068	*Sabal palmetto*	Field	Folly Beach, SC	32.64394	-79.96307	2022	M. Machesky and J. Morales Toledo
SP069	*Sabal palmetto*	Field	Folly Beach, SC	32.64389	-79.96342	2022	M. Machesky and J. Morales Toledo
SP070	*Sabal palmetto*	Field	Folly Beach, SC	32.64339	-79.96415	2022	M. Machesky and J. Morales Toledo
SP071	*Sabal palmetto*	Field	Folly Beach, SC	32.64248	-79.96647	2022	M. Machesky and J. Morales Toledo
SP072	*Sabal palmetto*	Field	Folly Beach, SC	32.6413	-79.96971	2022	M. Machesky and J. Morales Toledo
SP073	*Sabal palmetto*	Field	Richmond Hill, GA	31.95611	-81.32164	2022	M. Machesky and J. Morales Toledo
SP074	*Sabal palmetto*	Field	Jacksonville, FL	30.28203	-81.65156	2022	M. Machesky and J. Morales Toledo
SP075	*Sabal palmetto*	Field	Jacksonville, FL	30.28203	-81.65156	2022	M. Machesky and J. Morales Toledo
SP076	*Sabal palmetto*	Field	Jacksonville, FL	30.28203	-81.65156	2022	M. Machesky and J. Morales Toledo

Sample name	Species	Herbarium /Field Sample	Location	Latitude	Longitude	Year	Collector
SP077	*Sabal palmetto*	Field	Jacksonville, FL	30.18953	-81.62747	2022	M. Machesky and J. Morales Toledo
SP078	*Sabal palmetto*	Field	Jacksonville, FL	30.18953	-81.62747	2022	M. Machesky and J. Morales Toledo
SP079	*Sabal palmetto*	Field	Jacksonville, FL	30.18953	-81.62747	2022	M. Machesky and J. Morales Toledo
SP080	*Sabal palmetto*	Field	St. Augustine, FL	29.91618	-81.32469	2022	M. Machesky and J. Morales Toledo
SP081	*Sabal palmetto*	Field	St. Augustine, FL	29.91618	-81.32469	2022	M. Machesky and J. Morales Toledo
SP082	*Sabal palmetto*	Field	St. Augustine, FL	29.91618	-81.32469	2022	M. Machesky and J. Morales Toledo
SP083	*Sabal palmetto*	Field	Palm Coast, FL	29.47653	-81.20646	2022	M. Machesky and J. Morales Toledo
SP084	*Sabal palmetto*	Field	Palm Coast, FL	29.47653	-81.20646	2022	M. Machesky and J. Morales Toledo
SP085	*Sabal palmetto*	Field	Palm Coast, FL	29.47653	-81.20646	2022	M. Machesky and J. Morales Toledo
SP086	*Sabal palmetto*	Field	Daytona Beach, FL	29.20979	-81.02312	2022	M. Machesky and J. Morales Toledo
SP087	*Sabal palmetto*	Field	Daytona Beach, FL	29.20979	-81.02312	2022	M. Machesky and J. Morales Toledo
SP088	*Sabal palmetto*	Field	Cocoa, FL	28.35939	-80.79299	2022	M. Machesky and J. Morales Toledo
SP089	*Sabal palmetto*	Field	Cocoa, FL	28.35939	-80.79299	2022	M. Machesky and J. Morales Toledo
SP090	*Sabal palmetto*	Field	Cocoa, FL	28.35939	-80.79299	2022	M. Machesky and J. Morales Toledo
SP091	*Sabal palmetto*	Field	Palm Bay, FL	27.99822	-80.63298	2022	M. Machesky and J. Morales Toledo

Sample name	Species	Herbarium /Field Sample	Location	Latitude	Longitude	Year	Collector
SP092	*Sabal palmetto*	Field	Palm Bay, FL	27.99822	-80.63298	2022	M. Machesky and J. Morales Toledo
SP093	*Sabal palmetto*	Field	Palm Bay, FL	27.99822	-80.63298	2022	M. Machesky and J. Morales Toledo
SP094	*Sabal palmetto*	Field	Port Saint Lucie, FL	27.26414	-80.43213	2022	M. Machesky and J. Morales Toledo
SP095	*Sabal palmetto*	Field	Port Saint Lucie, FL	27.26414	-80.43213	2022	M. Machesky and J. Morales Toledo
SP096	*Sabal palmetto*	Field	Port Saint Lucie, FL	27.26414	-80.43213	2022	M. Machesky and J. Morales Toledo
SP097	*Sabal palmetto*	Field	West Palm Beach, FL	26.69177	-80.06908	2022	M. Machesky and J. Morales Toledo
SP098	*Sabal palmetto*	Field	West Palm Beach, FL	26.69177	-80.06908	2022	M. Machesky and J. Morales Toledo
SP099	*Sabal palmetto*	Field	West Palm Beach, FL	26.69177	-80.06908	2022	M. Machesky and J. Morales Toledo
SP100	*Sabal palmetto*	Field	Coral Gables, FL	25.67703	-80.27511	2022	M. Machesky and J. Morales Toledo
SP101	*Sabal palmetto*	Field	Coral Gables, FL	25.67703	-80.27511	2022	M. Machesky and J. Morales Toledo
SP102	*Sabal palmetto*	Field	Coral Gables, FL	25.67703	-80.27511	2022	M. Machesky and J. Morales Toledo
SP103	*Sabal palmetto*	Field	Coral Gables, FL	25.6764	-80.26925	2022	M. Machesky and J. Morales Toledo
SP104	*Sabal palmetto*	Field	Coral Gables, FL	25.6764	-80.26925	2022	M. Machesky and J. Morales Toledo
SP105	*Sabal palmetto*	Field	Fort Myers, FL	26.63749	-81.80719	2022	M. Machesky and J. Morales Toledo
SP106	*Sabal palmetto*	Field	Fort Myers, FL	26.63749	-81.80719	2022	M. Machesky and J. Morales Toledo
SP107	*Sabal palmetto*	Field	Fort Myers, FL	26.63749	-81.80719	2022	M. Machesky and J. Morales Toledo

Sample name	Species	Herbarium /Field Sample	Location	Latitude	Longitude	Year	Collector
SP108	*Sabal palmetto*	Field	Englewood, FL	26.92312	-82.35898	2022	M. Machesky and J. Morales Toledo
SP109	*Sabal palmetto*	Field	Englewood, FL	26.92331	-82.3585	2022	M. Machesky and J. Morales Toledo
SP110	*Sabal palmetto*	Field	Englewood, FL	26.92341	-82.35825	2022	M. Machesky and J. Morales Toledo
SP111	*Sabal palmetto*	Field	Englewood, FL	26.92351	-82.35802	2022	M. Machesky and J. Morales Toledo
SP112	*Sabal palmetto*	Field	Englewood, FL	26.92328	-82.35784	2022	M. Machesky and J. Morales Toledo
SP113	*Sabal palmetto*	Field	Englewood, FL	26.92323	-82.35805	2022	M. Machesky and J. Morales Toledo
SP114	*Sabal palmetto*	Field	Crystal River, FL	28.90914	-82.63802	2022	M. Machesky and J. Morales Toledo
SP115	*Sabal palmetto*	Field	Crystal River, FL	28.90914	-82.63745	2022	M. Machesky and J. Morales Toledo
SP116	*Sabal palmetto*	Field	Crystal River, FL	28.90923	-82.63664	2022	M. Machesky and J. Morales Toledo
SP117	*Sabal palmetto*	Field	Crystal River, FL	28.90913	-82.63636	2022	M. Machesky and J. Morales Toledo
SP118	*Sabal palmetto*	Field	Crystal River, FL	28.91193	-82.63459	2022	M. Machesky and J. Morales Toledo
SP119	*Sabal palmetto*	Field	Crystal River, FL	28.91236	-82.63462	2022	M. Machesky and J. Morales Toledo
SP120	*Sabal palmetto*	Field	Crystal River, FL	28.91313	-82.63468	2022	M. Machesky and J. Morales Toledo
SP121	*Sabal palmetto*	Field	Crystal River, FL	28.9141	-82.63435	2022	M. Machesky and J. Morales Toledo
SP122	*Sabal palmetto*	Field	Crystal River, FL	28.91451	-82.63226	2022	M. Machesky and J. Morales Toledo
SP123	*Sabal palmetto*	Field	Crystal River, FL	28.9193	-82.63647	2022	M. Machesky and J. Morales Toledo

Sample name	Species	Herbarium /Field Sample	Location	Latitude	Longitude	Year	Collector
SP124	*Sabal palmetto*	Field	Crystal River, FL	28.91927	-82.63626	2022	M. Machesky and J. Morales Toledo
SP125	*Sabal palmetto*	Field	Crystal River, FL	28.91935	-82.63655	2022	M. Machesky and J. Morales Toledo
SP126	*Sabal palmetto*	Field	Alachua, FL	29.79246	-82.49175	2022	M. Machesky and J. Morales Toledo
SP127	*Sabal palmetto*	Field	Alachua, FL	29.79246	-82.49175	2022	M. Machesky and J. Morales Toledo
SP128	*Sabal palmetto*	Field	Branford, FL	29.956	-82.92658	2022	M. Machesky and J. Morales Toledo
SP129	*Sabal palmetto*	Field	Branford, FL	29.95607	-82.9261	2022	M. Machesky and J. Morales Toledo
SP130	*Sabal palmetto*	Field	Branford, FL	29.95592	-82.92603	2022	M. Machesky and J. Morales Toledo
SP131	*Sabal palmetto*	Field	Branford, FL	29.95529	-82.92615	2022	M. Machesky and J. Morales Toledo
SP132	*Sabal palmetto*	Field	Carrabelle, FL	29.85124	-84.66378	2022	M. Machesky and J. Morales Toledo
SP133	*Sabal palmetto*	Field	Carrabelle, FL	29.85124	-84.66378	2022	M. Machesky and J. Morales Toledo
SP134	*Sabal palmetto*	Field	Carrabelle, FL	29.85124	-84.66378	2022	M. Machesky and J. Morales Toledo
SP135	*Sabal palmetto*	Field	Carrabelle, FL	29.85124	-84.66378	2022	M. Machesky and J. Morales Toledo
SP136	*Sabal palmetto*	Field	Carrabelle, FL	29.85124	-84.66378	2022	M. Machesky and J. Morales Toledo
SP137	*Sabal palmetto*	Field	Carrabelle, FL	29.85124	-84.66378	2022	M. Machesky and J. Morales Toledo
SP138	*Sabal palmetto*	Field	Port Saint Joe, FL	29.68863	-85.26492	2022	M. Machesky and J. Morales Toledo
SP139	*Sabal palmetto*	Field	Port Saint Joe, FL	29.68863	-85.26492	2022	M. Machesky and J. Morales Toledo

Sample name	Species	Herbarium /Field Sample	Location	Latitude	Longitude	Year	Collector
SP140	*Sabal palmetto*	Field	Port Saint Joe, FL	29.6888	-85.26438	2022	M. Machesky and J. Morales Toledo
SP141	*Sabal palmetto*	Field	Port Saint Joe, FL	29.68834	-85.26497	2022	M. Machesky and J. Morales Toledo
SP142	*Sabal palmetto*	Field	Port Saint Joe, FL	29.76538	-85.4039	2022	M. Machesky and J. Morales Toledo
SP143	*Sabal palmetto*	Field	Port Saint Joe, FL	29.76508	-85.4035	2022	M. Machesky and J. Morales Toledo
SP144	*Sabal palmetto*	Field	Port Saint Joe, FL	29.76502	-85.40344	2022	M. Machesky and J. Morales Toledo
SP145	*Sabal palmetto*	Field	Port Saint Joe, FL	29.76468	-85.40349	2022	M. Machesky and J. Morales Toledo
SP146	*Sabal palmetto*	Field	Port Saint Joe, FL	29.76431	-85.40326	2022	M. Machesky and J. Morales Toledo
SP147	*Sabal palmetto*	Field	Port Saint Joe, FL	29.76417	-85.40319	2022	M. Machesky and J. Morales Toledo
SP148	*Sabal palmetto*	Field	Port Saint Joe, FL	29.76402	-85.40309	2022	M. Machesky and J. Morales Toledo
SP149	*Sabal palmetto*	Field	Port Saint Joe, FL	29.76381	-85.40334	2022	M. Machesky and J. Morales Toledo
SP150	*Sabal palmetto*	Field	Port Saint Joe, FL	29.76352	-85.40333	2022	M. Machesky and J. Morales Toledo
SP151	*Sabal palmetto*	Field	Port Saint Joe, FL	29.76443	-85.40265	2022	M. Machesky and J. Morales Toledo
SP152	*Sabal palmetto*	Field	Port Saint Joe, FL	29.75607	-85.39584	2022	M. Machesky and J. Morales Toledo
SP153	*Sabal palmetto*	Field	Port Saint Joe, FL	29.75548	-85.39546	2022	M. Machesky and J. Morales Toledo
SP154	*Sabal palmetto*	Field	Port Saint Joe, FL	29.7553	-85.39549	2022	M. Machesky and J. Morales Toledo
SP155	*Sabal palmetto*	Field	Port Saint Joe, FL	29.7459	-85.39477	2022	M. Machesky and J. Morales Toledo

Sample name	Species	Herbarium /Field Sample	Location	Latitude	Longitude	Year	Collector
SP156	*Sabal palmetto*	Field	Port Saint Joe, FL	29.7459	-85.39477	2022	M. Machesky and J. Morales Toledo
SP157	*Sabal palmetto*	Field	Port Saint Joe, FL	29.74593	-85.39422	2022	M. Machesky and J. Morales Toledo
SP158	*Sabal palmetto*	Field	Mobile, AL	30.68266	-88.066	2022	M. Machesky and J. Morales Toledo
SP159	*Sabal palmetto*	Field	Mobile, AL	30.68266	-88.066	2022	M. Machesky and J. Morales Toledo
SP160	*Sabal palmetto*	Field	Mobile, AL	30.68266	-88.066	2022	M. Machesky and J. Morales Toledo
SP161	*Sabal palmetto*	Field	Grand Bay, AL	30.49869	-88.3344	2022	M. Machesky and J. Morales Toledo
SP162	*Sabal palmetto*	Field	Grand Bay, AL	30.49849	-88.33453	2022	M. Machesky and J. Morales Toledo
SP163	*Sabal palmetto*	Field	Grand Bay, AL	30.4988	-88.33447	2022	M. Machesky and J. Morales Toledo
SP164	*Sabal palmetto*	Field	Gulfport, MS	30.41916	-89.19079	2022	M. Machesky and J. Morales Toledo
SP165	*Sabal palmetto*	Field	Gulfport, MS	30.41916	-89.19079	2022	M. Machesky and J. Morales Toledo
SP166	*Sabal palmetto*	Field	Gulfport, MS	30.41866	-89.19063	2022	M. Machesky and J. Morales Toledo
SP167	*Sabal palmetto*	Field	Gulfport, MS	30.4187	-89.19008	2022	M. Machesky and J. Morales Toledo
SP168	*Sabal palmetto*	Field	New Orleans, LA	29.94008	-90.07572	2022	M. Machesky and J. Morales Toledo
SP169	*Sabal palmetto*	Field	New Orleans, LA	29.9401	-90.0757	2022	M. Machesky and J. Morales Toledo
SP170	*Sabal palmetto*	Field	New Orleans, LA	29.94011	-90.07576	2022	M. Machesky and J. Morales Toledo
SP171	*Sabal palmetto*	Field	Slidell, LA	30.28393	-89.74884	2022	M. Machesky and J. Morales Toledo

Sample name	Species	Herbarium /Field Sample	Location	Latitude	Longitude	Year	Collector
SP172	*Sabal palmetto*	Field	Slidell, LA	30.28377	-89.74873	2022	M. Machesky and J. Morales Toledo
SP173	*Sabal palmetto*	Field	Slidell, LA	30.28374	-89.74869	2022	M. Machesky and J. Morales Toledo
SPa001	*Sabal palmetto*	Herb.	Venice Beach, FL	27.074228	-82.450942	2003	J.L. Haynes
SPa002	*Sabal palmetto*	Herb.	Naples, FL	26.142208	-81.561922	2021	L.R. Noblick
SPa003	*Sabal palmetto*	Herb.	Clewiston, FL	26.74336	-81.12925	2021	L.R. Noblick
SPa004	*Sabal palmetto*	Herb.	Jacksonville, FL	30.482364	-81.491268	2005	L.R. Noblick
SPa005	*Sabal palmetto*	Herb.	Palm Beach County, FL	26.70419	-80.056838	1995	F.J. Dehring
SPa006	*Sabal palmetto*	Herb.	Monroe County, FL	25.173191	-80.370207	1977	L.A. Biernacki
SPa007	*Sabal palmetto*	Herb.	Zinder Point, FL	29.203909	-81.569302	1985	B. Hansen and R.P. Wunderlin
SPa008	*Sabal palmetto*	Herb.	Jonathan Dickinson State Park, FL	27.002397	-80.100447	1979	J. Popenoe
SPa009	*Sabal palmetto*	Herb.	Ft Meyers, FL	26.64053	-81.86619	2019	L.R. Noblick, A. Street, and L. Danielson
SPa010	*Sabal palmetto*	Herb.	North Bimini, Bahamas	25.749046	-79.256521	1974	D.S. Correll
SPa011	*Sabal palmetto*	Herb.	North Caicos, Turks and Caicos	21.952174	-71.972439	2010	J. Blaise
CU001	*Caryota urens*	Herb.	Granada, Nicaragua	11.934323	-85.955983	1982	J.C. Sandino

Sample name	Species	Herbarium /Field Sample	Location	Latitude	Longitude	Year	Collector
CU002	*Caryota urens*	Herb.	Summit Gardens, Panama	9.064255	-79.646533	1971	T.B. Croat
CU003	*Caryota urens*	Herb.	Summit Gardens, Panama	9.064255	-79.646533	1971	T.B. Croat
CU004	*Caryota urens*	Herb.	Villa Nizao, Dominican Republic	18.04167	-71.2	1981	T. Zanoni, M. Mejia, and C. Ramirez
CU005	*Caryota urens*	Herb.	Da Nang, Vietnam	16.054474	108.071706	1927	J. Clemens and M.S. Clemens
CU006	*Caryota urens*	Herb.	Fiji	-17.713399	178.065025	1941	D. Degenet
CU007	*Caryota urens*	Herb.	Chang Mai Province, Thailand	18.849268	98.970083	1990	W.J. Hahn
CU008	*Caryota urens*	Herb.	Oahu, Hawaii	21.275529	-157.823053	1967	H.H. Iltis
CU009	*Caryota urens*	Herb.	Singapore Botanic Gardens	1.313675	103.815907	1990	W.J. Hahn
CU010	*Caryota urens*	Herb.	Doi Phu Kha National Park, Thailand	19.198573	101.080352	1990	W.J. Hahn
CU011	*Caryota urens*	Herb.	Corrientes, Argentina	-27.469214	-58.830643	1970	V. Marunaka
CU012	*Caryota urens*	Herb.	San Diego Zoo, California	32.73333	-117.1667	1995	C.R. Annable and S. Haraszko
CU013	*Caryota urens*	Herb.	San Diego Zoo, California	32.73333	-117.1667	1995	C.R. Annable and S. Haraszko

Sample name	Species	Herbarium /Field Sample	Location	Latitude	Longitude	Year	Collector
CU014	*Caryota urens*	Herb.	San Diego Zoo, California	32.73333	-117.1667	1995	C.R. Annable and S. Haraszko
CU015	*Caryota urens*	Herb.	Kanehoe, Hawaii	21.45	-157.85	1997	C.R. Annable, H. Van Sickle, and G. Van Sickle
CU016	*Caryota urens*	Herb.	Villa Nizao, Dominican Republic	18.04167	-71.2	1981	T. Zanoni, M. Mejia, and C. Ramirez
CU017	*Caryota urens*	Herb.	St. Vincent	13.249528	-61.154946	1890	H.H. Smith and G.W. Smith
CU018	*Caryota urens*	Herb.	Wang Ching, Guangxi Zhuang, China	22.086165	110.21744	1928	R.C. Ching
CU019	*Caryota urens*	Herb.	Canton, Guangdong, China	22.464758	114.00572	1923	T.K. Ping
CU020	*Caryota urens*	Herb.	College of Agriculture, Sun Yat Sen University, Canton	23.096396	113.298943	1929	W.Y. Chun
CU021	*Caryota urens*	Herb.	Ba Na-Nui Chua Nature Reserve, Da Nang City, Vietnam	16	108.0167	2007	A. Henderson, N.Q. Dung, N. Canh, and L.V. Bo
CU022	*Caryota urens*	Herb.	Quang Binh Province, Vietnam	17.5	106.25	2007	A. Henderson, N.Q. Dung, P.X. Phuong, and L.V. Bo
CU023	*Caryota urens*	Herb.	Pu Mat National Park, Nghe An Province, Vietnam	18.95	104.8	2007	A. Henderson, B.V. Thanh, V.C.A. Tuan, P.V. Phuoc, and V.B. Huang

Sample name	Species	Herbarium /Field Sample	Location	Latitude	Longitude	Year	Collector
CU024	*Caryota urens*	Herb.	Pu Huong Nature Reserve, Nghe An Province, Vietnam	19.3	105.1167	2007	A. Henderson, B.V. Thanh, T.D. Dung, C.V. Dai, and V.B. Hung
CU025	*Caryota urens*	Herb.	Sao La Nature Reserve, Thua Thien-Hue Province, Vietnam	16.072	107.498	2009	A. Henderson, B.V. Thanh, and P.T. Ha
CU026	*Caryota urens*	Herb.	Bukit Fraser, Malaysia	3.716667	101.7	1987	R.D. Worthington
CU027	*Caryota urens*	Herb.	La Muda, Caguas, Puerto Rico	18.329051	-66.098161	1979	A.H. Liogier, P. Liogier, and L.F. Martorell
CU028	*Caryota urens*	Herb.	Pahang, Malaysia	3.358221	101.777008	2008	M. Jeanson, N. Yaakob, N. Yaakob, and E. Velautham
CU029	*Caryota urens*	Herb.	Baturaden, Java, Indonesia	-7.317879	109.236428	2008	M. Jeanson, J.R. Witono, P. Kartam
CU030	*Caryota urens*	Herb.	Bac Son City, Vietnam	21.89241	106.8775	2009	M. Jeanson and Q. Binh
CU031	*Caryota urens*	Herb.	Ding Hu Shan Park, Guangdong Province, China	23.17331	112.5469	2010	M. Jeanson and L. Guo
CU032	*Caryota urens*	Herb.	Doi Phuka National Forest, Thailand	19.18333	101.0833		A.S. Barfod and R. Pooma

Sample name	Species	Herbarium /Field Sample	Location	Latitude	Longitude	Year	Collector
PD001	*Phoenix dactlyifera*	Herb.	Phoenix, AZ	33.578915	-112.018005	1985	J. Ricketson and D. Vanderbur
PD002	*Phoenix dactlyifera*	Herb.	Big Pine Key, FL	24.669851	-81.353962	1940	E.P. Killip
PD003	*Phoenix dactlyifera*	Herb.	Big Pine Key, FL	24.669851	-81.353962	1936	E.P. Killip
PD004	*Phoenix dactlyifera*	Herb.	San Ignacio, Mexico	27.33333	-112.8333	1992	J.S. Miller, M. Merello, and A. Pool
PD005	*Phoenix dactlyifera*	Herb.	Santa Cruz, Bolivia	-17.78333	-63.2	1988	M. Nee
PD006	*Phoenix dactlyifera*	Herb.	Central Paraguay	-23.442499	-58.443829	1889	T. Morong
PD007	*Phoenix dactlyifera*	Herb.	Jericho, Palestine	31.861047	35.461766		American Colony, Jerusalem
PD008	*Phoenix dactlyifera*	Herb.	La Gomera, Canary Islands	28.103318	-17.219368	1905	C.J. Pitard
PD009	*Phoenix dactlyifera*	Herb.	Villa Giulia, Palermo, Italy	38.113415	13.375624	1900	W. Trelease
PD010	*Phoenix dactlyifera*	Herb.	Monte Bizen, Eritrea	15.325805	39.085577	1902	A. Pappi
PD011	*Phoenix dactlyifera*	Herb.	Jebel Uweinat, Sudan	21.923789	25.07994	1968	J. Leonard
PD012	*Phoenix dactlyifera*	Herb.	Tulear, Madagascar	-23.351607	43.685492	1975	T.B. Croat
PD013	*Phoenix dactlyifera*	Herb.	La Banda, Argentina	-27.734808	-64.241833	1971	A. Krapovickas and C.L. Cristobal
PD014	*Phoenix dactlyifera*	Herb.	Miami, Florida	25.812835	-80.191746	1929	H.N. Moldenke

Sample name	Species	Herbarium /Field Sample	Location	Latitude	Longitude	Year	Collector
PD015	*Phoenix dactlyifera*	Herb.	Ponce, Puerto Rico	17.99183	-66.592218	1901	L.M. Underwood and R.F. Griggs
PD016	*Phoenix dactlyifera*	Herb.	Puerto Real, Puerto Rico	18.079133	-67.183561	1885	P. Sintenis
PD017	*Phoenix dactlyifera*	Herb.	El Cobre, Cuba	20.046869	-75.949171	1902	C.L. Pollard and W. Palmer
PD018	*Phoenix dactlyifera*	Herb.	Camaguey, Cuba	21.549941	-77.269377	1909	J.A. Shafer
PD019	*Phoenix dactlyifera*	Herb.	Vieques, Puerto Rico	18.129973	-65.371078	1914	J.A. Shafer
PD020	*Phoenix dactlyifera*	Herb.	San Salvador, El Salvador	13.694706	-89.219372	1922	S. Calderon
PD021	*Phoenix dactlyifera*	Herb.	Trinidad, Paraguay	-27.130761	-55.703592	1889	T. Morong
PD022	*Phoenix dactlyifera*	Herb.	Cairo, Egypt	30.044013	31.242994	1889	Illegible
PD023	*Phoenix dactlyifera*	Herb.	Jardin Botanico de Orotava, Canary Islands	28.410811	-16.535241	1864	Illegible
PD024	*Phoenix dactlyifera*	Herb.	Hikutivake, Niue	-18.965157	-169.881546	1940	T.G. Yuncker
PD025	*Phoenix dactlyifera*	Herb.	Ulupau Head, Oahu, Hawaii	21.451696	-157.731055	1978	F.R. Fosberg and C.E. Evans III
Acowri .9930	*Acoelorrhaphe wrightii (Griseb. & H. Wendl.) H. Wendl. ex Becc.*	Herb.	North of the Everglades (Hammock)	25.6737	279.55	1921	Small & Dewinkeler

Sample name	Species	Herbarium /Field Sample	Location	Latitude	Longitude	Year	Collector
Acwr.4333	*Acoelorrhaphe wrightii (Griseb. & H. Wendl.) H. Wendl. ex Becc.*	Herb.	Belize River	17.4045	271.327	1933	Lundell
Acoewrig.3070	*Acoelorrhaphe wrightii (Griseb. & H. Wendl.) H. Wendl. ex Becc.*	Herb.	Mexico: Achotal, Balancan, Tabasco	17.875	268.48	1935	Matuda
Acme.2361	*Acrocomia aculeata (Jacq.) Lodd. ex Mart.*	Herb.	Veracruz, Mexico	19.1963	263.861	1976	Hernández
Aimi.1374	*Aiphanes minima (Gaertn.) Burret*	Herb.	Kingshell, Saint Vincent B.W.I	13.2805	298.816	2008	Beard
Arca.7653	*Areca catechu L.*	Herb.	Sumatra	2.967	99.12	1934	Boeea
Armo.28687	*Areca montana Ridl.*	Herb.	Malay Peninsula	3.1312	101.61	1935	Corner
Aral.6208	*Areca triandra Roxb. ex Buch.*	Herb.	Puerto Rico, La Jagua area, Federal Experiment Station, Mayaguez.	18.2141	292.869	1953	Muzik

Sample name	Species	Herbarium /Field Sample	Location	Latitude	Longitude	Year	Collector
Aren.6677	*Arenga engleri Becc.*	Herb.	Ryukyu Islands. Yaeyama Gunto: Iriomote Island; along the Urauchi River	24.3812	123.784	1951	Walker & Tawad
Armi.10578	*Arenga microcarpa Becc.*	Herb.	New Guinea (Kajabit, Markham Valley)	-6.7083	146.995	1939	Clemens
Arpi.34257	*Arenga pinnata (Wurmb) Merr.*	Herb.	Malay Peninsula	3.1312	101.61	1937	Simpah
Asma.80	*Asterogyne martiana (H. Wendl.) H. Wendl.*	Herb.	Costa Rica	10.2244	276.13	1964	Lent
Asme.10253	*Astrocaryum mexicanum Liebm. ex Mart.*	Herb.	Guatemala	15.8114	271.2	1947	Clover
Atco.4970-a	*Attalea cohune Mart.*	Herb.	British Honduras	16.9137	271.546	1934	Yuncker
Bacbar.16890	*Bactris barronis L. H. Bailey*	Herb.	Panamá	9.2705	280.521	1940	Bartlett & Lasser
Baco.16745	*Bactris coloniata L.H. Bailey*	Herb.	Panamá	9.1592	280.149	1940	Bartlett

Sample name	Species	Herbarium /Field Sample	Location	Latitude	Longitude	Year	Collector
Baga.10045	*Bactris gasipaes Kunth*	Herb.	Costa Rica	10.45	275.99		Hammel
Bagu.16996	*Bactris guineensis (L.) H.E. Moore*	Herb.	Panamá	9.2705	280.521	1940	Bartlett
Bama. 4842	*Bactris major Jacq.*	Herb.	Yucatan Peninsula	20.681	270.946	1963	Lundell
Bame. 1373	*Bactris mexicana Mart.*	Herb.	British Honduras	16.9137	271.546	1934	Gentle
Bapl.3379B	*Bactris plumeriana Mart.*	Herb.	Haiti	18.3725	287.737	1993	Skean Jr. & Judd
Brabra. 2917	*Brahea brandegeei (Purpus) H.E. Moore*	Herb.	Baja CA Mexico	25.72	248.67	1950	Carter & Kellog
Brca.16045	*Brahea calcarea Liebm.*	Herb.	Mexico	17.55	260.48	1962	Rzedowski
Brdu.11759	*Brahea dulcis (Kunth) Mart.*	Herb.	Mexico	19.5412	255.83	1989	Cochrane & Wetter & Cuevas
Brbe.3797	*Brahea dulcis var. berlandieri (Kunth) Mart.*	Herb.	Mexico	23.74	260.83	1976	Hansen & Cochran & Keller
Brpi.718	*Brahea pimo Becc.*	Herb.	Mexico	19.47	256.7	1990	Villa & Chávez

Sample name	Species	Herbarium /Field Sample	Location	Latitude	Longitude	Year	Collector
Brpr.13397	*Brahea prominens L.H. Bailey*	Herb.	Chapas, Mexico	15.8985	267.028	1965	Breedlove & Raven
Brsa.9654	*Brahea salvadorensis H. Wendl. ex Becc.*	Herb.	Guatemala	15.8114	271.2	1946	Clover
Buve.9197	*Burretiokentia veillardii (Brongn. & Gris) Pic. Serm.*	Herb.	New Caledonia	-21.659	165.843	1950	Guillaumin & Baumann-Bodenheim
Buca.21339	*Butia capitata (Mart.) Becc.*	Herb.	Uruguay	-33.595	304.14	1944	Bartlett
Buya.24939	*Butia yatay (Mart.) Becc.*	Herb.	Corrientes-Argentina	-28.754	301.937	1986	Schinini& Carnevali
Caac.33062	*Calamus acanthospathus Griff.*	Herb.	Assam, India	25.6215	91.7933	1953	Koelz
Caba.2287	*Calamus balanseanus Becc.*	Herb.	Indo-China, Tonkin	20.9976	105.85	1930	Petelot
Caca.8208	*Calamus caesius Blume*	Herb.	Sumatra (E. Coast)	1.7029	101.275	1927	Bartlett
Cade.198	*Calamus densiflorus Becc.*	Herb.	Sumatra (E. Coast)	1.7029	101.275	1928	Toroes
Cadie.7275	*Calamus diepenhorstii Miq.*	Herb.	Sumatra (E. Coast)	1.7029	101.275	1927	Bartlett

Sample name	Species	Herbarium /Field Sample	Location	Latitude	Longitude	Year	Collector
Cadi.78628	*Calamus discolor Mart.*	Herb.	Philippines	8.49	123.31	1929	Adaño
Caer.24380	*Calamus erectus Roxb.*	Herb.	Assam, India	25.6215	91.7933	1950	Koelz
Caer.27781	*Calamus erectus Roxb.*	Herb.	Assam, India	25.4995	90.255	1951	Koelz
Caex.8707	*Calamus exilis Griff.*	Herb.	Sumatra (E. Coast)	1.7029	101.275	1927	Bartlett
Dagr.445	*Calamus flexilis W.J. Baker*	Herb.	Island of Palawan, Philippines	8.49	123.31	1940	Ebalo
Cafl.27310	*Calamus floribundus Griff.*	Herb.	Assam, India	25.6215	91.7933	1951	Koelz
Caja.8095	*Calamus javensis Blume*	Herb.	Sumatra (E. Coast)	1.7029	101.275	1927	Bartlett
Dalo.4412	*Calamus longipes (Griff.) Mart.*	Herb.	Tapianoeli, Sumatra	1.376	99.2553	1933	Toroes
Cama.14133	*Calamus manillensis (Mart.) H. Wendl.*	Herb.	Mindanao	8.49	123.31	1912	Elmer
Came.743	*Calamus merrillii Becc.*	Herb.	Philippines	8.49	123.31	1940	Ebalo
Calmc.15515a	*Calamus microsphaerion Becc.*	Herb.	Philippines	11.8277	120.007	1935	Bartlett

Sample name	Species	Herbarium /Field Sample	Location	Latitude	Longitude	Year	Collector
Calmi. 227	*Calamus mindorensis Becc.*	Herb.	Philippines	8.49	123.31	1939	Ebalo
Damo. 783	*Calamus mollis (Blanco) Merr.*	Herb.	Ganiboc Mt., Philippines	8.49	123.31	1940	Ebalo
Cate.8563	*Calamus tetradactylus Hance*	Herb.	Hong Kong	22.4597	114.329	1969	Hu
Cabl.251	*Calamus usitasis Blanco*	Herb.	Philippines	8.49	123.31	1939	Ebalo
Cacl.1135	*Calyptrocalyx albertisianus Becc.*	Herb.	New Guinea	-6.7083	146.995	1940	Clemens
Cami.4811	*Caryota mitis Lour.*	Herb.	Sumatra, Tapaianoeli	1.376	99.2553	1933	Toroes
Caru.10826	*Caryota rumphiana Mart.*	Herb.	New Guinea, Morobe, Kajabit Mission	-6.7083	146.995	1939	Clemens
Caur.24789	*Caryota urens L.*	Herb.	Assam, India	25.4995	90.255	1950	Koelz
Ceal.10191	*Ceroxylon alpinum Bonpl. ex DC.*	Herb.	Colombia	4.711	285.928	1974	Moore Jr. & Anderson & Jaramillo
Cequ.10191	*Ceroxylon quindiuense (H. Karst.) H. Wendl.*	Herb.	Colombia	4.711	285.928	1974	Moore Jr. & Anderson & Jaramillo
Chqu.1929	*Chamaedorea*	Herb.	Mexico	15.69	267.38	1938	Matuda

Sample name	Species	Herbarium /Field Sample	Location	Latitude	Longitude	Year	Collector
	costaricana Oerst.						
Chel.10108	*Chamaedorea elegans Mart.*	Herb.	San Luis, Las crucitas, municipio/palmillo de Xilitla	22.2479	259.64	1959	Rzedowski
Cher.3443	*Chamaedorea ernesti-augustii H. Wendl.*	Herb.	Mexico	17.3	268.61	1939	Matuda
Chgr.6853	*Chamaedorea gramnifolia H. Wendl.*	Herb.	Honduras	17.0331	271.092	1936	Lundell
Chne.2943	*Chamaedorea neurochlamys Burret*	Herb.	Honduras	16.9137	271.546	1939	Yenile
Chob.402	*Chamaedorea oblongata Mart.*	Herb.	Mexico	17.875	268.48	1963	Gilly Sr. & Hernandez
Chco.49553	*Chamaedorea pinnatifrons (Jacq.) Oerst.*	Herb.	Chiapas Mexico	15.8985	267.028	1981	Breedlove & Keller
Chpo.12137	*Chamaedorea pochutlensis Liebm.*	Herb.	Nayarit Mexico	21.4712	255.05	1951	McVaugh

Sample name	Species	Herbarium /Field Sample	Location	Latitude	Longitude	Year	Collector
Chra.008	*Chamaedorea radicalis Mart.*	Herb.	Southwestern Tamaulipas (Gomez Farias Region)	22.938	260.616	1953	Martin
Chse.8075	*Chamaedorea seifrizii Burret*	Herb.	Campeche, Mexico	19.2722	269.25	1959	Moore Jr.
Chdi.221	*Chelyocarpus dianeures (Burrret) H.E. Moore*	Herb.	Choco, Colombia (6 degrees 7.5'N 77 degrees 26' W)	6.132	282.565	1991	Evans & Ramirez
Coar.1766	*Coccothrinax argentea (Lodd. ex Schult.& Schult. f.) Sarg. ex K. Schum.*	Herb.	Big Pine Key, Dade Co. Florida	24.6659	278.64	1955	Stoutamire
Conu.902	*Cocos nucifera L.*	Herb.	Honduras	18.3632	271.58	1933	Gentle
Crar.9175	*Cryosophila argentea Bartlett*	Herb.	San José Petén, Guatemala C.A.	16.8943	270.116	1996	Ucan & Taylor & Reyes & Tescunl
Crba.158	*Cryosophila bartlettii R.J. Evans*	Herb.	Panamá	9.1917	280.442	1989	Evans
Crycoo.162	*Cryosophila cookii Bartlett*	Herb.	Limón, Costa Rica	10.0833	276.64	1989	Evans
Daac.781	*Daemonorops*	Herb.	Philippines	8.49	123.31	1940	Ebalo

Sample name	Species	Herbarium /Field Sample	Location	Latitude	Longitude	Year	Collector
	achrolepis Becc.						
Dech.3196	*Desmoncus chinantlensis Liebm. ex Mart.*	Herb.	Tabasco, Mexico	17.875	268.48	1939	Matuda
Demy.16728	*Desmoncus myriacanthos Dugand*	Herb.	Panamá	9.1592	280.149	1940	Bartlett
Depo.50	*Desmoncus polyacanthos Mart.*	Herb.	British Guiana (now Guyana)	5.2366	301.938	1923	Persaud
Gama.3759	*Gaussia maya (O.F. Cook) H.J. Quero*	Herb.	Peten, Guatemala	16.8943	270.116	1933	Lundell
Gede.320	*Geonoma cuneata subsp. cuneata H. Wendl. ex Burret*	Herb.	Costa Rica	10.2244	276.13	1965	Lent
Gein.16748	*Geonoma interrupta (Ruiz & Pav.) Mart.*	Herb.	Panamá	9.2705	280.521	1940	Bartlett
Geap.9716	*Geonoma undata subsp. appuniana (Spruce) A.J. Hend.*	Herb.	Venezuela	5.7534	298.193	1970	Moore Jr. & Ambrose & Dietz IV & Pfister

Sample name	Species	Herbarium /Field Sample	Location	Latitude	Longitude	Year	Collector
Heca.14907	*Heterospathe cagayanensis Becc.*	Herb.	Cagayan Province, Philippines	18.0048	121.944	1935	Bartlett
Heel.218	*Heterospathe elata Scheff.*	Herb.	Philippines, Island of Mindoro: bongabon and Pinamalayan	12.7423	121.448	1941	Maliwanag
Irco.5739	*Iriartea deltoidea Ruiz & Pav.*	Herb.	Amazon Brazil (lat 9 degrees 20' S, long 69 degrees W)	-5.2127	289.843	1933	Krukoff
Koec.64	*Korthalsia echinometra Becc.*	Herb.	Sumatra, Silo Maradja, Asahan	3.0073	99.72	1927	Toroes
Lifo.17347	*Licuala fordiana Becc.*	Herb.	Kwangtung	23.2563	113.391	1934	Metcalf
Lipe.24940	*Licuala peltata Roxb.*	Herb.	Assam, India	25.6215	91.7933	1950	Koelz
Lisa.34149	*Livistona saribus (Lour.) Merr. ex A. Chev.*	Herb.	Selangor	3.1312	101.61	1937	Nur
Mesa.999	*Metroxylon sagu Rottb.*	Herb.	Philippines, Mindanao, near Kabasalan	8.49	123.31	1941	Ebalo
Nifru.6785	*Nypa fruticans Wurmb*	Herb.	Ryukyu Islands	24.3812	123.784	1951	Walker & Tawad

Sample name	Species	Herbarium /Field Sample	Location	Latitude	Longitude	Year	Collector
Orru.975	*Orania decipiens Becc.*	Herb.	Basilan Island	6.5425	121.89	1941	Ebalo
Orsy.5568	*Orania sylvicola (Griff.) H.E. Moore*	Herb.	Sumatra, Tapianoeli (Poelo Liman)	1.376	99.2553	1933	Toroes
Phou.28426	*Phoenix loureirii Kunth*	Herb.	Assam, India	25.6215	91.7933	1951	Koelz
Pipa.21619	*Pinanga patula Blume*	Herb.	Borneo	4.4432	117.925	1922	Elmer
Prka.10466	*Pritchardia kahukuensis Caum*	Herb.	Hawaii	21.5241	202.03	1935	Degener & Park, Bush, Potter, Topping
Regr.4990	*Reinhardtia gracilis (H. Wendl.) Burret*	Herb.	Honduras	14.9046	270.886	1934	Yuncker
Sam.8700	*Sabal mexicana Mart.*	Herb.	Texas	25.8521	262.581	1940	Lundell & Lundell
Sami.454	*Sabal minor (Jacq.) Pers.*	Herb.	Mississippi	33.8438	269.916	1955	Hardin
Sapu.22046	*Sabal pumos (Kunth) Burret*	Herb.	Mexico	19.2	258.3	1966	Rzedowski
Saya.3103	*Sabal yapa C. Wright ex Becc.*	Herb.	Honduras	16.9137	271.546	1939	Yentle?

Sample name	Species	Herbarium /Field Sample	Location	Latitude	Longitude	Year	Collector
Syfl.43 038	*Syagrus flexuosa (Mart.) Becc.*	Herb.	Brasil, MT	-15.227	304.19	1989	Krapovickas & Cristóbal
Trca.4 0637	*Trithrinax campestris (Burmeist.) Drude & Griseb.*	Herb.	Argentina	-30.738	300.38	1986	Krapovickas & Cristóbal
Wade. 30554	*Wallichia densiflora Mart.*	Herb.	Assam, India	25.6215	91.7933	1952	Koelz

Supplemental Table 3.2: Measured and calculated parameters from each palm sample.

Sample name	C:N	$\delta^{13}C$ (‰)	Δ_{leaf} (‰)	Stomatal index (%)	Stomatal density (mm^{-2})	Pore length (µm)	*VLA* (mm/mm^2)	Parallel *VLA* (mm/mm^2)	Cross *VLA* (mm/mm^2)	Calc c_a (ppm) [b=27]	Calc c_a (ppm) [b=30]	iWUE (µmol/mol) [b=27]	iWUE (µmol/mol) [b=30]
SP001				16.02	363.11	2.78	5.33	4.61	0.72				
SP002				21.51	806.22	1.72	5.94	4.73	1.21				
SP003	34.64	-29.04	21.40	13.12	306.18	2.37	5.55	4.95	0.60	994.09	733.41	59.51	80.66
SP004				19.71	623.13	2.42	5.95	5.00	0.95				
SP005							5.76	4.79	0.97				
SP006	35.73	-28.15	21.82	11.74	409.27	1.80	4.36	3.80	0.56	1090.77	782.61	44.51	62.03
SP007							5.14	4.53	0.61				
SP008							5.10	4.26	0.84				
SP009	34.82	-26.19	19.91				3.32	2.78	0.53			58.47	73.46
SP010							5.61	5.30	0.31				
SP011				21.53	709.29	2.27							
SP012	50.14	-26.72	19.85	17.95	707.75	1.54	4.52	4.30	0.22	694.29	553.97	65.28	81.81
SP013				18.72	789.30	2.33	5.43	4.93	0.50				
SP014	23.06	-29.28	22.07	12.49	605.74	1.68	5.26	5.00	0.26	1015.92	715.24	48.58	69.00
SP015				15.46	555.43	1.99							
SP016	24.13	-32.84	25.98	11.03	682.66		6.14	5.76	0.38			9.76	33.98
SP017	15.86	-26.87	20.09	13.00	822.07	1.68	6.31	5.99	0.32	655.24	517.43	62.20	78.76

Sample name	C:N	$\delta^{13}C$ (‰)	Δ_{leaf} (‰)	Stomatal index (%)	Stomatal density (mm^{-2})	Pore length (μm)	*VLA* (mm/mm^2)	Parallel *VLA* (mm/mm^2)	Cross *VLA* (mm/mm^2)	Calc c_a (ppm) [b=27]	Calc c_a (ppm) [b=30]	iWUE (μmol/mol) [b=27]	iWUE (μmol/mol) [b=30]
SP018	16.88	-23.94	17.49	13.86	980.72	1.58	5.91	5.46	0.45	463.07	398.72	80.50	93.49
SP019	20.78	-26.73	20.37	10.32	653.81	1.80	6.88	6.46	0.41	713.09	556.00	56.36	72.28
SP020	29.92	-25.37	18.29	8.01	548.05	1.86	5.24	4.87	0.36	572.71	482.55	80.42	95.45
SP021	30.5	-31.7	25.80	9.17	543.24	1.80	6.63	6.32	0.30	4231.01	1370.83	9.84	30.36
SP022	30.62	-26.79	20.00	15.40	396.96	2.30	4.06	3.69	0.36	729.08	578.02	63.02	79.49
SP023	36.7	-26.42	20.00		528.82	1.71	5.01	4.66	0.35	747.30	592.50	60.09	75.79
SP024	18.41	-27.14	20.38	9.11	447.09	1.78	5.07	4.54	0.54	832.91	649.35	59.65	76.52
SP025	21.5	-31.69	23.77	12.15	557.66	2.78	3.84	3.56	0.28	1324.48	777.34	37.15	63.30
SP026	24.2	-30.51	22.53	11.76	586.51	2.77	4.07	3.66	0.41	943.83	640.029	51.54	76.00
SP027	25.67	-30.64	22.66	18.51	572.08	2.94	4.55	3.89	0.66	962.80	644.57	49.93	74.58
SP028	28.5	-32.19	24.31				4.47	3.95	0.52			30.99	57.86
SP029	21.78	-30.28	22.29	10.93	716.31	3.20	2.42	2.11	0.32	827.61	572.58	54.21	78.36
SP030	21.053	-29.50	21.46	12.98	644.20	2.65	3.93	3.56	0.37	754.57	554.38	63.77	86.80
SP031	31.31	-28.98	20.92	10.90	740.34	2.62	6.23	5.67	0.55	667.28	506.13	70.03	92.32
SP032	25.6	-30.17	22.17	10.76	591.31	2.45	4.66	4.11	0.55	906.04	633.07	55.62	79.61
SP033	26.64	-28.38	20.28				5.15	4.58	0.57			77.35	98.79
SP034	21.94	-30.67	22.70	8.61	668.23	2.81	5.25	4.80	0.46	948.51	632.78	49.50	74.20
SP035	24.5	-29.49	21.46		548.05	2.82	3.24	3.00	0.24	770.54	566.27	63.82	86.85

Sample name	C:N	$\delta^{13}C$ (‰)	Δ_{leaf} (‰)	Stomatal index (%)	Stomatal density (mm^{-2})	Pore length (µm)	*VLA* (mm/mm^2)	Parallel *VLA* (mm/mm^2)	Cross *VLA* (mm/mm^2)	Calc c_a (ppm) [b=27]	Calc c_a (ppm) [b=30]	iWUE (µmol/mol) [b=27]	iWUE (µmol/mol) [b=30]
SP036	17.95	-30.14	22.14				5.52	4.93	0.59			55.97	79.91
SP037	29.77	-29.13	21.07		649.00	3.05	4.13	3.75	0.38	677.57	509.56	68.25	90.75
SP038	29.85	-29.73	21.71									60.94	84.30
SP039	28.14	-29.97	21.96	9.82	644.20	2.81	4.32	3.87	0.45	816.25	579.39	57.99	81.69
SP040	29.92	-30.50	22.52				5.60	5.12	0.48			51.64	76.09
SP041	30	-31.05	23.10				3.68	2.89	0.80			44.94	70.17
SP042	24.75	-28.38	20.29	9.51	697.08	3.02	4.59	4.20	0.39	591.13	462.74	77.29	98.73
SP043	23.2	-29.97	21.96	12.33	663.43	2.94	4.37	3.67	0.70	800.92	568.60	58.01	81.72
SP044	24.56	-30.03	22.02				2.91	2.36	0.55			57.35	81.13
SP045	23	-29.05	20.99	7.34	471.13	2.75	3.90	3.33	0.57	746.43	564.00	69.22	91.61
SP046	22.41	-31.06	23.11	13.89	528.82	4.21	3.81	3.33	0.48	1000.03	639.33	44.76	70.02
SP047	29.62	-28.43	20.34									76.74	98.25
SP048	28.36	-30.27	22.27	11.05	649.00	3.19	5.13	4.65	0.49	840.48	582.46	54.45	78.57
SP049	26	-30.05	22.04	11.31	639.39	2.81				829.85	585.66	57.10	80.91
SP050	25.8	-29.96	21.95	13.43	697.08	3.26	4.86	4.33	0.53	771.9	548.52	58.16	81.85
SP051	19.95	-28.71	20.63	9.81	740.34	2.91	4.40	3.77	0.63	620.07	477.49	73.35	95.26
SP052	21.56	-29.69	21.67	9.82	538.43	2.65	3.55	2.78	0.77	819.67	594.27	61.44	84.74
SP053	26.067	-30.29	22.30	10.42	687.46	3.02	4.56	3.90	0.67	845.48	584.57	54.13	78.29

Sample name	C:N	$\delta^{13}C$ (‰)	Δ_{leaf} (‰)	Stomatal index (%)	Stomatal density (mm^{-2})	Pore length (μm)	*VLA* (mm/mm^2)	Parallel *VLA* (mm/mm^2)	Cross *VLA* (mm/mm^2)	Calc c_a (ppm) [b=27]	Calc c_a (ppm) [b=30]	iWUE (μmol/mol) [b=27]	iWUE (μmol/mol) [b=30]
SP054	29.69	-29.65	21.63	14.27	605.74	2.64	4.72	4.21	0.51	789.73	573.97	61.86	85.11
SP055	23	-29.75	21.72	11.01	673.04	3.19	5.36	4.79	0.57	747.23	539.59	60.76	84.14
SP056	20.71	-30.45	22.47	11.05	624.97	3.38	3.69	3.24	0.46	870.43	593.29	52.20	76.59
SP057	22.67	-28.99	20.93	12.12	706.69	2.74	3.65	3.12	0.53	666.25	505.12	69.93	92.24
SP058	23.33	-29.84	21.82	11.46	673.04	3.32	5.29	4.58	0.71	754.03	540.87	59.66	83.17
SP059	26.13	-33.61	25.81	11.71	557.66	2.76	4.64	4.23	0.41	3585.72	1154.68	13.72	42.62
SP060	27.07	-31.82	23.91	10.07	600.93	2.92	5.31	4.90	0.41	1336.55	767.85	35.56	61.89
SP061	36.64	-32.05	24.16	10.06	509.59	2.75				1544.86	850.73	32.69	59.36
SP062	49.38	-31.36	23.42	8.65	610.54	3.44	5.66	5.35	0.31	1103.52	679.88	41.20	66.88
SP063	43.11	-29.11	21.06				5.03	4.89	0.14			68.47	90.94
SP064	28.86	-30.95	22.99		644.20	3.22	4.23	3.78	0.46	989.36	641.00	46.17	71.26
SP065	29.15	-30.60	22.63	9.39	581.70	3.36	5.60	5.24	0.37	916.52	615.81	50.37	74.97
SP066	36.18	-32.99	25.15	8.08	509.59	2.61	5.13	4.68	0.45	2415.09	1042.62	21.28	49.29
SP067	37.36	-30.48	22.50		509.59	3.30	4.12	3.67	0.46	921.97	626.69	51.84	76.27
SP068	22.88	-28.09	19.99	9.70	673.04	2.76	4.52	4.01	0.51	582.31	462.02	80.79	101.82
SP069	34.17	-28.79	20.72	11.80	798.03	2.77	4.64	4.11	0.53	627.30	480.82	72.31	94.34
SP070	45.75	-28.44	20.35	10.80	730.73	2.31	4.76	4.11	0.65	633.32	494.38	76.59	98.12
SP071	34.2	-27.99	19.88	10.17	740.34	2.83	5.69	5.23	0.45	558.93	445.38	81.96	102.86

Sample name	C:N	$\delta^{13}C$ (‰)	Δ_{leaf} (‰)	Stomatal index (%)	Stomatal density (mm^{-2})	Pore length (μm)	*VLA* (mm/mm^2)	Parallel *VLA* (mm/mm^2)	Cross *VLA* (mm/mm^2)	Calc c_a (ppm) [b=27]	Calc c_a (ppm) [b=30]	iWUE (μmol/mol) [b=27]	iWUE (μmol/mol) [b=30]
SP072	32.55	-30.04	22.03	12.23	735.54	2.95	5.77	5.24	0.53	793.67	560.47	57.20	81.00
SP073	55.57	-31.32	23.39	10.10	701.89	2.85	5.06	4.67	0.38	1110.72	687.32	41.60	67.23
SP074	56.57	-30.50	22.52	12.49	711.50	3.30	5.98	5.68	0.31	861.77	584.87	51.64	76.09
SP075	23.76	-32.30	24.42	10.67	716.31	2.86	5.89	5.46	0.43	1546.13	809.67	29.71	56.73
SP076	31.58	-30.38	22.39	10.52	706.69	3.27	6.06	5.56	0.50	841.93	577.53	53.05	77.33
SP077	25.44	-32.41	24.54	10.14	668.23	3.02	4.07	3.56	0.52	1623.59	828.24	28.31	55.49
SP078	29.62	-31.31	23.37	10.64	620.16	3.17	3.83	3.44	0.38	1103.77	684.49	41.80	67.40
SP079	42.44	-31.22	23.27	9.92	605.74	2.70	4.71	4.34	0.37	1128.24	707.95	42.91	68.38
SP080	30.69	-30.42	22.43	9.31	639.39	2.82	5.83	5.55	0.28	898.11	614.01	52.60	76.94
SP081	27.36	-31.27	23.33	8.32	653.81	2.41	4.53	4.11	0.42	1162.37	724.60	42.29	67.83
SP082	25.25	-29.59	21.56	11.21	649.00	2.83	5.61	5.10	0.51	750.68	547.99	62.62	85.79
SP083	38.4	-30.05	22.05		576.89	2.98	5.54	5.11	0.43	835.55	589.42	57.04	80.85
SP084	32.83	-29.98	21.97	9.07	730.73	2.80	5.15	4.66	0.49	793.70	563.12	57.92	81.63
SP085	22.41	-29.32	21.27	9.61	610.54	3.08	5.81	5.34	0.47	707.17	525.63	65.94	88.72
SP086	38.8	-31.86	23.96	10.96	706.69	3.01	4.67	4.13	0.54	1297.93	740.11	35.02	61.42
SP087	31.15	-29.70	21.68				3.03	1.71	1.33			61.28	84.60
SP088	31.75	-30.52	22.54	10.53	836.49	2.90	5.91	5.46	0.45	865.09	585.68	51.33	75.81
SP089	37.6	-30.80	22.83				3.30	2.07	1.24			47.99	72.87

Sample name	C:N	$\delta^{13}C$ (‰)	Δ_{leaf} (‰)	Stomatal index (%)	Stomatal density (mm^{-2})	Pore length (µm)	*VLA* (mm/mm^2)	Parallel *VLA* (mm/mm^2)	Cross *VLA* (mm/mm^2)	Calc c_a (ppm) [b=27]	Calc c_a (ppm) [b=30]	iWUE (µmol/mol) [b=27]	iWUE (µmol/mol) [b=30]
SP090	28.071	-30.02	22.02	8.97	586.51	2.66	5.47	5.12	0.36	854.12	603.80	57.36	81.14
SP091	28.64	-30.16	22.17	9.53	663.43	3.12	5.66	5.24	0.43	819.22	572.61	55.67	79.65
SP092	34.09	-28.25	20.15	10.69	754.77	3.06	5.44	5.11	0.34	566.60	446.30	78.87	100.13
SP093	28.31	-31.78	23.87				3.54	2.32	1.23			35.99	62.28
SP094	25.53	-28.78	20.71				3.84	2.30	1.55			72.41	94.43
SP095	27.71	-28.09	19.98	10.22	721.11	2.74	5.34	4.89	0.45	572.56	454.33	80.82	101.85
SP096	22.18	-29.54	21.51		562.47	2.64				784.40	574.70	63.27	86.36
SP097	23.73	-29.39	21.35	10.50	682.66	2.51	4.82	4.22	0.60	735.99	544.67	65.11	87.98
SP098	23.33	-30.73	22.76	8.11	576.89	3.13	4.67	4.33	0.34	961.49	637.65	48.80	73.58
SP099	32.58	-29.37	21.33	8.90	649.00	2.78	4.85	4.54	0.30	721.57	534.53	65.30	88.15
SP100	22.35	-32.36	24.48	7.85	552.85	3.01	5.79	5.46	0.33	1649.73	852.87	29.01	56.11
SP101	24.87	-28.38	20.29	10.26	605.74	2.61	5.32	4.69	0.63	630.40	493.48	77.29	98.73
SP102	26.57	-30.56	22.59	6.87	413.44	3.05	3.04	1.86	1.19	1011.56	682.23	50.84	75.39
SP103	29.62	-33.32	25.50	8.38	456.71	3.49	5.53	5.23	0.30	2786.28	1050.70	17.24	45.72
SP104	23.71	-31.04	23.09				2.83	1.70	1.12			44.98	70.21
SP105	24.73	-32.57	24.70	9.76	528.82	2.81	4.51	4.11	0.40	1867.64	917.45	26.46	53.86
SP106	19.7	-29.71	21.68	12.68	947.06	3.12	5.46	4.99	0.46	700.23	507.06	61.23	84.56
SP107	21.44	-30.22	22.22				3.24	1.90	1.35			54.99	79.05

Sample name	C:N	$\delta^{13}C$ (‰)	Δ_{leaf} (‰)	Stomatal index (%)	Stomatal density (mm^{-2})	Pore length (µm)	*VLA* (mm/mm^2)	Parallel *VLA* (mm/mm^2)	Cross *VLA* (mm/mm^2)	Calc c_a (ppm) [b=27]	Calc c_a (ppm) [b=30]	iWUE (µmol/mol) [b=27]	iWUE (µmol/mol) [b=30]
SP108	26.07	-29.45	21.41				4.35	2.64	1.72			64.38	87.34
SP109	27.07	-29.85	21.83	9.52	745.15	2.60	4.77	4.00	0.77	783.12	561.19	59.50	83.03
SP110	27.54	-28.02	19.91	11.86	730.73	2.76	4.45	3.91	0.54	563.78	448.82	81.70	102.63
SP111	22.87	-28.97	20.91	12.53	759.57	2.24	4.65	4.01	0.64	688.36	522.50	70.18	92.46
SP112	28.85	-31.04	23.09				5.52	5.11	0.41			45.02	70.24
SP113	27.25	-29.61	21.58		754.77	2.10				791.03	576.89	62.46	85.64
SP114	35.1	-30.12	22.12									56.16	80.08
SP115	26	-30.45	22.47	9.80	749.96	2.68				884.92	603.12	52.19	76.58
SP116	29	-29.79	21.77	8.90	600.93	2.75	5.17	4.56	0.62	800.51	576.34	60.26	83.70
SP117	31.08	-30.80	22.84	8.82	524.01	2.82	5.94	5.36	0.59	1034.80	681.03	47.91	72.80
SP118	35.82	-29.36	21.32	11.02	706.69	2.73	5.34	4.89	0.46	711.34	527.35	65.44	88.27
SP119	29.46	-27.54	19.40	10.11	740.34	2.89	4.06	3.56	0.50	519.81	422.13	87.50	107.75
SP120	32.4	-28.47	20.39		600.93	2.48	5.68	5.35	0.33	653.56	509.32	76.18	97.75
SP121	29.62	-30.55	22.57				4.58	2.99	1.60			50.96	75.49
SP122	27.79	-29.53	21.50	8.32	548.05	2.68	5.36	5.02	0.34	785.68	575.89	63.35	86.43
SP123	29.23	-32.51	24.64				6.58	6.22	0.36			27.19	54.50
SP124	30.15	-30.46	22.47									52.14	76.53
SP125	30	-31.32	23.38									41.66	67.28

Sample name	C:N	$\delta^{13}C$ (‰)	Δ_{leaf} (‰)	Stomatal index (%)	Stomatal density (mm^{-2})	Pore length (μm)	*VLA* (mm/mm^2)	Parallel *VLA* (mm/mm^2)	Cross *VLA* (mm/mm^2)	Calc c_a (ppm) [b=27]	Calc c_a (ppm) [b=30]	iWUE (μmol/mol) [b=27]	iWUE (μmol/mol) [b=30]
SP126	33.91	-30.91	23.00		596.12	2.85				1027.58	668.30	46.58	71.62
SP127	30.2	-29.54	21.50	10.49	533.62	2.54	3.91	3.56	0.35	807.01	591.31	63.29	86.37
SP128	30.13	-29.47	21.43				4.22	2.64	1.59			64.12	87.10
SP129	32.46	-30.08	22.07		749.96	3.00	5.67	5.46	0.20	793.43	558.67	56.76	80.61
SP130	27.23	-29.74	21.72				2.47	1.51	0.96			60.86	84.23
SP131	31.87	-28.63	20.55		528.82	2.89				661.68	511.50	74.25	96.05
SP132	26.76	-32.68	24.82	9.16	524.01	2.87	5.09	4.34	0.76	1966.27	937.34	25.11	52.67
SP133	26.83	-31.54	23.61	8.14	581.70	3.06	5.89	5.45	0.44	1210.62	727.25	39.01	64.94
SP134	25.39	-30.02	22.01		509.59	0.58	4.87	4.56	0.31	2581.84	1826.26	57.45	81.22
SP135	26.94	-30.53	22.55				4.03	3.66	0.37			51.29	75.78
SP136	25.94	-31.43	23.50	10.64	528.82	3.35				1169.86	713.52	40.31	66.08
SP137	28.12	-31.15	23.20									43.75	69.12
SP138	29.38	-28.29	20.19		735.54	2.85	5.67	5.21	0.46	583.10	458.53	78.44	99.75
SP139	26.94	-31.16	23.21	12.16	697.08	3.07	4.82	4.24	0.58	1041.69	658.38	43.61	69.00
SP140	30.93	-29.87	21.85	9.92	634.58	2.87	4.11	3.69	0.43	794.85	568.76	59.26	82.82
SP141	29.13	-29.26	21.22				4.52	2.84	1.68			66.61	89.30
SP142	27.72	-28.51	20.42	10.62	730.73	2.87	5.04	4.44	0.60	603.81	469.71	75.75	97.37
SP143	27.76	-28.84	20.78				4.34	2.60	1.74			71.68	93.78

Sample name	C:N	$\delta^{13}C$ (‰)	Δ_{leaf} (‰)	Stomatal index (%)	Stomatal density (mm^{-2})	Pore length (μm)	*VLA* (mm/mm^2)	Parallel *VLA* (mm/mm^2)	Cross *VLA* (mm/mm^2)	Calc c_a (ppm) [b=27]	Calc c_a (ppm) [b=30]	iWUE (μmol/mol) [b=27]	iWUE (μmol/mol) [b=30]
SP144	25.24	-29.57	21.54	10.63	725.92	2.54	5.69	5.00	0.69	750.81	548.99	62.92	86.04
SP145	25.63	-28.82	20.75		629.77	3.25	5.16	4.90	0.26	635.84	486.62	71.97	94.04
SP146	23.08	-28.50	20.42									75.80	97.42
SP147	21.36	-29.10	21.04	10.12	629.77	3.19	6.23	5.68	0.55	669.43	504.41	68.64	91.10
SP148	23.44	-27.86	19.74	10.02	673.04	2.88	5.94	5.35	0.58	555.70	445.46	83.64	104.34
SP149	28.41	-29.19	21.14		735.54	2.73				685.51	513.50	67.46	90.05
SP150	25.5	-29.38	21.34	11.79	586.51	3.14	4.65	4.23	0.42	718.26	531.89	65.23	88.09
SP151	23.2	-28.85	20.78				5.74	5.33	0.41			71.61	93.72
SP152	32.67	-29.99	21.99	7.85	543.24	2.79	4.60	4.22	0.39	854.01	605.24	57.74	81.48
SP153	38	-30.23	22.23	11.15	673.04	2.84	5.28	5.01	0.27	849.52	590.53	54.88	78.95
SP154	22.29	-30.17	22.18		716.31	2.64				844.41	589.71	55.55	79.54
SP155	28.56	-28.95	20.88				3.64	2.28	1.36			70.44	92.68
SP156	29.25	-29.20	21.15		745.15	2.67	4.57	4.00	0.58	688.23	515.19	67.32	89.93
SP157	32.38	-27.12	18.96				4.52	2.87	1.65			92.55	112.21
SP158	22.62	-29.69	21.67				2.40	1.31	1.09			61.41	84.71
SP159	26.47	-30.10	22.09		524.01	2.86				875.71	615.56	56.50	80.38
SP160	26.22	-33.36	25.55				3.78	2.20	1.58			16.71	45.25
SP161	21.04	-29.57	21.54	10.10	807.65	2.67	4.68	4.23	0.45	725.78	530.48	62.84	85.98

Sample name	C:N	$\delta^{13}C$ (‰)	Δ_{leaf} (‰)	Stomatal index (%)	Stomatal density (mm^{-2})	Pore length (μm)	*VLA* (mm/mm^2)	Parallel *VLA* (mm/mm^2)	Cross *VLA* (mm/mm^2)	Calc c_a (ppm) [b=27]	Calc c_a (ppm) [b=30]	iWUE (μmol/mol) [b=27]	iWUE (μmol/mol) [b=30]
SP162	18.56	-29.96	21.95	9.66	475.94	2.76	4.38	3.90	0.48	882.49	627.26	58.20	81.88
SP163	22.62	-30.33	22.34									53.68	77.89
SP164	32.57	-30.69	22.72				3.71	2.30	1.42			49.27	73.99
SP165	28.94	-29.32	21.28		576.89	3.78	4.99	4.33	0.66	683.26	507.65	65.86	88.65
SP166	30.19	-28.33	20.23	10.30	788.42	2.49	6.03	5.23	0.81	598.76	469.91	77.93	99.30
SP167	29.27	-29.03	20.97	9.95	663.43	2.35	5.11	4.79	0.31	711.77	538.43	69.46	91.82
SP168	25.75	-30.90	22.94									46.79	71.80
SP169	40.08	-32.61	24.75	9.37	581.70	3.06	5.28	4.90	0.38	1818.76	883.99	25.97	53.43
SP170	34.38	-32.78	24.93									23.84	51.55
SP171	27.13	-29.68	21.66		543.24	2.50	3.94	3.56	0.38	831.73	603.26	61.51	84.80
SP172	26.5	-29.37	21.33				5.94	5.34	0.60			65.33	88.18
SP173	39.82	-29.18	21.13		538.43	3.08	4.76	4.33	0.42	710.50	532.58	67.59	90.17
SPa001	15.67	-27.95	20.37		528.82	2.91	5.60	5.42	0.18	640.64	499.65	68.96	88.41
SPa002	16.08	-30.24	22.31	10.48	865.34	2.84	5.71	5.32	0.39	820.01	566.42	54.00	78.17
SPa003	15.2	-30.37	22.45	9.99	605.74	3.06	6.18	5.88	0.31	891.63	608.62	52.39	76.75
SPa004	16.96	-28.76	21.16	8.18	711.50	2.79	5.96	5.55	0.41	687.76	514.738874	61.39	82.03
SPa005	12.72	-26.11	18.68	9.74	706.69	3.17	6.40	6.11	0.29	468.34	389.91	83.05	99.76
SPa006	19.3	-25.42	18.34	8.71	629.77	2.93	5.38	5.00	0.37	469.01	394.56	79.94	95.02

Sample name	C:N	$\delta^{13}C$ (‰)	Δ_{leaf} (‰)	Stomatal index (%)	Stomatal density (mm^{-2})	Pore length (µm)	*VLA* (mm/mm^2)	Parallel *VLA* (mm/mm^2)	Cross *VLA* (mm/mm^2)	Calc c_a (ppm) [*b*=27]	Calc c_a (ppm) [*b*=30]	iWUE (µmol/mol) [*b*=27]	iWUE (µmol/mol) [*b*=30]
SPa007	16.42				495.17	3.07	6.16	5.88	0.28				
SPa008	13.64			10.40	759.57	2.56	6.69	6.43	0.25				
SPa009	16.83			11.11	668.23	3.11	5.10	4.65	0.45				
SPa010	18				557.66	3.10	5.10	4.77	0.33				
SPa011	21.06				591.31	2.63	6.76	6.34	0.42				
CU001	20.4	-27.37	20.29	8.42	115.38	14.07	5.76	5.45	0.31	601.09	470.56	63.39	80.97
CU002				9.17	113.86								
CU003	31.3	-27.76	21.02	5.04	62.50	14.73	5.08	4.80	0.28	784.26	591.73	54.01	71.58
CU004	15.62	-31.71	24.88	6.51	91.34	19.65	5.03	4.72	0.31	1866.30	874.29	19.90	42.48
CU005				11.35	183.09								
CU006													
CU007	17.09	-28.6	21.35	13.47	225.95	12.62				649.06	480.17	55.36	74.84
CU008	34.22	-28.64	21.98	5.69	100.01	4.61				1298.59	920.50	44.70	63.06
CU009	18.05	-30.66	23.53	5.21	81.73	13.11	4.51	4.21	0.30	1290.52	784.46	34.06	56.03
CU010	12.12	-29.65	22.45	7.20	124.99	9.83	5.96	5.47	0.49	957.41	653.46	44.58	65.32
CU011	25.64	-26.36	19.55	10.77	100.96	21.35				513.50	414.63	67.07	83.07
CU012	30.01	-28.40	21.07				3.66	3.31	0.35			59.15	78.66
CU013	46.43	-28.65	21.35									56.44	76.26

Sample name	C:N	$\delta^{13}C$ (‰)	Δ_{leaf} (‰)	Stomatal index (%)	Stomatal density (mm^{-2})	Pore length (µm)	*VLA* (mm/mm^2)	Parallel *VLA* (mm/mm^2)	Cross *VLA* (mm/mm^2)	Calc c_a (ppm) [b=27]	Calc c_a (ppm) [b=30]	iWUE (µmol/mol) [b=27]	iWUE (µmol/mol) [b=30]
CU014	46.46	-25.48	18.02	5.31	52.88	18.37	4.72	4.57	0.15	518.00	439.78	89.61	105.55
CU015	46.41	-28.12	20.73		48.07	34.82	5.12	4.91	0.20	637.03	488.18	63.14	82.39
CU016	34.35	-32.23	25.44	5.38	67.30	15.94	4.23	3.90	0.33	2868.11	1112.84	14.70	37.89
CU017	51.37	-31.51	25.61		81.73	17.61	5.02	4.66	0.36	2977.54	1068.04	11.26	31.40
CU018	38.02	-30.37	24.24	5.93	67.30	21.55	4.50	4.14	0.37	1501.39	814.35	23.31	42.98
CU019	54.30	-25.85	19.50									63.10	77.98
CU020	45.21	-27.55	21.27				4.92	4.57	0.35			48.53	65.27
CU021	37.62	-30.22	22.64	9.09	72.11	34.90	4.37	4.12	0.25	853.90	572.93	46.29	68.99
CU022	31.52	-28.97	21.33		62.50	21.91	3.95	3.58	0.37	738.70	547.32	60.25	81.31
CU023	43.44	-27.423	19.71		62.50	24.23	5.89	5.70	0.20	561.79	450.86	77.44	96.49
CU024	29.28	-30.58	23.02	8.18	62.50	29.78	4.94	4.59	0.35	984.04	635.452	42.25	65.42
CU025	12.6	-30.55	22.96									43.34	66.65
CU026	16.23	-28.98	21.86	6.61	72.11	21.79	4.52	4.19	0.33	792.76	566.88	49.62	69.39
CU027	25.76923077	-28.11944	21.1542867									54.45437139	72.74389818
CU028	13.31	-27.77	20.05		105.76	22.20	8.42	8.14	0.27	541.84	428.74	74.17	93.74
CU029	21.44	-26.99	19.23									82.90	101.44
CU030	25	-26.53					4.83	4.42	0.40				

Sample name	C:N	$\delta^{13}C$ (‰)	Δ_{leaf} (‰)	Stomatal index (%)	Stomatal density (mm^{-2})	Pore length (µm)	*VLA* (mm/mm^2)	Parallel *VLA* (mm/mm^2)	Cross *VLA* (mm/mm^2)	Calc c_a (ppm) [b=27]	Calc c_a (ppm) [b=30]	iWUE (µmol/mol) [b=27]	iWUE (µmol/mol) [b=30]
CU031	11.60	-31.67	24.12									31.04	55.98
CU032	22.87						4.06	3.90	0.16				
PD001	61.33			14.99	340.03								
PD002	68.2			2.96	187.49	2.92				228.65			
PD003				16.95	496.97								
PD004				5.74	121.55								
PD005													
PD006				9.48	216.94								
PD007				10.93	296.95								
PD008													
PD009													
PD010													
PD011													
PD012	34.2	-25.82	18.86									74.50	90.02
PD013	21.47	-27.21	20.44		379.79	3.69	9.66	9.31	0.35	658.21	511.63	59.20	76.17
PD014	24.375	-25.84	19.47									63.76	78.71
PD015	19.94	-25.70	19.46	12.73	427.86	2.78	4.33	4.12	0.21	604.67	490.04	61.79	76.24
PD016	26.57	-26.54	20.38		389.40	3.57	6.20	5.90	0.30	651.15	507.61	53.27	68.33

Sample name	C:N	$\delta^{13}C$ (‰)	Δ_{leaf} (‰)	Stomatal index (%)	Stomatal density (mm^{-2})	Pore length (µm)	*VLA* (mm/mm^2)	Parallel *VLA* (mm/mm^2)	Cross *VLA* (mm/mm^2)	Calc c_a (ppm) [b=27]	Calc c_a (ppm) [b=30]	iWUE (µmol/mol) [b=27]	iWUE (µmol/mol) [b=30]
PD017	25	-25.72	19.48		302.87	3.30	5.47	5.22	0.25	635.17	514.41	61.68	76.16
PD018	27.62	-25.36	19.02		389.40	3.54	5.65	5.33	0.32	541.88	446.04	65.97	80.15
PD019	35.1	-26.48	20.15									56.91	72.26
PD020	15.55	-28.20	21.95		456.71	2.91				874.65	621.52	42.44	59.72
PD021	17.43	-25.53	19.32									62.16	76.31
PD022		-27.90	21.80									42.11	58.61
PD023	18.90	-27.53	21.47		269.22	3.46	6.67	6.13	0.54	889.48	653.19	43.75	59.58
PD024	26.93	-26.17	19.74		389.40	3.45	5.82	5.56	0.25	600.19	481.16	62.38	77.81
PD025	30.08	-25.64	18.57	10.67	413.44	3.82	5.43	5.21	0.22	494.72	413.36	78.23	93.63
Acowri. 9930		-28.80	22.40				5.00	4.49	0.51			38.67	56.38
Acwr.4 333		-26.72	20.48				5.50	4.90	0.60			55.47	71.50
Acoewr ig.3070		-27.24	20.98									51.37	67.94
Acme.2 361		-28.55	21.75	6.05	116.93		8.65	8.30	0.36			48.02	66.62
Aimi.13 74		-29.47	21.92									54.17	76.05
Arca.76 53		-27.05	20.76				5.26	4.83	0.43			53.01	69.29

Sample name	C:N	$\delta^{13}C$ (‰)	Δ_{leaf} (‰)	Stomatal index (%)	Stomatal density (mm^{-2})	Pore length (µm)	*VLA* (mm/mm^2)	Parallel *VLA* (mm/mm^2)	Cross *VLA* (mm/mm^2)	Calc c_a (ppm) [*b*=27]	Calc c_a (ppm) [*b*=30]	iWUE (µmol/mol) [*b*=27]	iWUE (µmol/mol) [*b*=30]
Armo.28687		-31.16	25.10				2.22	1.88	0.34			16.17	36.86
Aral.6208		-26.41	20.09									59.70	75.57
Aren.6677		-30.10	24.00				4.12	3.65	0.47			25.88	45.67
Armi.10578		-28.22	21.96				5.96	5.50	0.46			43.21	60.86
Arpi.34257		-29.30	23.17				4.78	4.43	0.35			32.75	51.56
Asma.80		-33.05	26.95									0.48	23.74
Asme.10253		-28.11	21.85				4.58	4.04	0.54			44.29	61.86
Atco.4970-a		-31.52	25.47				7.27	5.61	1.66			13.06	34.09
Bacbar.16890		-30.18	24.12				2.64	2.02	0.61			24.69	44.54
Baco.16745		-32.64	26.73				5.23	4.72	0.51			2.31	24.78
Baga.10045		-30.22	31.16										
Bagu.16996		-31.20	25.21	8.67	170.78		5.07	4.49	0.58			15.39	36.33
Bama.4842		-29.53	23.29									32.59	52.05

Sample name	C:N	$\delta^{13}C$ (‰)	Δ_{leaf} (‰)	Stomatal index (%)	Stomatal density (mm^{-2})	Pore length (µm)	*VLA* (mm/mm^2)	Parallel *VLA* (mm/mm^2)	Cross *VLA* (mm/mm^2)	Calc c_a (ppm) [*b*=27]	Calc c_a (ppm) [*b*=30]	iWUE (µmol/mol) [*b*=27]	iWUE (µmol/mol) [*b*=30]
Bame.1373		-26.73	20.42	6.30	163.09							56.01	72.00
Bapl.3379B		-26.72	19.49									73.76	91.12
Brabra.2917		-24.23	17.79	6.61	140.01		9.06	8.48	0.57			79.223	92.74
Brca.16045		-26.92	20.52	13.22	370.80		6.82	6.40	0.42			56.87	73.44
Brdu.11759		-26.57	19.36				10.22	9.42	0.80			73.78	90.71
Brbe.3797		-24.86	17.89									83.35	97.81
Brpi.718		-25.33	18.03									87.06	102.55
Brpr.13397		-23.10	16.46				11.31	10.08	1.22			92.99	105.46
Brsa.9654		-26.62	20.30				5.84	5.25	0.58			57.56	73.58
Buve.9197		-34.66	28.79	5.47	104.62		4.71	4.26	0.45			-17.34	10.38
Buca.21339		-23.71	17.27				7.96	6.80	1.16			83.70	96.67
Buya.24939		-26.79	19.69				7.44	6.32	1.12			69.70	86.78
Caac.33062		-23.97	17.54				4.11	3.40	0.71			81.71	95.00

Sample name	C:N	$\delta^{13}C$ (‰)	Δ_{leaf} (‰)	Stomatal index (%)	Stomatal density (mm^{-2})	Pore length (μm)	*VLA* (mm/mm^2)	Parallel *VLA* (mm/mm^2)	Cross *VLA* (mm/mm^2)	Calc c_a (ppm) [b=27]	Calc c_a (ppm) [b=30]	iWUE (μmol/mol) [b=27]	iWUE (μmol/mol) [b=30]
Caba.2287		-30.83	24.84				7.19	6.39	0.80			18.31	38.62
Caca.8208		-26.94	20.72									53.02	69.18
Cade.198		-26.65	20.43				6.26	5.68	0.58			55.58	71.47
Cadie.7275		-30.21	24.16				6.73	6.32	0.41			24.00	43.56
Cadi.78628		-28.91	22.80									35.55	53.81
Caer.24380		-29.73	23.56				4.07	3.37	0.70			29.57	48.90
Caer.27781		-30.14	24.03									25.56	45.38
Caex.8707		-32.06	26.11									7.49	28.98
Dagr.445		-29.56	23.47									30.28	49.47
Cafl.27310		-34.38	28.53				5.65	5.10	0.55			-13.17	11.19
Caja.8095		-36.35	30.69									-31.16	-5.14
Dalo.4412		-30.31	24.25									23.35	43.15
Cama.14133		-27.24	21.09				5.63	4.69	0.94			49.01	65.22

Sample name	C:N	$\delta^{13}C$ (‰)	Δ_{leaf} (‰)	Stomatal index (%)	Stomatal density (mm^{-2})	Pore length (µm)	*VLA* (mm/mm^2)	Parallel *VLA* (mm/mm^2)	Cross *VLA* (mm/mm^2)	Calc c_a (ppm) [b=27]	Calc c_a (ppm) [b=30]	iWUE (µmol/mol) [b=27]	iWUE (µmol/mol) [b=30]
Came.743		-27.04	20.82				9.85	8.83	1.01			53.07	69.59
Calmc.15515a		-24.75	18.37				6.61	5.98	0.63			73.63	87.59
Calmi.227		-27.91	21.63				7.41	6.72	0.69			46.27	63.67
Damo.783		-27.80	21.62									46.21	63.53
Cate.8563		-27.62	21.21				6.42	5.08	1.34			51.70	69.28
Cabl.251		-27.39	21.09				5.86	5.49	0.37			50.71	67.48
Cacl.1135		-27.34	21.14				3.25	2.58	0.67			50.33	67.18
Cami.4811		-29.82	23.73				6.85	6.63	0.22			27.78	47.06
Caru.10826		-26.99	20.66									54.33	70.68
Caur.24789		-30.45	24.32									23.05	43.14
Ceal.10191		-25.05	18.21									79.90	94.59
Cequ.10191		-24.17	17.29									88.19	101.91
Chqu.1929		-31.13	25.11				6.70	6.05	0.65			16.17	36.95

Sample name	C:N	$\delta^{13}C$ (‰)	Δ_{leaf} (‰)	Stomatal index (%)	Stomatal density (mm^{-2})	Pore length (µm)	*VLA* (mm/mm^2)	Parallel *VLA* (mm/mm^2)	Cross *VLA* (mm/mm^2)	Calc c_a (ppm) [b=27]	Calc c_a (ppm) [b=30]	iWUE (µmol/mol) [b=27]	iWUE (µmol/mol) [b=30]
Chel.10108		-28.97	22.71									37.47	56.21
Cher.3443		-33.18	27.20									-1.75	21.17
Chgr.6853		-32.48	26.51				5.26	4.83	0.43			4.15	26.28
Chne.2943		-32.91	26.91				3.49	3.03	0.46			0.74	23.37
Chob.402		-34.31	28.36				3.38	2.98	0.40			-11.93	12.75
Chco.49553		-31.46	24.77									20.82	43.08
Chpo.12137		-33.33	27.42				5.10	4.85	0.25			-3.59	19.65
Chra.008		-30.91	24.83				4.90	4.51	0.39			18.73	39.40
Chse.8075		-31.77	25.66				5.11	4.77	0.34			11.66	33.42
Chdi.221		-36.52	29.83				3.14	2.36	0.78			-27.52	1.50
Coar.1766		-26.44	20.12									59.69	75.65
Conu.902		-26.81	20.57									54.68	70.80
Crar.9175		-31.43	24.33									26.53	49.76

Sample name	C:N	$\delta^{13}C$ (‰)	Δ_{leaf} (‰)	Stomatal index (%)	Stomatal density (mm^{-2})	Pore length (μm)	*VLA* (mm/mm^2)	Parallel *VLA* (mm/mm^2)	Cross *VLA* (mm/mm^2)	Calc c_a (ppm) [*b*=27]	Calc c_a (ppm) [*b*=30]	iWUE (μmol/mol) [*b*=27]	iWUE (μmol/mol) [*b*=30]
Crba.158		-33.36	26.52									4.63	29.67
Crycoo.162		-28.72	21.62									51.96	71.45
Daac.781		-28.51	22.36									39.81	57.88
Dech.3196		-29.10	22.88									35.31	53.88
Demy.16728		-27.55	21.35									48.48	65.54
Depo.50		-29.10	22.77									35.54	53.65
Gama.3759		-29.79	23.70									28.03	47.28
Gede.320		-32.45	26.29									6.29	28.92
Gein.16748		-30.94	24.93									17.79	38.45
Geap.9716		-30.47	24.20									25.11	45.89
Heca.14907		-31.50	25.47									13.08	34.13
Heel.218		-28.67	22.52									38.47	56.73
Irco.5739		-27.93	21.74									44.72	62.01

Sample name	C:N	$\delta^{13}C$ (‰)	Δ_{leaf} (‰)	Stomatal index (%)	Stomatal density (mm^{-2})	Pore length (μm)	*VLA* (mm/mm^2)	Parallel *VLA* (mm/mm^2)	Cross *VLA* (mm/mm^2)	Calc c_a (ppm) [b=27]	Calc c_a (ppm) [b=30]	iWUE (μmol/mol) [b=27]	iWUE (μmol/mol) [b=30]
Koec.64		-29.54	23.45									30.00	48.85
Lifo.17347		-32.23	26.23									6.58	28.37
Lipe.24940		-28.72	22.50									43.70	64.27
Lisa.34149		-26.02	19.72									62.25	77.60
Mesa.999		-25.92	19.64									63.23	78.58
Nifru.6785		-25.11	18.75									71.03	85.52
Orru.975		-29.65	23.56									29.59	48.88
Orsy.5568		-26.06	19.78									61.41	76.75
Phou.28426		-27.15	20.89									52.62	69.27
Pipa.21619		-36.78	30.70										
Prka.10466		-26.43	20.12									58.66	74.37
Regr.4990		-33.65	27.73									-6.24	17.05
Sam.8700		-27.57	21.38									48.23	65.32

Sample name	C:N	$\delta^{13}C$ (‰)	Δ_{leaf} (‰)	Stomatal index (%)	Stomatal density (mm^{-2})	Pore length (μm)	*VLA* (mm/mm^2)	Parallel *VLA* (mm/mm^2)	Cross *VLA* (mm/mm^2)	Calc c_a (ppm) [b=27]	Calc c_a (ppm) [b=30]	iWUE (μmol/mol) [b=27]	iWUE (μmol/mol) [b=30]
Sami.454		-30.68	24.57									21.03	41.52
Sapu.22046		-27.05	20.54									57.12	73.85
Saya.3103		-26.96	20.64									54.58	70.90
Syfl.43038		-29.04	21.95									48.73	68.61
Trca.40637		-25.50	18.34									82.61	98.18
Wade.30554		-28.45	22.22									41.18	59.19

Supplemental Table 3.3: Climate data for each palm sample.

Sample name	MAP (mm/year)	MAT (°C)	VPD (hPa)	c_a (ppm)	$\delta^{13}CO_2$ (‰)
SP001	1138.85	25.47	9.23	294.6	-6.72
SP002	1446.94	22.59	8.81	309.6	-6.93
SP003	1361.05	21.42	10.19	384.02	-8.26
SP004	1400.55	18.83	7.06	366.84	-8.03
SP005	1321.68	19.13	7.46	355.7	-7.86
SP006	1137.65	25.46	9.24	310.5	-6.95
SP007	1334.19	19.02	7.42	337.3	-7.61
SP008	1332.29	19.28	6.16	323.9	-7.32
SP009	1203.04	19.73	6.65	298.3	-6.8
SP010	1138.85	25.47	9.23	289.6	-6.68
SP011	495.76	23.92	16.19	296.2	-6.74
SP012	1312.08	19.43	7.92	330.19	-7.4
SP013	1501.18	18.03	6.3	296	-6.72
SP014	1402.18	23.51	10.63	356.54	-7.85
SP015	1382	25.37	6.68	297	-6.76
SP016	1372.56	22.55	8.17	346.35	-7.71
SP017	1342.55	24.03	9.41	325.68	-7.32
SP018	1398.01	22.01	7.75	306.2	-6.87
SP019	1619.52	25.12	9.72	307.6	-6.9
SP020	1268.45	19.4	6.75	333.84	-7.54
SP021	1501.18	18.03	6.3	296	-6.72
SP022	1332.29	19.28	6.16	325.68	-7.32
SP023	1348.01	22.9	10.49	310.5	-6.95
SP024	1444.88	21.03	9.21	325.68	-7.32
SP025	1217.04	17.41	8.57	416.45	-8.67

Sample name	MAP (mm/year)	MAT (°C)	VPD (hPa)	c_a (ppm)	$\delta^{13}CO_2$ (‰)
SP026	1217.04	17.41	8.57	416.45	-8.67
SP027	1217.04	17.41	8.57	416.45	-8.67
SP028	1553.04	17.55	8.07	416.45	-8.67
SP029	1563.19	17.93	7.61	416.45	-8.67
SP030	1485.49	17.93	6.3	416.45	-8.67
SP031	1485.49	17.93	6.3	416.45	-8.67
SP032	1485.49	17.93	6.3	416.45	-8.67
SP033	1485.49	17.93	6.3	416.45	-8.67
SP034	1383.94	17.77	6.9	416.45	-8.67
SP035	1383.94	17.77	6.9	416.45	-8.67
SP036	1383.94	17.77	6.9	416.45	-8.67
SP037	1383.94	17.77	6.9	416.45	-8.67
SP038	1383.94	17.77	6.9	416.45	-8.67
SP039	1383.94	17.77	6.9	416.45	-8.67
SP040	1383.94	17.77	6.9	416.45	-8.67
SP041	1383.94	17.77	6.9	416.45	-8.67
SP042	1383.94	17.77	6.9	416.45	-8.67
SP043	1441.19	17.95	6.68	416.45	-8.67
SP044	1441.19	17.95	6.68	416.45	-8.67
SP045	1441.19	17.95	6.68	416.45	-8.67
SP046	1441.19	17.95	6.68	416.45	-8.67
SP047	1441.19	17.95	6.68	416.45	-8.67
SP048	1441.19	17.95	6.68	416.45	-8.67
SP049	1441.19	17.95	6.68	416.45	-8.67
SP050	1437.46	17.95	6.77	416.45	-8.67
SP051	1306.4	19.02	5.34	416.45	-8.67

Sample name	MAP (mm/year)	MAT (°C)	VPD (hPa)	c_a (ppm)	$\delta^{13}CO_2$ (‰)
SP052	1306.4	19.02	5.34	416.45	-8.67
SP053	1306.4	19.02	5.34	416.45	-8.67
SP054	1306.4	19.02	5.34	416.45	-8.67
SP055	1306.4	19.02	5.34	416.45	-8.67
SP056	1307.79	19.42	6.04	416.45	-8.67
SP057	1307.79	19.42	6.04	416.45	-8.67
SP058	1306.4	19.02	5.34	416.45	-8.67
SP059	1364.9	19.09	6.95	416.45	-8.67
SP060	1364.9	19.09	6.95	416.45	-8.67
SP061	1364.9	19.09	6.95	416.45	-8.67
SP062	1364.9	19.09	6.95	416.45	-8.67
SP063	1364.9	19.09	6.95	416.45	-8.67
SP064	1364.9	19.09	6.95	416.45	-8.67
SP065	1364.9	19.09	6.95	416.45	-8.67
SP066	1364.9	19.09	6.95	416.45	-8.67
SP067	1364.9	19.09	6.95	416.45	-8.67
SP068	1330.2	19.08	5.99	416.45	-8.67
SP069	1330.2	19.08	5.99	416.45	-8.67
SP070	1330.2	19.08	5.99	416.45	-8.67
SP071	1330.2	19.08	5.99	416.45	-8.67
SP072	1330.2	19.08	5.99	416.45	-8.67
SP073	1310.67	19.31	8.77	416.45	-8.67
SP074	1304.52	21.28	9.78	416.45	-8.67
SP075	1304.52	21.28	9.78	416.45	-8.67
SP076	1304.52	21.28	9.78	416.45	-8.67
SP077	1311.17	21.28	9.85	416.45	-8.67

Sample name	MAP (mm/year)	MAT (°C)	VPD (hPa)	c_a (ppm)	$\delta^{13}CO_2$ (‰)
SP078	1311.17	21.28	9.85	416.45	-8.67
SP079	1311.17	21.28	9.85	416.45	-8.67
SP080	1355.5	21.18	7.56	416.45	-8.67
SP081	1355.5	21.18	7.56	416.45	-8.67
SP082	1355.5	21.18	7.56	416.45	-8.67
SP083	1343.43	21.33	8.21	416.45	-8.67
SP084	1343.43	21.33	8.21	416.45	-8.67
SP085	1343.43	21.33	8.21	416.45	-8.67
SP086	1295.02	21.98	8.28	416.45	-8.67
SP087	1295.02	21.98	8.28	416.45	-8.67
SP088	1453.11	22.43	9.46	416.45	-8.67
SP089	1453.11	22.43	9.46	416.45	-8.67
SP090	1453.11	22.43	9.46	416.45	-8.67
SP091	1516.71	22.93	9.21	416.45	-8.67
SP092	1516.71	22.93	9.21	416.45	-8.67
SP093	1516.71	22.93	9.21	416.45	-8.67
SP094	1402.84	22.88	9.02	416.45	-8.67
SP095	1402.84	22.88	9.02	416.45	-8.67
SP096	1402.84	22.88	9.02	416.45	-8.67
SP097	1601.72	24.22	9.25	416.45	-8.67
SP098	1601.72	24.22	9.25	416.45	-8.67
SP099	1601.72	24.22	9.25	416.45	-8.67
SP100	1612.69	25.07	9.48	416.45	-8.67
SP101	1612.69	25.07	9.48	416.45	-8.67
SP102	1612.69	25.07	9.48	416.45	-8.67
SP103	1600.81	24.89	9.16	416.45	-8.67

Sample name	MAP (mm/year)	MAT (°C)	VPD (hPa)	c_a (ppm)	$\delta^{13}CO_2$ (‰)
SP104	1600.81	24.89	9.16	416.45	-8.67
SP105	1469.93	23.61	10.25	416.45	-8.67
SP106	1469.93	23.61	10.25	416.45	-8.67
SP107	1469.93	23.61	10.25	416.45	-8.67
SP108	1305.41	22.95	7.51	416.45	-8.67
SP109	1305.41	22.95	7.51	416.45	-8.67
SP110	1305.41	22.95	7.51	416.45	-8.67
SP111	1305.41	22.95	7.51	416.45	-8.67
SP112	1305.41	22.95	7.51	416.45	-8.67
SP113	1305.41	22.95	7.51	416.45	-8.67
SP114	1444.32	21.91	8.78	416.45	-8.67
SP115	1444.32	21.91	8.78	416.45	-8.67
SP116	1448.21	21.9	8.83	416.45	-8.67
SP117	1448.21	21.9	8.83	416.45	-8.67
SP118	1448.21	21.9	8.83	416.45	-8.67
SP119	1448.21	21.9	8.83	416.45	-8.67
SP120	1449.93	21.87	8.9	416.45	-8.67
SP121	1449.93	21.87	8.9	416.45	-8.67
SP122	1449.93	21.87	8.9	416.45	-8.67
SP123	1449.93	21.87	8.9	416.45	-8.67
SP124	1449.93	21.87	8.9	416.45	-8.67
SP125	1449.93	21.87	8.9	416.45	-8.67
SP126	1353.43	20.67	9.37	416.45	-8.67
SP127	1353.43	20.67	9.37	416.45	-8.67
SP128	1364.07	20.33	9.28	416.45	-8.67
SP129	1364.07	20.33	9.28	416.45	-8.67

Sample name	MAP (mm/year)	MAT (°C)	VPD (hPa)	c_a (ppm)	$\delta^{13}CO_2$ (‰)
SP130	1364.07	20.33	9.28	416.45	-8.67
SP131	1364.07	20.33	9.28	416.45	-8.67
SP132	1418.82	20.33	7.11	416.45	-8.67
SP133	1418.82	20.33	7.11	416.45	-8.67
SP134	1418.82	20.33	7.11	416.45	-8.67
SP135	1418.82	20.33	7.11	416.45	-8.67
SP136	1418.82	20.33	7.11	416.45	-8.67
SP137	1418.82	20.33	7.11	416.45	-8.67
SP138	1509.8	20.59	6.68	416.45	-8.67
SP139	1509.8	20.59	6.68	416.45	-8.67
SP140	1509.8	20.59	6.68	416.45	-8.67
SP141	1509.8	20.59	6.68	416.45	-8.67
SP142	1523.23	20.38	6.32	416.45	-8.67
SP143	1523.23	20.38	6.32	416.45	-8.67
SP144	1523.23	20.38	6.32	416.45	-8.67
SP145	1523.23	20.38	6.32	416.45	-8.67
SP146	1523.23	20.38	6.32	416.45	-8.67
SP147	1523.23	20.38	6.32	416.45	-8.67
SP148	1523.23	20.38	6.32	416.45	-8.67
SP149	1523.23	20.38	6.32	416.45	-8.67
SP150	1523.23	20.38	6.32	416.45	-8.67
SP151	1523.23	20.38	6.32	416.45	-8.67
SP152	1522.21	20.48	6.24	416.45	-8.67
SP153	1523.3	20.4	6.34	416.45	-8.67
SP154	1523.3	20.4	6.34	416.45	-8.67
SP155	1522.17	20.42	6.29	416.45	-8.67

Sample name	MAP (mm/year)	MAT (°C)	VPD (hPa)	c_a (ppm)	$\delta^{13}CO_2$ (‰)
SP156	1522.17	20.42	6.29	416.45	-8.67
SP157	1522.17	20.42	6.29	416.45	-8.67
SP158	1760.84	19.81	7.7	416.45	-8.67
SP159	1760.84	19.81	7.7	416.45	-8.67
SP160	1760.84	19.81	7.7	416.45	-8.67
SP161	1740.68	19.75	8.15	416.45	-8.67
SP162	1740.68	19.75	8.15	416.45	-8.67
SP163	1740.68	19.75	8.15	416.45	-8.67
SP164	1751.95	19.72	8.47	416.45	-8.67
SP165	1751.95	19.72	8.47	416.45	-8.67
SP166	1751.95	19.72	8.47	416.45	-8.67
SP167	1751.95	19.72	8.47	416.45	-8.67
SP168	1669.14	21.27	9.53	416.45	-8.67
SP169	1669.14	21.27	9.53	416.45	-8.67
SP170	1669.14	21.27	9.53	416.45	-8.67
SP171	1674.36	20.15	8.49	416.45	-8.67
SP172	1674.36	20.15	8.49	416.45	-8.67
SP173	1674.36	20.15	8.49	416.45	-8.67
SPa001	1320.51	22.93	7.56	375.98	-8.15
SPa002	1473.72	23.82	10.53	416.45	-8.61
SPa003	1209.99	23.26	9.58	416.45	-8.61
SPa004	1319.32	21.03	8.35	379.98	-8.21
SPa005	1633.35	24.4	9.18	360.97	-7.92
SPa006	1210.46	25.18	8.8	333.84	-7.54
SPa007	1388.59	21.54	9.44	346.35	-7.71
SPa008	1613.06	24.18	9.44	336.84	-7.56

Sample name	MAP (mm/year)	MAT (°C)	VPD (hPa)	c_a (ppm)	$\delta^{13}CO_2$ (‰)
SPa009	1494.89	23.75	10.19	411.66	-8.59
SPa010	1216	24.57	8.25	330.19	-7.4
SPa011	760	26.22	9.32	390.1	-8.31
CU001	1538	26.74	8.45	341.48	-7.64
CU002	2305	26.42	5.95	326.32	-7.33
CU003	2305	26.42	5.95	326.32	-7.33
CU004	1032	24.34	7.44	340.12	-7.61
CU005	2085	25.78	7.6	305.4	-6.86
CU006	3133	22.55	3.01	310.8	-6.96
CU007	1058	25.66	9.7	354.45	-7.86
CU008	856	24.7	9.86	322.18	-7.29
CU009	2376	26.88	6.06	354.45	-7.86
CU010	1224	21.82	8.17	354.45	-7.86
CU011	1485	21.12	7.32	325.68	-7.32
CU012	265.38	17.44	7.25	360.97	-7.92
CU013	265.38	17.44	7.25	360.97	-7.92
CU014	265.38	17.44	7.25	360.97	-7.92
CU015	2337	23.14	7.55	363.88	-7.98
CU016	1025	24.32	7.5	340.12	-7.61
CU017	2026	25.95	7.55	293	-6.71
CU018	1680	22.35	6.51	305.8	-6.86
CU019	1939	22.86	6.78	304.1	-6.86
CU020	1724	22.32	7.2	306.2	-6.87
CU021	2333	21.97	5.08	384.02	-8.26
CU022	2205	23.5	7.3	384.02	-8.26
CU023	1606	21.81	5.41	384.02	-8.26

Sample name	MAP (mm/year)	MAT (°C)	VPD (hPa)	c_a (ppm)	$\delta^{13}CO_2$ (‰)
CU024	1375	23.62	5.93	384.02	-8.26
CU025	2387	23.38	6.2	387.64	-8.29
CU026	2739	19.72	1.62	349.31	-7.75
CU027	1845	25.42	7.46	336.84	-7.56
CU028	2534	22.57	3.58	385.83	-8.28
CU029	4033	23.27	5.31	385.83	-8.28
CU030	1317	21.78	5.39	387.64	-8.29
CU031	1785	21.41	6.06	390.1	-8.31
CU032	1221	21.74	8.06		0
PD001	248.15	22.71	23.05	346.35	-7.71
PD002	1137.65	25.46	9.24	310.5	-6.95
PD003	1137.65	25.46	9.24	308.7	-6.93
PD004	130	21.74	10.04	356.54	-7.85
PD005	1308	24.27	9.49	351.69	-7.8
PD006	1072	23.82	9.62	292.6	-6.71
PD007	184	22.78	13.54		0
PD008	367	15.38	6.48	297.4	-6.78
PD009	461	18.67	6.69	296.1	-6.73
PD010	466	18.15	9.2	296.4	-6.75
PD011	15	21.75	22.8	323.05	-7.3
PD012	571	25.45	10.28	331.12	-7.44
PD013	671	20.59	9.34	326.32	-7.33
PD014	1621.75	25.04	9.84	306.2	-6.87
PD015	882	26.31	7.99	296.2	-6.74
PD016	1296	25.82	6.63	290.9	-6.7
PD017	1247	25.42	5.95	296.4	-6.75

Sample name	MAP (mm/year)	MAT (°C)	VPD (hPa)	c_a (ppm)	$\delta^{13}CO_2$ (‰)
PD018	1161	25.85	7.01	299.1	-6.82
PD019	1159	26.5	8.77	300.6	-6.86
PD020	1848	23.22	6.61	303.9	-6.87
PD021	1694	21.37	7.39	292.6	-6.71
PD022	29	21.72	13.32	292.6	-6.71
PD023	263	19.85	7.18	286.1	-6.65
PD024	2354	24.95	5.54	310.5	-6.95
PD025	696	23.87	8.65	335.41	-7.55
Acowri.9930	1476.478	23.72	7.81	303.7	-7.05
Acwr.4333	1878.44	25.61	7.34	307.6	-6.79
Acoewrig.3070	1875.159	26.56	7.63	308.4	-6.84
Acme.2361	1355.605	25.6	6.96	330.8	-7.42
Aimi.1374	2417.386	23.53	1.67	385.46	-8.2
Arca.7653	2890.227	25.14	4	307.1	-6.85
Armo.28687	2257.992	26.5	6.1	308.4	-6.84
Aral.6208	2018.274	25.45	7.45	312.2	-6.85
Aren.6677	2320.984	23.62	5.94	311.5	-6.83
Armi.10578	3805.806	26.49	7.14	310.1	-6.88
Arpi.34257	2257.992	26.5	6.1	309.2	-6.81
Asma.80	4042.543	25	4.48	318.4	-7
Asme.10253	3001.68	26.47	5.82	310.8	-6.88
Atco.4970-a	2548.683	22.73	2.52	308	-6.85
Bacbar.16890	2932.61	24.4	2.9	310.5	-6.78
Baco.16745	2655.389	25.77	4.62	310.5	-6.78
Baga.10045	3963.518	26.37	4.52		0
Bagu.16996	2932.61	24.4	2.9	310.5	-6.78

Sample name	MAP (mm/year)	MAT (°C)	VPD (hPa)	c_a (ppm)	$\delta^{13}CO_2$ (‰)
Bama.4842	1145.249	26.43	9.36	317.8	-6.93
Bame.1373	2548.683	22.73	2.52	308	-6.85
Bapl.3379B	1728.864	27.22	13.43	355	-7.75
Brabra.2917	245.249	23.76	10.64	311.2	-6.87
Brca.16045	976.598	22.2	7.13	317.2	-6.96
Brdu.11759	878.205	21.48	7.91	349.3	-7.72
Brbe.3797	588.276	23.93	13.37	330.8	-7.42
Brpi.718	1021.082	21.63	7.42	350.8	-7.76
Brpr.13397	1874.691	24.36	7.44	319.1	-7.02
Brsa.9654	3001.68	26.47	5.82	310.8	-6.86
Buve.9197	1678.362	20.2	2.95	350.8	-6.87
Buca.21339	1242.739	17.44	5.75	311	-6.85
Buya.24939	1319.892	20.74	7.06	344.8	-7.63
Caac.33062	5414.482	17.53	1.71	312.2	-6.85
Caba.2287	1667.487	23.89	7.59	306.6	-6.76
Caca.8208	2268.076	27.18	5.77	305.4	-6.78
Cade.198	2268.076	27.18	5.77	305.8	-6.77
Cadie.7275	2268.076	27.18	5.77	305.4	-6.78
Cadi.78628	2331.04	27.82	7.19	306.2	-6.77
Caer.24380	5414.482	17.53	1.71	311.2	-6.87
Caer.27781	3250.705	18.33	0.38	311.5	-6.83
Caex.8707	2268.076	27.18	5.77	305.4	-6.78
Dagr.445	1478.453	25.91	3.47	310.5	-6.78
Cafl.27310	5414.482	17.53	1.71	311.5	-6.83
Caja.8095	2268.076	27.18	5.77	305.4	-6.78
Dalo.4412	2409.532	25.28	4.41	307.6	-6.79

Sample name	MAP (mm/year)	MAT (°C)	VPD (hPa)	c_a (ppm)	$\delta^{13}CO_2$ (‰)
Cama.14133	2331.04	27.82	7.19	299.8	-6.73
Came.743	2331.04	27.82	7.19	310.5	-6.78
Calmc.15515a	2504.609	26.66	5.78	308.4	-6.84
Calmi.227	2331.04	27.82	7.19	311.6	-6.88
Damo.783	2331.04	27.82	7.19	310.5	-6.78
Cate.8563	2201.175	22.96	6.96	322.8	-7
Cabl.251	2331.04	27.82	7.19	310.1	-6.88
Cacl.1135	3630.947	21.25		310.5	-6.78
Cami.4811	2409.532	25.28	4.41	307.6	-6.79
Caru.10826	3630.947	25.03	3.92	310.1	-6.88
Caur.24789	3250.705	18.33	0.38	311.2	-6.87
Ceal.10191	926.683	17.52	3.86	328.5	-7.3
Cequ.10191	926.683	17.52	3.86	328.5	-7.3
Chqu.1929	2211.648	16.83	0.04	309.6	-6.8
Chel.10108	408.157	23.94	14.63	315.7	-6.92
Cher.3443	2127.678	26.48	8.59	310.1	-6.88
Chgr.6853	1955.448	22.79	0.79	308.7	-6.83
Chne.2943	2548.683	22.73	2.52	310.1	-6.88
Chob.402	1875.159	26.56	7.63	317.8	-6.93
Chco.49553	1874.691	24.36	7.44	337.3	-7.47
Chpo.12137	1200.522	22.52	5.04	311.5	-6.83
Chra.008	954.57	20.05	4.53	312.2	-6.85
Chse.8075	1184.485	25.89	8.1	315.7	-6.92
Chdi.221	5273.382	26.13	4.08	352.2	-7.78
Coar.1766	1094.551	25.62	9.53	313.5	-6.86
Conu.902	1421.386	25.7	5.12	307.6	-6.79

Sample name	MAP (mm/year)	MAT (°C)	VPD (hPa)	c_a (ppm)	$\delta^{13}CO_2$ (‰)
Crar.9175	2257.102	25.65	5.16	359.6	-7.86
Crba.158	2543.353	26	4.92	349.3	-7.72
Crycoo.162	3685.733	26.18	5.68	349.3	-7.72
Daac.781	2331.04	27.82	7.19	310.5	-6.78
Dech.3196	1875.159	26.56	7.63	310.1	-6.88
Demy.16728	2655.389	25.77	4.62	310.5	-6.78
Depo.50	2687.253	26.47	10.57	304.1	-6.99
Gama.3759	2257.102	25.65	5.16	307.6	-6.79
Gede.320	4042.543	25	4.48	319.1	-7.02
Gein.16748	2932.61	24.4	2.9	310.5	-6.78
Geap.9716	2468.291	18.11	0.04	323.9	-7.01
Heca.14907	2192.529	25.85	6.48	308.4	-6.84
Heel.218	2373.694	26.71	7.68	310.8	-6.79
Irco.5739	2554.867	26.03	3.05	307.6	-6.79
Koec.64	2357.403	27.03	6.47	305.4	-6.78
Lifo.17347	1730.867	21.27	4.77	308	-6.85
Lipe.24940	5414.482	17.53	1.71	350.8	-6.87
Lisa.34149	2354.624	24.42	0.55	309.2	-6.81
Mesa.999	2331.04	27.82	7.19	310.8	-6.79
Nifru.6785	2320.984	23.62	5.94	311.5	-6.83
Orru.975	1925.219	26.2	6	310.8	-6.79
Orsy.5568	2409.532	25.28	4.41	307.6	-6.79
Phou.28426	5414.482	17.53	1.71	311.5	-6.83
Pipa.21619	1917.702	23.99		303.9	-7.21
Prka.10466	2351.97	22.81	6.94	308.4	-6.84
Regr.4990	2078.147	25.78	10.88	308	-6.85

Sample name	MAP (mm/year)	MAT (°C)	VPD (hPa)	c_a (ppm)	$\delta^{13}CO_2$ (‰)
Sam.8700	689.959	23.24	7.35	310.5	-6.78
Sami.454	1384.837	16.88	6.24	313.5	-6.86
Sapu.22046	1216.995	25.3	14.8	319.9	-7.06
Saya.3103	2548.683	22.73	2.52	310.1	-6.88
Syfl.43038	1401.331	24.92	6.16	349.3	-7.72
Trca.40637	1114.642	19.17	5.87	344.8	-7.63
Wade.30554	5414.482	17.53	1.71	311.8	-6.86